CANADA

DEPARTMENT OF
ENERGY, MINES AND RESOURCES
MINES BRANCH
OTTAWA

STUDIES OF THE DOUBLE LAYER AT THE OXIDE-SOLUTION INTERFACE

S. M. AHMED AND D. MAKSIMOV

MINERAL SCIENCES DIVISION

FEBRUARY 1968

Research Report R 196 Price $1.25

Available by mail from the Queen's Printer, Ottawa,
and at the following Canadian Government bookshops:

OTTAWA
Daly Building, Corner Mackenzie and Rideau

TORONTO
221 Yonge Street

MONTREAL
Æterna-Vie Building, 1182 St. Catherine St. West

WINNIPEG
Mall Center Building, 499 Portage Avenue

VANCOUVER
657 Granville Avenue

HALIFAX
1737 Barrington Street

or through your bookseller

A deposit copy of this publication is also available
for reference in public libraries across Canada

Price $1.25 Catalogue No. M38-1/196

Price subject to change without notice

ROGER DUHAMEL, F.R.S.C.
Queen's Printer and Controller of Stationery
Ottawa, Canada
1968

Mines Branch Research Report R 196

STUDIES OF THE DOUBLE LAYER AT THE OXIDE-SOLUTION INTERFACE

by

S. M. Ahmed* and D. Maksimov**

ABSTRACT

The double layer at the oxide-solution interface has been examined by studying the equilibrium distribution of the potential-determining ions (H^+ and OH^-) at the interface as a function of their electrochemical potentials. The oxides investigated were alumina, cassiterite, hematite, magnetite, rutile, thoria, and zirconia in solutions of KNO_3, KCl and $NaClO_4$. Information has been obtained on the zero point of charge, the surface charge densities ($q^{\pm}$), the differential capacities ($C^{\pm}$), and the effect of $q^{\pm}$ on the interfacial tension. The data are discussed with respect to current theories of the double layer.

*Research Scientist, Mineral Sciences Division, Mines Branch, Department of Energy, Mines and Resources, Ottawa, Canada.

**Visiting Scientist (1964-68), from Skochinski Mining Institute, Moscow, U.S.S.R.

ÉTUDE DE LA DOUBLE COUCHE ÉLECTRIQUE A L'INTERFACE OXYDE-SOLUTION

par

S. M. Ahmed* et D. Maksimov**

RÉSUMÉ

On a examiné la double couche électrique à l'interface oxyde-solution en étudiant la distribution à l'équilibre des ions qui déterminent le potentiel (H^+ et OH^-) à l'interface en fonction de leurs potentiels électrochimiques. Les travaux ont porté sur l'alumine, la cassitérite, l'hématite, la magnétite, le rutile, ainsi que les oxydes de thorium et de zirconium dans des solutions de KNO_3, KCl et $NaClO_4$.

On a obtenu des renseignements sur la valeur du point de charge zéro, des densités superficielles de charge ($q^{\pm}$), des capacités différentielles ($C^{\pm}$), ainsi que sur l'effet de $q^{\pm}$ sur la tension interfaciale. On a discuté les résultats en regard des théories courantes sur la double couche.

---

* Prépose au recherches scientifiques, Division des sciences minérales, Direction des mines, ministère de l'Energie, des Mines et des Ressources, Ottawa, Canada.

** Scientifique visitant, de l'institut minier Skochinski (Moscou), à la Direction des mines (1964-68).

CONTENTS

= = =

FIGURES

TABLES

PART A. THEORETICAL BACKGROUND

I. INTRODUCTION

The double layer plays an important role wherever interfacial science is involved in mineral research and technology; for example, in flotation (1-5), agglomeration, adhesion, surface spreading and wetting (6), or leaching with micro-organisms. Most minerals are either non-metals or semiconductors. An understanding of the double layer at the mineral-solution interface could prove useful in helping to solve many industrial problems. However, improper use of double-layer theory may also lead to drastic errors. Most of the reviews (7-11) that have been published recently on double-layer phenomena are concerned with the academic point of view, and very few reviews (4, p. 91; 12) are particularly oriented towards minerals. The following survey of the subject is undertaken to show its usefulness in the above fields of work. There are numerous modern techniques (13-16) available for studying interfaces in general, and some of these techniques have been reviewed recently by Zettlemoyer (17). Double-layer phenomena, in particular, can be investigated by a variety of well-known methods, not including such indirect studies as electrode kinetics. Which method would be most suitable depends on the nature and physical form of the material and also the kind of information needed. A thorough study of the semiconductor-electrolyte interface, however, requires a

wider variety of measurements, including the electrical properties of the semiconductor surface, as will be reviewed briefly in a later section.

Polarizable Interfaces

A metal surface in contact with an electrolyte solution can be polarized electrically by applying a D.C. voltage across the interface. An electrode is said to be ideally polarizable (7-10) if no significant amount of charge crosses the interface. If the metal is a liquid such as Hg, or a metal amalgam, electrocapillary methods are used in which the variation of interfacial tension is measured directly as a function of the applied potential and the composition of the solution.

If one of the phases is a metal (liquid or solid) or a semiconductor, the double-layer capacity can be measured directly by both A.C. or D.C. methods. Further information on the double layer, and also on the nature of adsorption, can be derived from the measured values of capacity.

Reversible and Nonpolarizable Interfaces

Metals and elementary semiconductors in contact with their respective potential-determining ions, e.g. Hg in equilibrium with Hg^{++}, constitute reversible electrodes (18; 8, p. 636) whose potential E is determined by the activity of the potential-determining ions in solution, according to the Nernst equation,

$$E = E_o + \frac{RT}{z_+ F} \ln a_{cation},$$

where E_o is the standard electrode potential when the activity, a, of the cation in solution is equal to unity. The characteristics of the interface may be studied by electrocapillary methods if the metal is a liquid, whereas solids can be studied as galvanic cells, in conjunction with another half-cell.

Many inorganic salts and compound semiconductors -- such as Ag halides (19-21), metal oxides (22-27) and metal sulphides (28-29) -- that are sparingly soluble in water give rise to a reversible double layer when in contact with their potential-determining ions. These potential-determining ions are the constituents of the lattice itself, and for oxides they are H^+ and OH^- (27). Such systems, as above, are also known as electrodes of the second kind (30, p. 256). The electrode potential or the double-layer potential, as before, is determined by the activity of the potential-determining ions according to the Nernst equation. These can be studied as electrodes in rod form, e.g., AgCl (31), Ag_2S (32, 33), and metal oxides (30, p. 293; 34, 35). The metal oxides can also be studied as half-cells, when suspended as powders in electrolyte solutions (19-29). If the surface areas of powders are precisely known, much of the information on the double layer that is usually obtained by electrocapillarity can be obtained by this method (23), although with much less precision. Considerable work has been carried out on mineral-solution interfaces by this method. Contact-angle measurements on solid surfaces can also give some information on the double layer, although these measurements essentially represent the over-all result of several microscopic effects at the interface.

Electrokinetic Methods

An electrokinetic potential (zeta potential) is developed at the solid-solution interface when there is a relative movement between the mobile and the fixed phases. The zeta potential is mainly responsible for the following types of electrokinetic effects encountered in surface chemistry: electrophoresis, sedimentation potential, electro-osmosis, and streaming potential. Streaming-potential methods can be used both on solid surfaces and on coarse powdered materials, whereas electrophoretic methods are used on colloidal or finely divided solids for determining the zeta potential, the nature of charge ($\pm$), and also the potential of the zero charge. Due to several uncertainties arising from the location of the shear plane, surface conductivity, dielectric constant, etc., a quantitative interpretation of electrokinetic effects is difficult. Electrokinetic techniques are only complementary to other methods, and will not be dealt with further here.

Colloid-Solution Interface

Besides electrophoretic methods, several other techniques are well established for studying the colloid-electrolyte interface (13, 36).

The present survey will be confined mainly to the solution side of the double layer on solids, which in general is essentially the same whether the solid is a metal, a non-metal, or a semiconductor. However, the nature of solid surfaces, particularly those of semiconductors, plays a major role in the nature and degree of adsorption. At the semiconductor-electrolyte interface, the double layer is known to extend for a considerable distance ($\sim 10^{-4}$ cm) into the solid.

Colloid-solution interfaces will not be dealt with in detail here, as excellent reviews are available (13, 36). Because the basic thermodynamics and the present knowledge of the double layer were developed mainly from electrocapillary work with Hg, electrocapillarity will be considered in detail first; an understanding of it is essential for any further work on double-layer phenomena.

II. INTERFACIAL PHENOMENA

When two phases in which electrons have different electrochemical potentials* are brought into contact, charge transfer or charge adjustment occurs between them until, at equilibrium, a potential difference (Galvani potential) is established at the boundary layer. The subject of potential differences at interphases has been discussed in detail by Grahame (7, p. 487), Conway (37, p. 13), and Parsons (38). The nature of interfacial equilibria, as will be seen later, also depends on whether the material is a metal, a non-metal, a semiconductor, or a solution. The residual chemical bonds on surfaces ($\sim 10^{15}/cm^2$), produced, for example, by the fracture of solids, also participate in establishing potential differences at interphases. During the establishment of interfacial equilibria, the following types of interactions may occur:

---

* For metals the electrochemical potential is the work function, i.e., the work required to remove an electron at the Fermi level to a point in free space.

a) diffusion of reactant ions or molecules towards the surface;

b) adsorption of ions, dipoles or molecules;

c) charge transfer across the interface, involving ions or molecules;

d) formation of chemical compounds on the surface, followed by dissociation of the surface groups.

The tendency for an ion or molecule to be adsorbed on a solid surface may be attributed to the phenomenon of polarization caused by an induced dipole interaction. If the free energy, G, of such interaction is greater than the thermal energy, the average adsorption time, τ, of an ion or molecule on the surface will be longer than the average molecular vibration time ($\tau_o \sim 10^{-13}$ seconds), according to the relationship $\tau = \tau_o \cdot e^{\Delta G/RT}$. The magnitude of the adsorption energy depends on various factors, such as, for example, the charge, size, hydration and polarizability of the ions or the molecules. Details of such interaction energies may be found in reviews by Zettlemoyer (17) and others (8). Anions, being less hydrated and more polarizable than cations, show a greater and more specific (covalent) tendency for adsorption on surfaces than cations. The adsorption of organic compounds on electrodes has been discussed in detail by Frumkin and Damaskin (39). In organic salts the tendency for adsorption may also depend on the nature and size of the non-ionogenic part of the compound (40). Large molecules of non-polar organic compounds show a tendency (6) for adhesion to non-polar solid surfaces by van der Waals forces. Organic compounds, such as alcohols, that have a lower surface tension than water may show a marked tendency (6) to accumulate at the

solid-solution interface, provided other conditions are favourable.

As a result of the above interactions, an unequal distribution of electrical charges occurs in the boundary region. Thus, there will be an excess $\pm$ of surface charge on the solid side and an excess $\mp$ of space charge on the solution side of the interfacial boundary plane. This distribution of charges at the boundary is called the double layer. In the following sections, the double layers on polarizable interfaces and on non-polarizable or reversible interfaces will be considered separately, together with the theoretical and experimental methods of investigating them.

III. POLARIZABLE ELECTRODES

A mercury surface in contact with an electrolyte solution can be polarized electrically by applying a variable voltage through a potentiometer (7-9). The applied voltage, E, is measured in combination with a reference electrode and is designated E^- or E^+, depending on whether the reference electrode is reversible to an anion or to a cation present in solution. At a certain applied potential, the interface acquires a net zero charge and the "coulombic" potential difference across the interface is zero (a dipole adsorption potential, χ, however may still be present). This potential, E_z, is known as the potential of zero charge (p.z.c.). In NaF solutions, it occurs at -0.48 volt, with respect to a normal calomel electrode (7). At the p.z.c., each phase retains its original (maximum) surface tension. When the applied potential is greater than or less than E_z,

the Hg-surface, obviously, acquires a positive or negative surface charge ($q^{\pm}$) composed of excess metal ions or excess electrons, respectively. An excess space charge ($\bar{+}$) accumulates on the solution side of the interface so that the whole system is electrically neutral, and a double layer is thus formed. The charges tend to expand the surface as a result of electrostatic repulsion, and hence decrease the surface tension (tendency to contract the surface). Therefore, the greater the charge density at the interface, the lesser will be the interfacial tension or interfacial energy*.

The variation of the surface tension of Hg, with applied potential and solution composition, can be measured in the capillary electrometer originated by Lippmann. Several modifications of this apparatus have been used, including the dropping Hg-electrode, and the details may be found elsewhere (41-43). The Hg electrode is known as an ideally polarizable electrode because no significant amount of charge (in the absence of Hg^{++}) crosses the interface when it is polarized electrically. The electrode, in effect, behaves as an electrical condenser without leakage. The high over-voltage of Hg for hydrogen evolution also favours its polarizability.

Thermodynamics of Electrocapillarity

Applying Gibbs' adsorption equation to the polarizable mercury electrode, Grahame and Whitney (44) have shown that the decrease in the interfacial energy, γ, is given, at constant temperature and pressure, as

*The interfacial tension in dynes/cm is numerically equivalent to the interfacial energy in ergs/cm^2.

$$-d\gamma = qdE + \sum^{soln} \Gamma_i d\bar{\mu}_i + qd(\Delta\psi), \qquad \text{(Eq. 1)}$$

where q is the surface charge ($\pm$) density (per cm^2) on the Hg; E is the applied potential as described earlier; and $\bar{\mu}_i$ and Γ_i are the electrochemical potential (37) and surface excess (moles/cm^2) of component i, respectively. $\Delta\psi$ is a term arising from changes in the liquid junction potentials, if any, on changing the composition of the solution or the reference electrode. The surface excess, Γ, is recognized (7, p. 454) with reference to a hypothetical plane drawn parallel to but not coincident with the physical interface. The summation, $\sum \Gamma_i d\mu_i$, includes all the charged and neutral components of the solution, although $\Gamma_{H_2O} d\mu_{H_2O}$ is generally taken as zero. At constant composition, Equation 1 reduces to the well-known Lippmann's equation:

$$q = -\left(\frac{\partial\gamma}{\partial E}\right)_{\mu}. \qquad \text{(Eq. 2)}$$

The surface charge density, q, can thus be obtained by the graphical differentiation of the γ-E plots, which are also known as the electrocapillary curves. The value of q with the sign reversed also represents the total ionic charge in the double layer, so that:

$$q^{\pm} = -F \sum^{soln} \Gamma_i^{\pm} z_i \qquad \text{(Eq. 3)}$$

where F is the Faraday constant, and z_i is the valence of component i (including the sign). If the solution consists of a z-z valent salt of type AB,

$$q = -zF(\Gamma_A^{+} - \Gamma_B^{-}). \qquad \text{(Eq. 4)}$$

The electrocapillary curves and the q-E plots for some electrolyte solutions are reproduced in Figures 1 and 2. In these curves, q equals zero when γ is maximum, as may be seen from Equation 2, and hence the corresponding potential, p.z.c. = E_z, is also known as the potential of electrocapillary maximum (e.c.m.). In Figure 1 it is seen that the potential of the e.c.m. in KI solution is shifted to a more negative value as compared with the E_z of Hg in NaF solutions. This shift is due to the specific adsorption of I^- on Hg, which will be discussed in more detail later. The anodic branch of the electrocapillary curve (left-hand side of the e.c.m.) represents the decrease in the interfacial energy, due to a predominant adsorption of anions (Γ^-) on the positively charged Hg (charge density = q^+). The cathodic branch (right-hand side of the e.c.m.) represents, similarly, adsorption of cations (Γ^+) on the negatively charged Hg (charge density = q^-). It is seen in Figure 1 that the electrocapillary curves vary markedly with the nature of anions at the extreme positive potentials, whereas the curves for most of the common cations coincide at the extreme negative potentials.

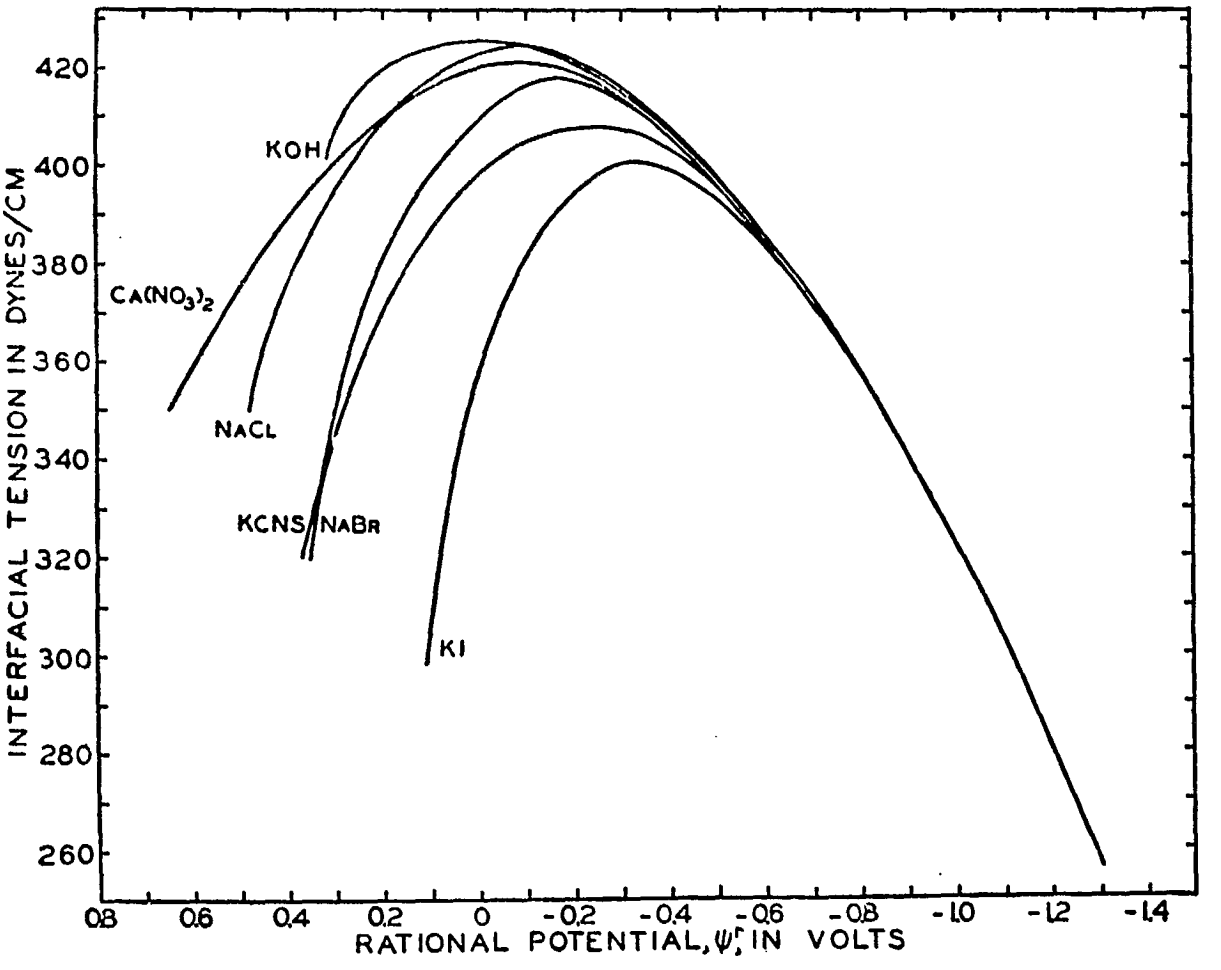

Figure 1. Electrocapillary curves of Hg in different electrolyte solutions at 19°C. ψ^r is measured relative to the potential of e.c.m. in NaF solution (= -0.48 volt). (After Grahame, Ref. 7, p. 448)

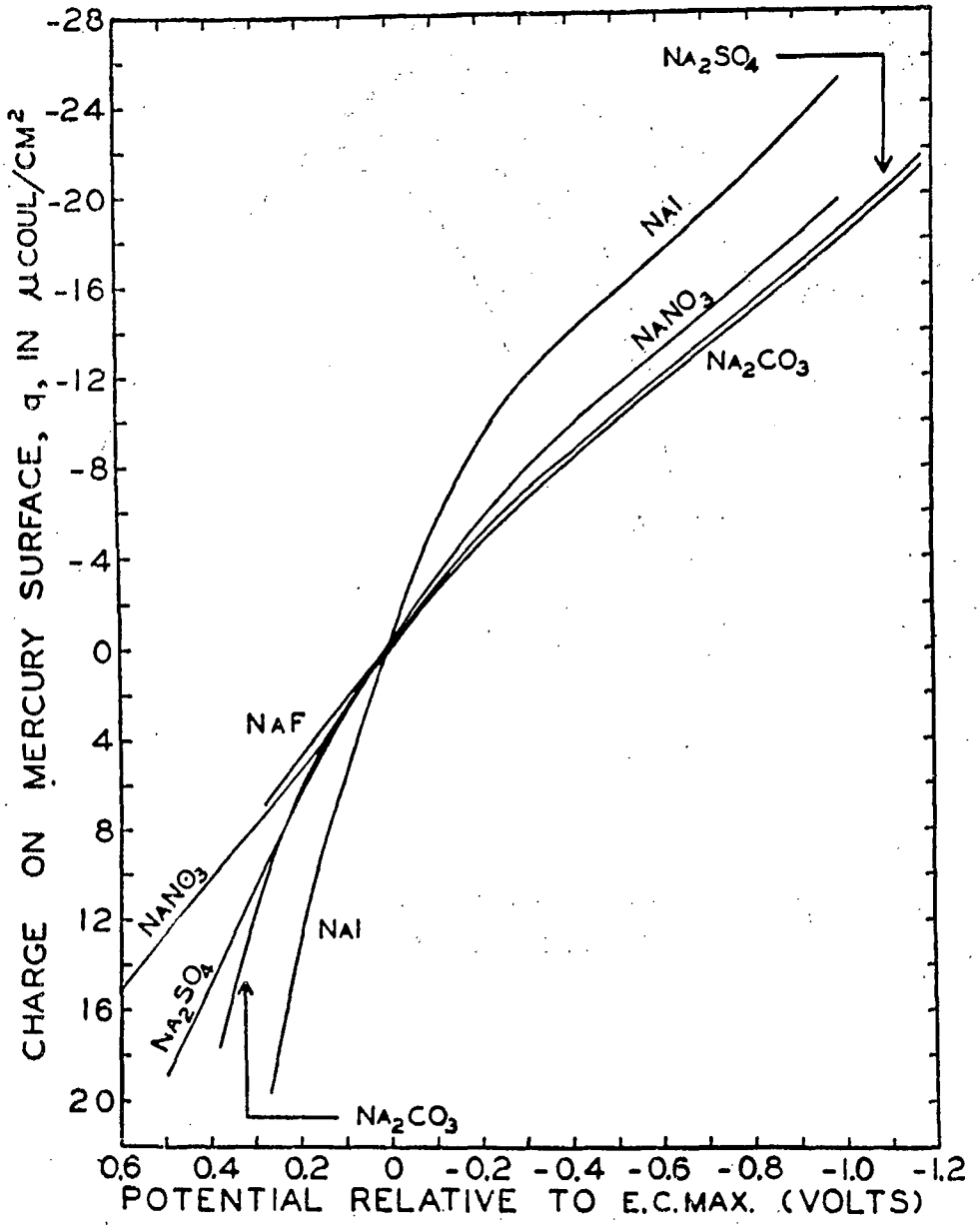

Figure 2. Surface charge density ($q^{\pm}$) of Hg in contact with 1 M solutions at 25°C. (After Grahame, Ref. 7, p. 456)

The differential capacity, C, of the entire double layer can be obtained by differentiation of the q-E plots, according to Equation 5, which is obtained from the Lippmann's relationship (Equation 2):

$$-\left(\frac{\partial^2\gamma}{\partial E^2}\right)_\mu = \left(\frac{\partial q}{\partial E}\right)_\mu = C \qquad \text{(Eq. 5)}$$

The integral capacity, K, of the double layer is given by $K = q/E$. Some typical differential capacity curves, along with those calculated from double-layer theories, are shown in Figures 3, 4 and 5. The shapes of these curves have important theoretical significance and will be discussed further after the theories of the double layer are considered.

As q and C are obtained by first and second graphical differentiation of the electrocapillary curves, their values are not very accurate. Moreover, this method is not applicable to solids. Hence, direct measurements of the double-layer capacity, C, are preferred, by using either A.C. or D.C. methods. The surface charge density, q, and the electrocapillary (γ-E) curves may then be evaluated by integration of the C-E and q-E plots, respectively, viz.,

$$q = \int_{E_z}^{E} C\,dE \qquad \text{(Eq. 6)}$$

$$\gamma - \gamma_{E_z} = -\int_{E_z}^{E} q\,dE = -\iint_{E_z}^{E} C\,dE^2 \qquad \text{(Eq. 7)}$$

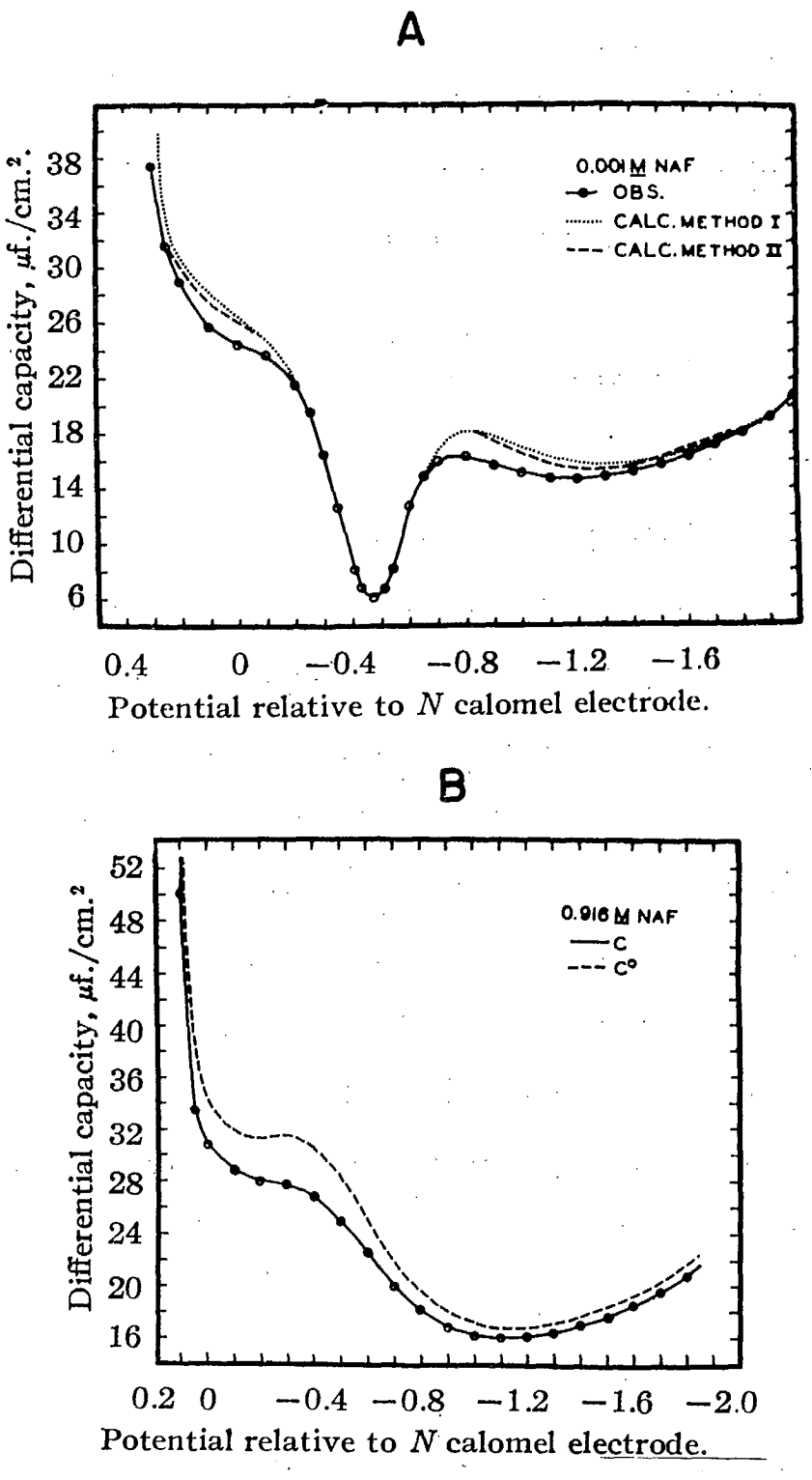

Figure 3. Experimental and calculated values of the differential capacity of the Hg-solution interface. Dashed line in B represents the differential capacity of the compact layer C^{o}. (After Grahame, Ref. 76, p. 4820)

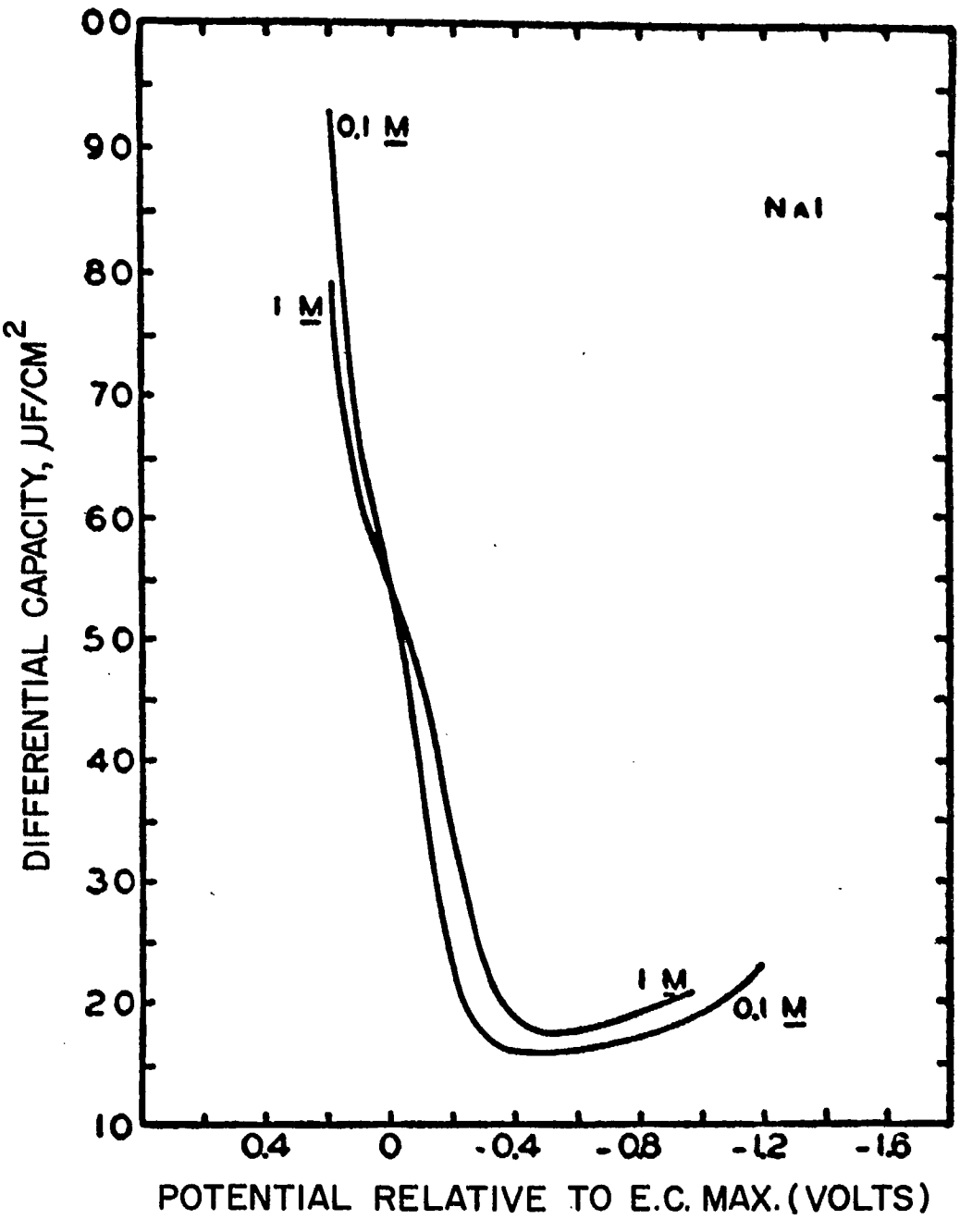

Figure 4. Differential capacity of the electrical double layer between Hg and aqueous NaI solutions. (After Grahame, Ref. 7, p.463)

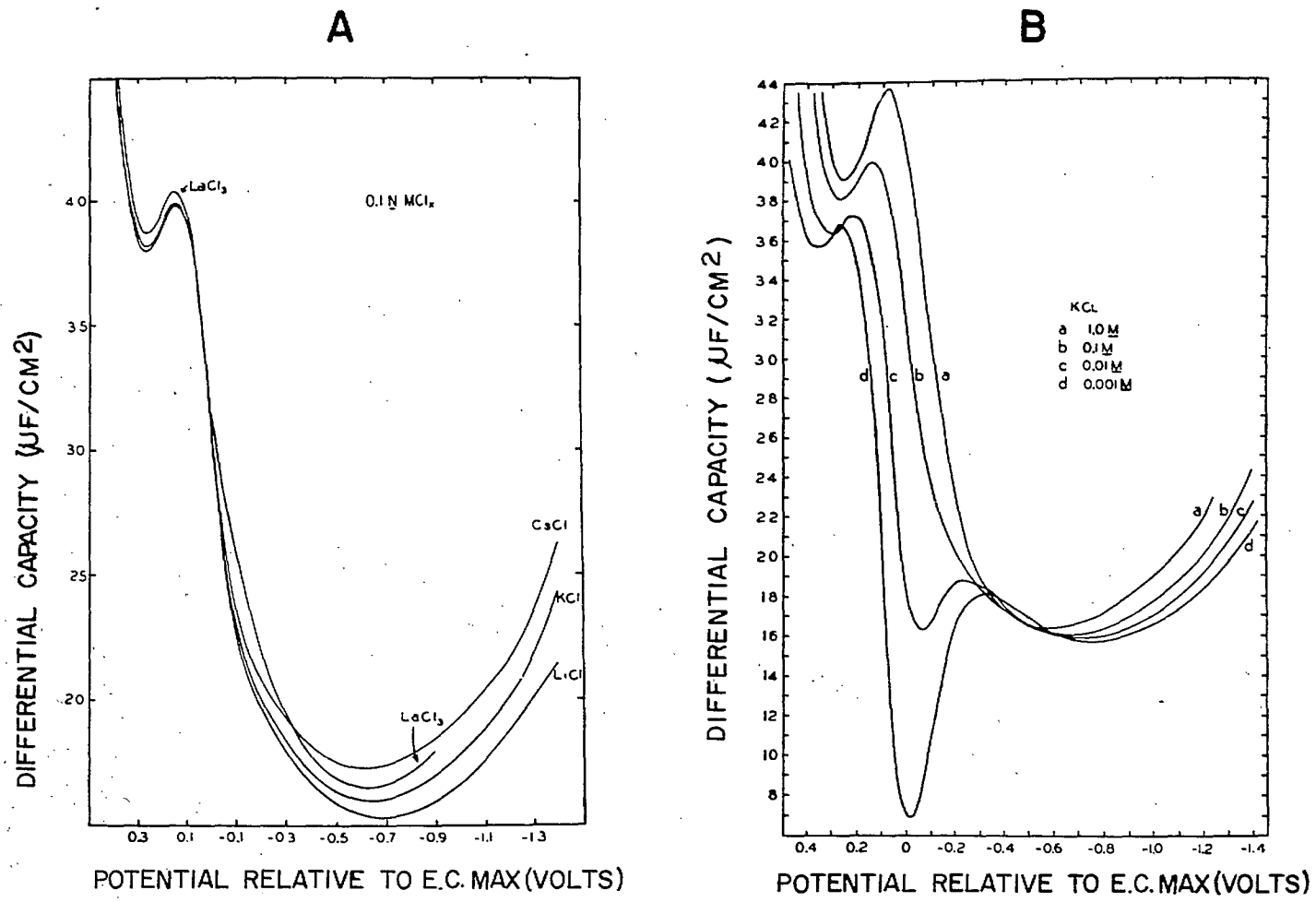

Figure 5. Differential capacity of the Hg-solution interface in different electrolyte solutions. (After Grahame, Ref. 41, p.332)

With D.C. transient methods, the electrode capacity is measured by observing the rate of change of potential with time, when the electrode is charged with D.C. A cathode ray oscilloscope is used as an indicating instrument. With A.C. methods of measuring the double-layer capacity, the electrode is introduced into a high-impedance A.C. bridge and balanced against a known standard capacity, while the potential of the interface is varied by superimposing a D.C. voltage upon the A.C. The measured capacity, particularly in the case of solid electrodes, is also known to vary with the A.C. frequency. Several modifications of these techniques have been developed (30, p. 590; 41, 45-48). Ramaley and Enke (45) have also recently reviewed the instrumentation required for capacity measurements and have described two methods in detail.

So far, we have been dealing with only variations in the applied voltage E on γ. We shall now consider the effect on γ of varying the composition of the solution ($\bar{\mu}_i$) at constant $E^{\pm}$. If E^+ or E^- are the applied polarizing potentials, when the reference electrode is reversible to a cation or an anion respectively, it can be shown (cf. Equation 1) at zero liquid-junction potentials, for the simple case of a uni-univalent electrolyte, that

$$-d\gamma = qdE^{\pm} + \Gamma^{\pm}_i d\mu_i. \qquad \text{(Eq. 8)}$$

The terms Γ^+ and Γ^- represent surface excesses of cations and anions. The more complicated cases of z-z' valent electrolytes has also been dealt with by Grahame (49). If the chemical potentials (μ_i) are defined as in Equation 9, in which the mean activity coefficients ($f_{\pm}$) are used instead

of the individual activity coefficients, we have

$$d\mu_i = RT\, d\ln m_{\pm} f_{\pm}, \qquad \text{(Eq. 9)}$$

where $m_{\pm}$ is the mean molality of the 1-1 valent salt, i.

Equation 8 may now be considered further under three important conditions:

a) At constant composition, it reduces to Lippmann's equation.

b) When q = o, i.e. at the p.z.c. (E_z) or the e.c.m.,

$$-\left(\frac{d\gamma}{\partial\mu_1}\right)^{max} = \Gamma_i^{+max} = \Gamma_i^{-max}, \qquad \text{(Eq. 10)}$$

i.e., any change or shift of the e.c.m. as a function of electrolyte concentration is related to the salt adsorbed, which can be determined from the plots of the e.c.m. against log $a_{\pm}$ (activity) of the electrolyte.

c) At constant E^- or E^+,

$$-\left(\frac{\partial\gamma}{\partial\mu_i}\right)_{E^-} = \Gamma_i^+ \text{ and } -\left(\frac{\partial\gamma}{\partial\mu_i}\right)_{E^+} = \Gamma_i^-. \qquad \text{(Eq. 11)}$$

Hence, the surface excess, $\Gamma^{\pm}$, at any value of $E^{\mp}$, can be determined by differentiation of the γ versus log $a_{\pm}$ plots.

Alternative equations can also be derived to evaluate $\Gamma^{\pm}$ by the graphical integration of the following derivatives with respect to E^- or E^+, from the q versus log $a_{\pm}$ plots:

$$\left(\frac{\partial q}{\partial\mu}\right)_{E^{\mp}} = \left(\frac{\partial\Gamma^{\pm}}{\partial E^{\mp}}\right)_{\mu}. \qquad \text{(Eq. 12)}$$

Such graphical analysis of the double layer may also be performed from the experimental measurements of differential capacity, since the components $C_{\pm}$ are related to the surface excess $\Gamma^{\pm}$ as

$$z^{\pm} F \left(\frac{\partial \Gamma^{\pm}}{\partial E^{\mp}}\right)_{\mu_i} = -C_{\pm} \cdot \qquad \text{(Eq. 13)}$$

Graham and Soderberg (50) have given details for the complete analysis of the double-layer components. The subject has been reviewed by Bockris (10) and others (8, 9).

Structure of the Double Layer on Metals and Non-Metals

The problem of ionic distribution in the double layer cannot be solved from thermodynamics alone. Different models have been proposed and detailed reviews (7; 9, p. 33) are available. The first model was that of Helmholtz and Quinke, who proposed a compact double layer similar to a parallel-plate condenser, whereas Gouy and Chapman proposed a diffuse double layer in which the potential drop is gradual. According to the first model, the double-layer capacity should be constant with change of potential, while the second model predicts a high value of $C \sim 250\,\mu F/cm^2$ in 0.1 N electrolyte solutions at low potentials. Neither of the above predictions is found to be true experimentally. In the Holmholtz model the effect of temperature on the distribution of ions is neglected, whereas in the Gouy-Chapman model the finite size of the ions was not considered.

The present double-layer theories are based on the Stern model. This consists of a combination of the Helmholtz compact layer, followed by the Gouy-Chapman diffuse double layer, combined in series like two parallel-plate condensers, but not with a constant capacity. Grahame (7, p. 466) proposed a further refinement to the double-layer theory by splitting the Helmholtz layer into the inner Helmholtz layer (abbreviated as I.H.L. $\approx$2 Å thick) and the outer Helmholtz layer (abbreviated as O.H.L. $\approx$3 Å thick). Many anions (7, 8, 51), such as Cl^-, Br^-, I^-, BrO_3^-, etc., which are less hydrated and more polarizable than cations, can approach much closer to the surface of Hg and can occupy the I.H.L., so that there are no solvent molecules between the surface and the I.H.L. Such adsorption is known as specific adsorption. In addition to the energy of dehydration of ions, covalent forces and other short range forces, such as van der Waals interaction, also take part in the specific adsorption. However, at low values of E, anions (7, 8, 51) such as F^-, NO_3^-, ClO_4^-, and HSO_4^- show little tendency for specific adsorption on Hg. Specific adsorption also depends on the nature of the solid surfaces. Cations, which are more hydrated and less polarizable (8, 52) than anions, in general stay in the O.H.L., so that the space between the surface and the O.H.L. is occupied by a layer of oriented solvent molecules. Such adsorption is shown by most of the alkali and alkaline earth ions. However, Cs^+, Tl^+ (53, 54), polyvalent cations such as Al^{3+} and La^{3+}, and tetraalkylammonium ions are known to possess a considerable tendency for specific adsorption on Hg. The I.H.L. layer, therefore, loses its significance when there is

no specific adsorption of ions on the surface. The effect of specific or non-specific adsorption on the double-layer characteristics (γ, p.z.c., and C) is an interesting and useful subject and will be discussed further in the next section. The questions of hydration of the adsorbed ions, hydration of the surface, and the orientation and dielectric properties of solvent molecules in the I.H.L. have been the subject of many controversial discussions. Several refinements of double-layer theories have been proposed by Conway et al. (55), Grahame (56), Macdonald and Barlow (57), Watts-Tobin (58)and Bockris et al. (59). Not all of the experimental facts have been satisfactorily explained, and a number of discrepancies have been summarized by Conway (37, p. 39) and others (9, 60, 61). More exact theories of the double layer, taking into account the discreteness-of-charge effects and the particle-particle interaction in the compact double layer, have been proposed (62-66). The subject has also been reviewed recently by Levine et al. (61). For most practical purposes, however, the Stern-Gouy-Chapman model as modified by Grahame is satisfactory (Figure 6).

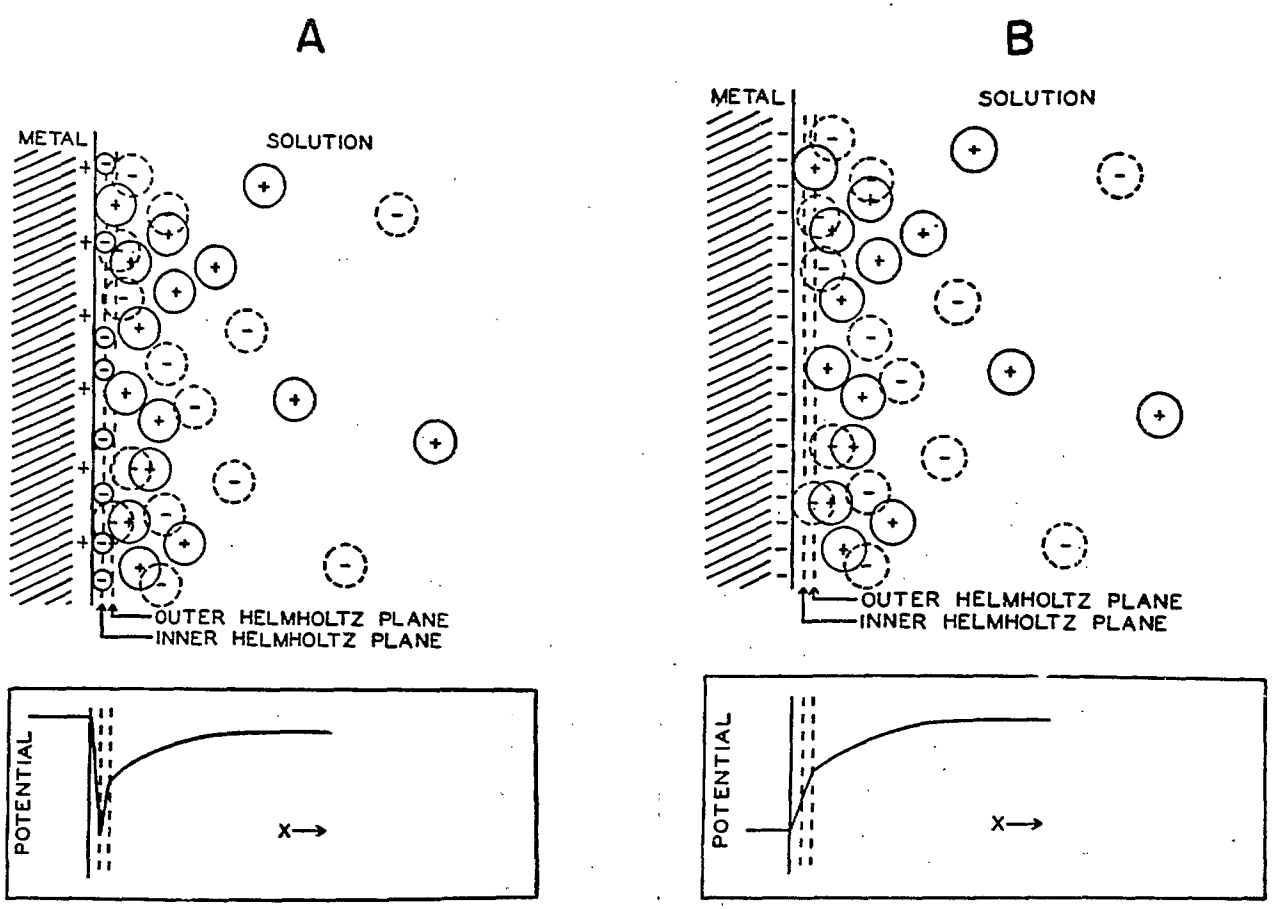

Figure 6. Stern-Gouy-Chapman model of the double layer as modified by Grahame. A: Under positive polarization with specific adsorption of anions. B: Under negative polarization. The larger circles represent ions in hydrated form and the smaller circles represent ions in dehydrated form. (After Grahame, Ref. 7, pp. 490 and 491)

Kinetic Theory of the Double Layer

If η refers to the charge density (in μ coulombs/cm^2) on the solution side of the total double layer, and q the surface charge density on the solid side, then $\eta = -q$. If η^i and η^d refer to the charge densities in the compact and diffuse parts of the double layer, then

$$-q = \eta = \eta^i + \eta^d. \qquad \text{(Eq.14)}$$

The charge densities η^d and η^i can be calculated from the kinetic theory of the double layer (Equations 16 and 21) as outlined below. Further, η^i and η^d are composed of the cation surface-excess, Γ^+, and anion surface-excess, Γ^-, in moles/cm^2 (the experimental quantities, cf. Equations 11 and 12), so that

$$zF\Gamma^- = \eta^i_- + \eta^d_- \qquad \text{and}$$

$$zF\Gamma^+ = \eta^i_+ + \eta^d_+. \qquad \text{(Eq.15)}$$

In the absence of specific adsorption, $\eta^i = 0$ in the above equations. A complete analysis of the double-layer components in terms of q, η, η^i_+, η^d_+ and $\Gamma^\pm$ can be carried out, making use of the above relationships. Details of such analyses are given by Grahame and Soderberg (50) and others (7, 9, 10).

The Diffuse Double Layer

From the kinetic theory of the diffuse double layer (7, 9), the charge density η^d and its components η^d_+ and η^d_- have been calculated, as shown in Equations 16, 17 and 18. For a z-z valent electrolyte,

$$\eta^d = -2A \sinh (zF\psi^o/2RT), \qquad \text{(Eq. 16)}$$

$$= -11.72\sqrt{c} \sinh 19.46\, z\psi^o \ \mu \text{ coul/cm}^2 \text{ at } 25°;$$

$$\eta_+^d = A(e^{-zF\psi^o/RT} - 1), \qquad \text{(Eq. 17)}$$

$$\eta_-^d = -A(e^{zF\psi^o/RT} - 1), \qquad \text{(Eq. 18)}$$

where $A = \left(\frac{DRTn_i}{2\pi}\right)^{\frac{1}{2}}$, ψ^o is in volts, and D is the dielectric constant of water (78.5 assumed).

In the above equations, c is the concentration in moles/litre, z is the valence of the ion including the sign, F is the Faraday constant, R is the gas constant, T is the temperature on the absolute scale, n_i is the number of ions/unit volume of the bulk solution, and ψ^o is the electrical potential of the outer Helmholtz plane relative to the interior of the solution. The term $zF\psi^o$ in Equation 16 represents the work done to transfer a gram-ion of charge zF from the interior of the solution to the outer Helmholtz plane. The potential ψ^o is closely related to the electrokinetic (ζ) potential and can be calculated from Equation 16 if η^d is known. η^d ($\pm$) and ψ^o ($\mp$) are opposite in sign. The calculations are more involved for z-z' electrolytes (49). The charge density, η^d, hardly reaches a value of 20 μ coul/cm^2 even with the highest attainable values of ψ^o. Russell (67) has tabulated the calculated values of the surface charge density, q, as a function of electrode potential and NaF concentration. The corresponding values for the differential capacity, C^d, of the diffuse double layer may also be calculated as:

$$C^d = \frac{zFA}{RT} \cosh (zF\psi^o/2RT), \qquad \text{(Eq. 19)}$$

$$= 228.5\ z\sqrt{c} \cosh 19.46\ z\psi^o\ \mu F/cm^2 \text{ at } 25°C.$$

Values of C^d, thus calculated for different values of C and ψ^o, are listed by Grahame (7). If C^o represents the differential capacity of the region between the surface and the outer Helmholtz plane which is occupied by solvent molecules, then, in the absence of specific adsorption,

$$\frac{1}{C} = \frac{1}{C^o} + \frac{1}{C^d}, \qquad \text{(Eq. 20)}$$

where C is the differential capacity of the entire double layer. Equations similar to 19 and 20 may also be written for the corresponding integral capacities K, K^o, and K^d. Grahame obtained values of C^o on Hg (in the absence of specific adsorption--NaF used) from Equation 20, where C was obtained experimentally, and C^d calculated from Equation 19. Assuming this value of C^o, C has been calculated for different values of the potential, E, and the concentration. These calculated values, as shown in Figures 3A and 3B, are in close agreement with the experimental values and lend confirmation for the validity of the assumptions made in the double-layer theories.

The Compact Double Layer

From the Stern theory of the compact layer, as modified by Grahame, it is also possible to calculate (7) the charge density, η^i, in the compact layer. For the simple case where only anions are specifically adsorbed and cations stay in the outer Helmholtz plane,

$$\eta^i = 2z_- Frn_i \exp\left\{-z_- F(\psi^i - \phi^i_-)/RT\right\}, \qquad \text{(Eq. 21)}$$

$$= 3.86\, cz_- \exp\left\{-38.92\, z_-(\psi^i - \phi^i_-)\right\} \quad \mu \text{ coul/cm}^2 \text{ at } 25°C,$$

if $r = 2\text{Å}$.

In the above equation, ψ^i is the electrical potential of the inner Helmholtz plane ($= E_z$, when $q = 0$ at e.c.m.), ϕ^i_- is defined as the adsorption potential of anions, r is the radius of the non-solvated ion, and the other terms have their usual meaning, as defined before. A value of about 25 μ coul/cm^2 for η^i represents about 25% of the surface coverage. A 100% surface coverage is never attained, although a maximum surface charge of 60 to 70 μ coul/cm^2 has been reported for solid surfaces. Both ψ^i and ϕ^i_- have been evaluated indirectly for the Hg-solution interface, so that η^i can be either calculated theoretically or computed from experimental results (7, 65, 66). A number of more complicated systems have also been worked out, where specific adsorption of anions (e.g. I^-) (65, 66, 68-70) and cations (53, 54, 60) (e.g. Tl^+) occurs separately or simultaneously (60). Bockris (59), Devanathan (71), Parsons (66, 72), Delahay (9, 54) and several others (73, 74) have also formulated isotherms for the specific adsorption of ions in the inner Helmholtz layer and have calculated the standard free energy (ΔG^o) for such adsorption. Wroblova et al. (75) found that the ΔG^o for the specific adsorption of anions on Hg decreases in the order $I^- > CNS^- > CN^- > BrO_3^- > ClO_4^- > ClO_3^- > Cl^-$.

The Potential of Zero Charge and Specific Adsorption

The p.z.c. is a characteristic electrochemical property of each metal and is related directly to the electronic work function of the metal (37, p. 65). Hence it varies with different crystal faces and also depends on the adsorbed solvent dipoles and the nature and the amount of the specifically adsorbed ions. As also seen from Equation 10, the e.c.m. and, hence, the p.z.c. shift towards increasingly positive or negative potentials, depending upon whether the cations or the anions are specifically adsorbed. When both anions and cations are specifically adsorbed, the sign of the shift of potential may be reversed as the concentration changes. Equation 11, when substituted for γ, may be written as:

$$\left(\frac{\partial E^{\pm}}{\partial \mu_i}\right)_q = -\left(\frac{\partial \Gamma}{\partial q^{\mp}}\right)_{\mu}, \qquad \text{(Eq. 22)}$$

where $d\mu_i = RT/nF \, d\ln a_i$ for the component i.

Esin and Markov showed that, in the presence of specific adsorption, the p.z.c. varies with the concentration of the electrolyte at a rate $>RT/nF$; and this is known as the Esin and Markov effect. A detailed discussion on this effect may be found elsewhere (8, 9, p. 53).

The Differential Capacity Curves and Nature of Adsorption

If there is no specific adsorption of ions at the p.z.c., the capacity curves, as shown in Figures 3 to 5, have V-shaped minima for low electrolyte concentrations (< 0.1M). Such minima are expected from theory, because of the low electrical potential, low charge densities, and hence

greater average distance of ions in the double layer at the p.z.c. On the slightly anodic side (q^+) of the p.z.c., the V-shaped curves show a characteristic "hump", which is followed by a steep rise in C at higher anodic potentials. While this rapid increase in C with positive potentials is attributed (76) to increasing specific adsorption of anions (in the inner Helmholtz layer), the origin of the "hump" has been a subject of considerable controversy (8). According to Macdonald et al. (57), the dielectric constant of the medium, and hence C, begins to decrease as the highly polarizable anions begin to be adsorbed in the compact layer, which then reaches a saturation limit. The hump is thus caused by the two opposing effects of specific adsorption of anions and dielectric saturation. For intense specific adsorption, e.g. I^- on Hg (Figure 4), no minimum at the p.z.c. and no hump are found, because of the major effect of specific adsorption. The hump is also found to disappear (77) with increasing temperature (>25°C). The subject has been discussed further, with alternative suggestions, by a number of authors (8, 9, 50, 58, 59, 77, 78).

In the cathodic region (q^-) of the C curves, the capacity (Figures 3 to 5) is found to be almost independent of the nature of the cations as well as their concentration (except for Tl^+, Cs^+, tetraalkylammonium, and polyvalent cations), although the cations differ considerably in their ionic sizes. The differential capacity reaches a minimum of about 16 $\mu F/cm^2$ ($q \sim 13\ \mu c/cm^2$) at a potential of about -1.15 volts relative to a normal calomel electrode, or -0.7 volt relative to the potential of e.c.m. The following explanation for this behaviour has been proposed by several

workers (8, 76). In the absence of specific adsorption, the compact layer is occupied by water (solvent) molecules which are subjected to a high electric-field strength ($d\psi/dx \sim 10^8$ volts/cm) and hence undergo dielectric saturation. The dielectric constant (37, p. 29; 59) thus varies from about 7 in the compact layer to about 30-40 in the vicinity of the outer Helmholtz plane, and is 78.5 in the diffuse double-layer. As most of the monovalent cations stay outside the compact layer, they exert negligible influence on C. Hence, C is effectively controlled by the highly polarized solvent molecules in the compact layer and is almost independent of the nature, as well as the concentration, of cations. A slight increase in C at higher positive potentials may be due to a slight tendency for cations to enter the compact layer. The above behaviour, of course, does not apply for those cations which show a profound tendency for specific adsorption on solid surfaces. Water and other solvent molecules play a significant role at the interface. The subject of the polarizability of water and the adsorption of organic compounds on Hg surfaces has been reviewed elsewhere (8, 39).

IV. SOLID METAL-SOLUTION INTERFACE

The interfacial tension at the metal-solution interface can be studied only indirectly by studying properties such as contact angles and friction coefficients (79). These studies are only qualitative, because of uncertainties arising from factors such as interfacial tension between the solid-gas phase, hysteresis, surface roughness, surface heterogeneity, etc. In recent work

on polarized surfaces of Ge, Sparnaay (80) has observed, qualitatively, the variation of contact angles with the applied potential at the Ge-solution interface.

Direct measurements of the capacity of the double layer on Pt, Pb, Zn, Tl, Cd, Sn, Cn, Ag and other metals have provided (8, 43, 45, 81-85) valuable information on the nature of adsorption on these metals. The most recent work is on Ag (45, 81) and Cd (82) in various electrolyte solutions. In general, the behaviour is similar to that of Hg surfaces.

V. THE SEMICONDUCTOR-ELECTROLYTE INTERFACE

When a metal-electrolyte interface is polarized electrically, no appreciable drop in potential and no excess space charge occur inside the metallic phase itself, because of the high concentration of free carriers (electrons) present in metals. The dielectric constant, as well as the capacity of the metallic phase, is considered to be infinite (7, p. 483). Hence, for a given electrode potential, the double-layer characteristics of a metal-electrolyte interface are determined entirely by the nature and concentration of the electrolyte. This is, however, not the case for a semiconductor-electrolyte interface where a substantial drop in potential and a space-charge region can occur within the semiconductor phase close to the surface ($\sim 10^{-4}$ cm for Ge).

This difference between metals and semiconductors arises because of the low concentration of free carriers (electrons and holes) present in semiconductors, $\approx 2.5 \times 10^{13}/cm^3$ for Ge ($\approx 4 \times 10^{-8}$ moles/litre, which is of the same order of magnitude as the number of moles/litre of H^+ and OH^- in water). The dielectric constant of most semiconductors is also low, about 10-20. Hence, unlike a metal, a semiconductor phase can support an extensive space charge. Several reviews (86-94) are available on the theory and on the experimental methods of investigating semiconductor surfaces, their space charge and the semiconductor-electrolyte interface. The space charge (or charge excess Γ) in the semiconductor phase is induced by the presence of what are known as surface states on the semiconductor. These are the surface-localized electron-energy levels, that are different from the energy levels in the bulk of the semiconductor. The surface states can be induced in one or more of the following ways:

a) by the presence of the "dangling bonds" on an uncontaminated surface as a result of lattice terminations (Tamm states $\approx 10^{15}/cm^2$);

b) lattice imperfections, chemical inhomogeneity, geometrical irregularities, etc;

c) adsorbed impurities;

d) electrical polarization;

e) contact with another phase with a different work function.

There can be several types of space-charge regions, depending on whether the semiconductor is n-type or p-type and also whether there is a surface excess or depletion of charge carriers. In what is known as the "inverse layer", for example, an n-type or p-type semiconductor may have a p-type or n-type surface respectively. The presence of a space charge,

therefore, can change the nature and magnitude of adsorption of ions and molecules from solution. Thus, adsorption at the liquid-semiconductor interface could be much different from what is expected from the bulk properties of the solid, depending on the nature of space charge. The distribution of charge in the space-charge region of the semiconductor phase is similar to the distribution of ions in the diffuse double layer of the solution phase. Hence, the total measured differential capacity (C_t) of the semiconductor-electrolyte interface (47, 95) includes the capacities of the space-charge region ($C_{s.c.}$), the Helmholtz region (C_H), and the diffuse double-layer region (C_d), so that

$$\frac{1}{C_t} = \frac{1}{C_{s.c.}} + \frac{1}{C_H} + \frac{1}{C_d} . \qquad \text{(Eq. 23)}$$

In concentrated solutions, C_d can be ignored and, by measuring C_t, the space-charge layer and the mode of adsorption at the liquid-solid interface can be investigated. In addition to measuring $C_{s.c.}$, several other techniques have been used to investigate the space-charge region. The details may be found elsewhere (8, p. 670; 43, 45, 47, 81-85, 95). Since several of the naturally occurring oxides (e.g. magnetite) and sulphides (e.g. galena) are semiconductors (47, 96), a knowledge of their surface properties is essential for a better understanding of mineral dressing processes. Mular (97) has recently considered several aspects of semiconductor surfaces that could play a major role in mineral dressing.

VI. REVERSIBLE INTERFACES

Thermodynamics

A detailed treatment of the thermodynamics of reversible interfaces, and of other fundamental aspects of the double layer, may be found in several publications (11, 19-24, 28, 29, 98-104). When sparingly soluble compounds, such as AgCl (31), AgI (19-21, 99), Ag_2S (28, 29, 32, 33, 100) or metal oxides (22-26, 30, 34, 101-108), are suspended in solutions of an indifferent electrolyte (e.g. KNO_3), equilibrium is soon established between the surfaces and the potential-determining ions, e.g., Ag^+ and I^- for AgI, or H^+ and OH^- for oxides. For the present discussion, the equilibria may be represented as:

$$MX_s \mid M^+ \underset{X^-}{\overset{M^+}{\rightleftharpoons}} \mid MX_s \mid \underset{M^+}{\overset{X^-}{\rightleftharpoons}} X^- \mid MX_s$$

$$q^+ \xleftarrow{E_r^+} \left| \begin{array}{l} \text{z.p.c.} \\ q = 0 \\ E_r = 0 \end{array} \right| \xrightarrow{E_r^-} q^-,$$

where MX is a solid uni-univalent compound (e.g. AgI) in equilibrium with ions M^+ and X^-, and "s" refers to the solid phase. $E_r^{\pm *}$ refers to the cell potential relative to the potential of zero charge, say E_z, at which the potential of the outer Helmholtz plane (ψ^o), relative to the interior of solution,

---

*$E_r^{\pm}$, thus, would correspond to ψ^r, the rational potential at the reversible Hg-solution interface, as used by Grahame (7).

may be taken as zero. Hence $E_r^{\pm}$ may also be taken, in the absence of specific adsorption, as the potential across the double layer. If E_z and $a_{M_o^+}$ refer to the cell potential and the activity of M^+, respectively, at the z.p.c., and E is the cell potential at any other value of a_{M^+}, then E_r is given from the Nernst equation as:

$$E_r = E - E_z = \frac{2.303RT}{F} \log \frac{a_{M^+}}{a_{M_o^+}} \qquad \text{(Eq. 24)}$$

$$= -0.05914\,(pM - pM_o), \text{ at } 25°C.$$

When Gibbs' adsorption equation is applied to the above equilibria, the change in interfacial energy, γ, in the presence of an indifferent electrolyte such as KNO_3, is:

$$d\gamma = -\left(\Gamma_{M^+} d\bar{\mu}_{M^+}\right) - \left(\Gamma_{X^-} d\bar{\mu}_{X^-}\right) - \left(\Gamma_{K^+} d\bar{\mu}_{K^+}\right) - \left(\Gamma_{NO_3^-} d\bar{\mu}_{NO_3^-}\right) \qquad \text{(Eq. 25)}$$

The individual ionic activity coefficients that are used in the form of chemical potentials, as above, are usually replaced at a final stage of calculation by the mean activity coefficients (Equation 9). For constant ionic strength, and also if K^+ and NO_3^- are not specifically adsorbed, the last two terms in Equation 25 are zero, and the above equation may be simplified to

$$d\gamma = -F\left[\Gamma_{M^+} - \Gamma_{X^-}\right] dE^{\pm}_{\mu_{KNO_3}} . \qquad \text{(Eq. 26)}$$

Using Equation 4 as the definition of the surface charge density, q,

$$d\gamma = -(q^{\pm}\, dE^{\pm})_{\mu_{KNO_3}} \quad \text{or} \quad \left(\frac{d\gamma}{dE^{\pm}}\right)_{\mu_{KNO_3}} = -q^{\pm} . \qquad \text{(Eq. 27)}$$

The charge density, q, is positive, zero or negative in sign, depending on whether $\Gamma_{M^+} >$, =, or $< \Gamma_{X^-}$. The differential capacity, C, of the double layer is given by:

$$-\left(\frac{d^2\gamma}{dE^2}\right)_{\mu_{KNO_3}} = \left(\frac{dq}{dE}\right)_{\mu_{KNO_3}} = C. \qquad \text{(Eq. 28)}$$

If γ_o (absolute value not known) represents the interfacial energy at the z.p.c., then at any other cell potential the total change in the interfacial energy, with respect to γ_o, may be obtained by integration of the more general form of Equation 27, so that

$$\gamma - \gamma_o = \left(\int_{E_z}^{E_r} q^{\pm} dE^{\pm}\right)_{\mu_{KNO_3} = -\infty} - \left(\int_{-\infty}^{\mu} \Gamma_{K^+NO_3^-} \, d\mu_{KNO_3}\right)_E . \qquad \text{(Eq. 29)}$$

If the chemisorption of K^+ and NO_3^- is negligible, the last term in the above equation may be omitted. The curves of $(\gamma - \gamma_o)$ against E_r, obtained by the integration of q-E plots, will be similar in character to the electrocapillary curves. At constant cell potential, any change in the interfacial energy is due to the effect of increasing the ionic strength of the solution on the adsorption, if any, of K^+ or NO_3^- on the surface; so that, from Equation 25,

$$d\gamma = -\Gamma_{K^+} \, d\mu_{KNO_3} \text{ in the } q^- \text{ region,} \qquad \text{(Eq. 30)}$$

where $\Gamma_{NO_3^-} \simeq 0$, and

$$d\gamma = -\Gamma_{NO_3^-} \, d\mu_{KNO_3} \text{ in the } q^+ \text{ region,} \qquad \text{(Eq. 31)}$$

where $\Gamma_{K^+} \simeq 0$.

The above equations are the same as those developed for the polarizable Hg-solution interface. Equations 10, 11 and 12, describing the variation of the interfacial energy, and of the surface charge, on Hg with the chemical potential or activity of the electrolyte in solution, at constant electrode potentials, are also applicable to the present system. Hence, by studying the equilibrium distribution of the potential-determining ions at the interface in the presence of an indifferent electrolyte, at a constant ionic strength, and by knowing the specific surface areas of the powders, information can be obtained on all the double-layer characteristics. By comparing the experimental values with theory, conclusions can also be drawn on the nature of adsorption at the interface and on the chemical composition of the surface.

The AgI and Ag_2S Systems

Silver iodide, as a colloidal suspension in solutions of KNO_3, $NaNO_3$ and $NaClO_4$, has been studied exhaustively by several workers (19-21, 99). The adsorption of Ag^+ and I^- on AgI suspensions was measured by potentiometric titrations. The surface area was not known precisely and was derived by assuming a theoretical value of 6 $\mu F/cm^2$ for the differential capacity of the double layer in 0.001 M solutions of the uni-univalent salt, in the absence of specific adsorption. In all this work, the material was left to equilibrate with solutions for several hours, and this aspect of slow equilibrium has been discussed to some extent in a recent publication (21). As is seen from Figures 7 and 8, the surface charge densities and the

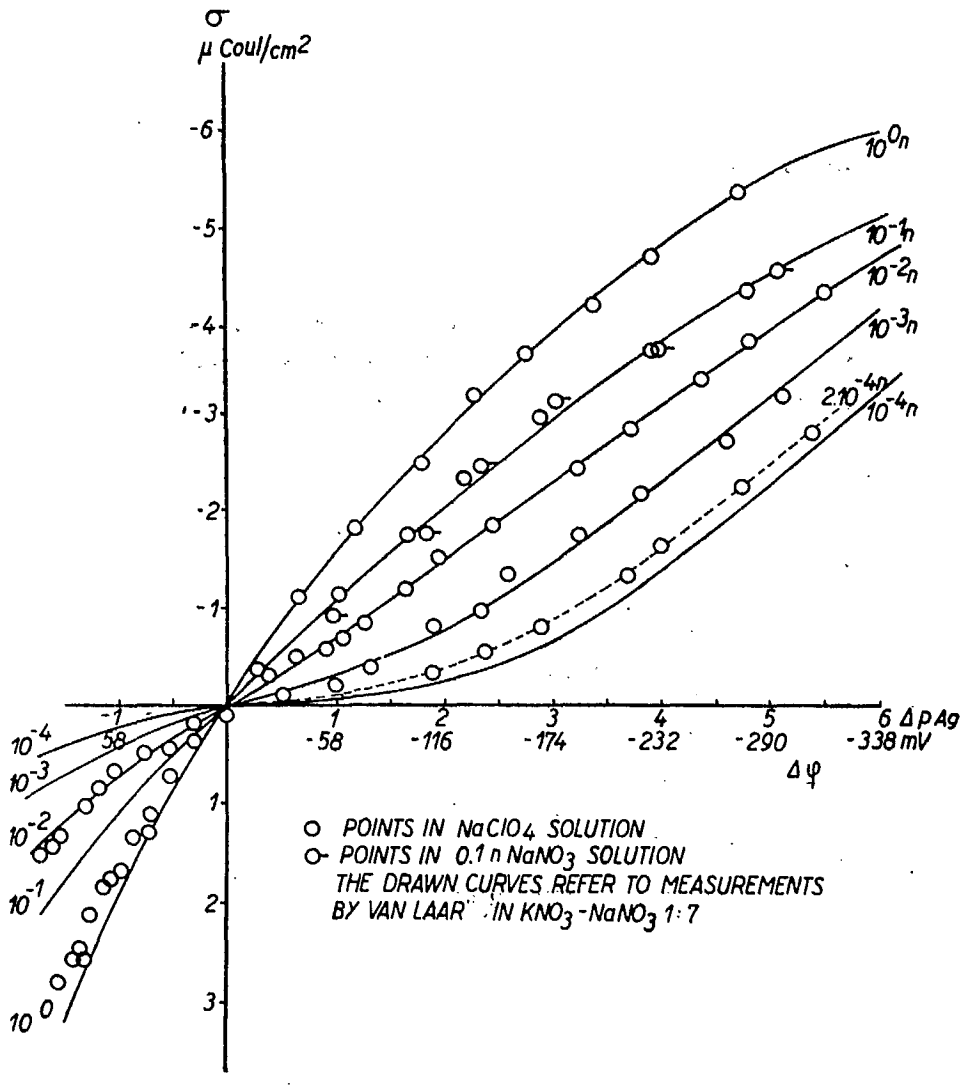

Figure 7. Adsorption of Ag^+ and I^- on AgI surfaces plotted against the potential $\Delta\phi$ relative to the z.p.c. (After Mackor, Ref. 19, p. 774)

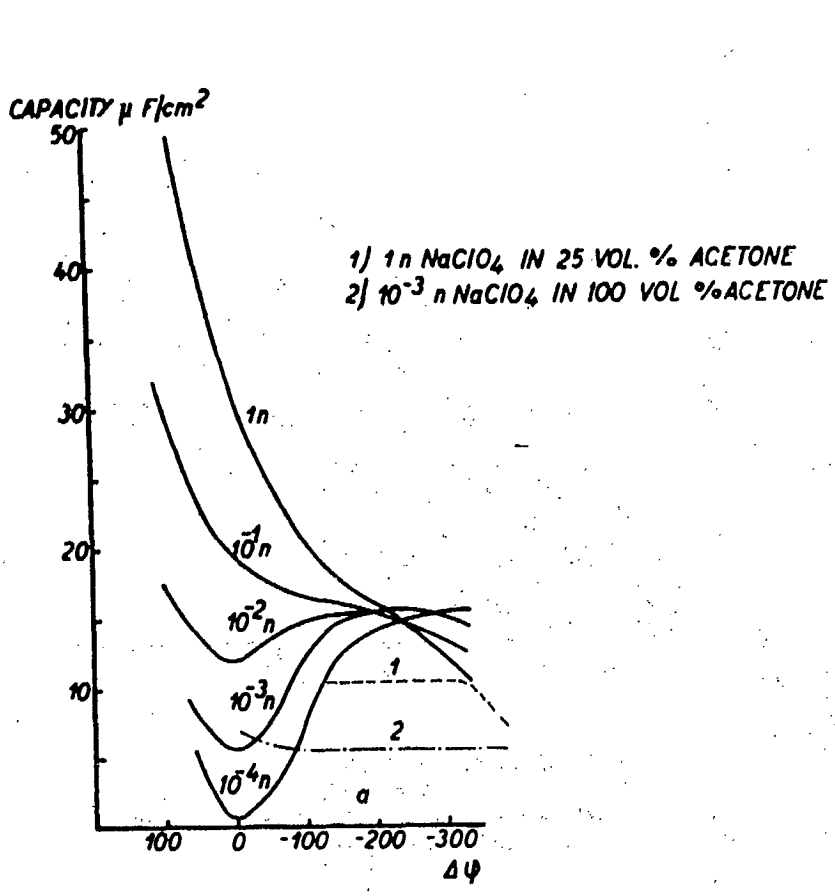

Figure 8. Differential capacity of the double layer on AgI in $NaClO_4$ solutions, plotted against the potential $\Delta\phi$ relative to the z.p.c. (After Mackor, Ref. 19, p. 775)

differential capacity curves are very similar to the respective plots for the Hg-solution interface. The z.p.c. of AgI was found to occur at pI = 10.56 ($C_{Ag} \approx 2.8 \times 10^{-6}$ moles/litre). The variation in the shape of the capacity curves also has the same significance as in the case of the polarizable Hg-solution interface. Very minor differences between the two systems have been discussed by Lyklema and Overbeek (99). These authors have also inferred that the influence of cations and anions on the capacity curves of AgI follows the lyotropic order $NH_4^+ > RB^+ > K^+ > Na^+ > Li^+$ on cathodic surfaces and the order $NO_3^- > ClO_4^- > F^-$ on anodic surfaces. The influence of polyvalent cations such as Th^{4+}, La^{3+}, Ca^{2+}, etc., on the capacity curves of AgI has also been investigated.

Bijsterbosch and Lyklema (21) have studied the influence of urea and six different alcohols on the surface-charge densities, and on the shifts in the z.p.c., of AgI in KNO_3 solutions. From the direction of the shifts in the z.p.c., it was concluded that the alcohols were adsorbed with their hydrophobic part facing the AgI surface. Using Equation 32,

$$\frac{\theta}{1-\theta} = C_A \exp\left[-\frac{\Delta G^o}{RT}\right], \qquad \text{(Eq. 32)}$$

where θ is the fractional surface coverage by alcohols of concentration C_A, the Gibbs' molar free energy (ΔG^o) for the adsorption process was calculated to be -2 to -3 kcal/mole. Levine and Letijevic (11) have taken into account the discreteness-of-charge effect and the size of the counter ions, to obtain isotherms for the specific adsorption of counter ions on AgI.

The Ag_2S-solution interface has been investigated by De Bruyn and coworkers (28, 29, 100) in the same way as the AgI system. The potential-determining ions were found to be Ag^+ and $S^=$ whilst, between pH 5 to 9, H^+ and OH^- showed no specific interaction with Ag_2S. In solutions of sodium acetate and sodium metaborate, the z.p.c. was found to occur at pAg 10.2. In general, the behaviour of the Ag_2S system was very similar to that of AgI and was in reasonable agreement with theories of the double layer. Iwasaki and De Bruyn (29) have studied the shift in the z.p.c. of Ag_2S on the adsorption of dodecylammonium acetate (D.D.A.) on Ag_2S. The chemisorption of the dodecylammonium ions ($D.A.^+$) on Ag_2S, as expected from theory (cf. Equation 10), resulted in shifting the z.p.c. to a more positive potential (i.e., to a lesser pAg). These shifts in the z.p.c., as a function of the concentration of D.D.A., are shown in Figure 9. The slope of these plots (cf. Equation 22) was found to be independent of the surface charge density, which is in qualitative agreement with the behaviour of the polarized Hg-solution interface. The adsorption of D.D.A. itself was found to obey the Freundlich isotherm $\Gamma_i = KC_i^n$, where C_i is the concentration of ions or molecules, i, in solution; K is a constant; and n is related to adsorption energy. The decrease in the interfacial tension, and the shifts of the maxima of the γ-γ_o curves, due to adsorption of D.D.A. on Ag_2S, may also be seen in Figure 10. As expected from theory (Equation 12), the slopes

$$\left(\frac{\partial q}{\partial \mu_{D.D.A.}}\right)_E \quad \text{and} \quad \left(\frac{\partial \Gamma_{D.A.^+}}{\partial E}\right)_{\mu_{D.A.A.}}$$

were also found to be equal ($\sim$(5 to 8) x 10^{-14} moles/cm^2 mV).

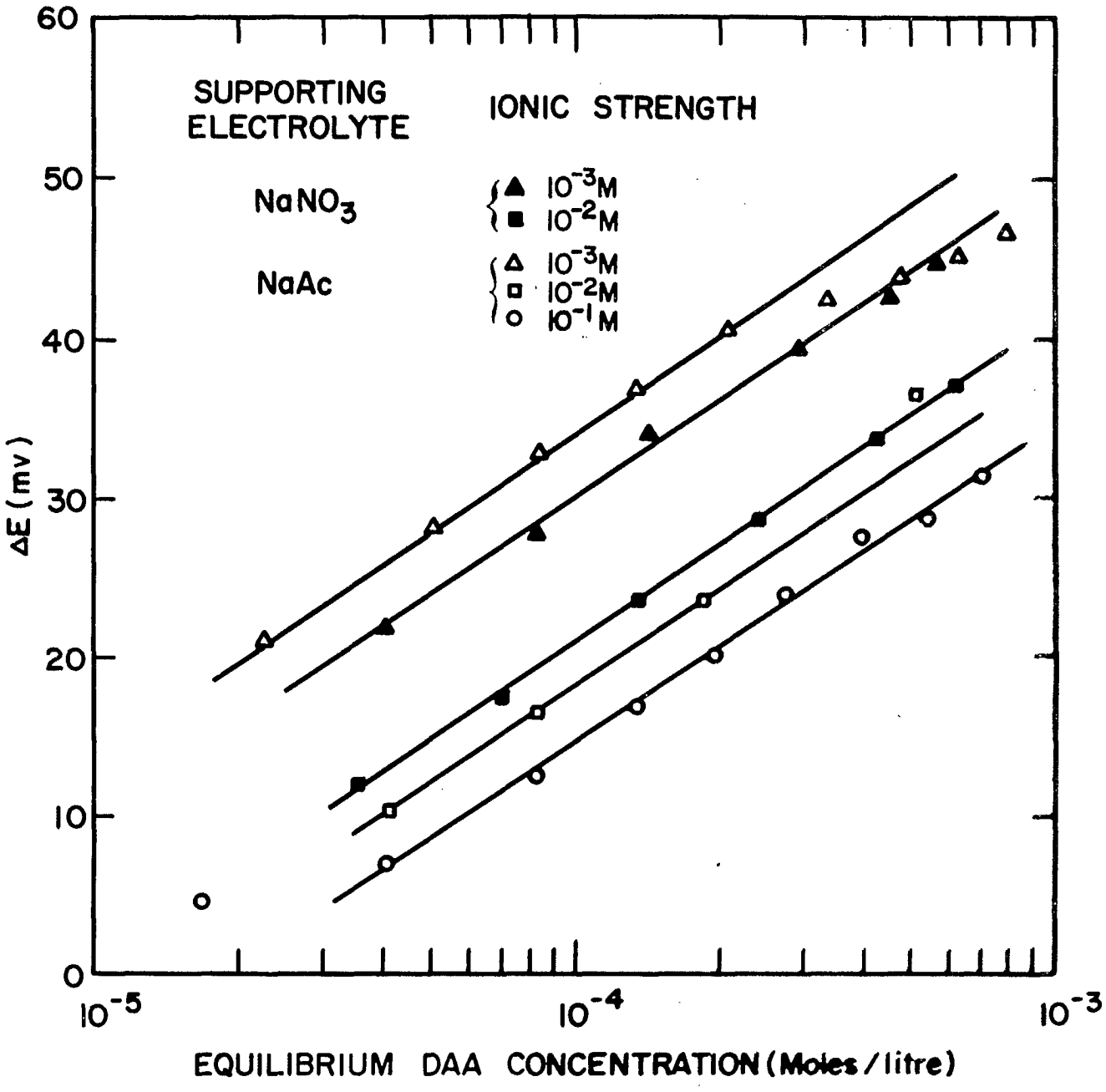

Figure 9. Shifts in Z.P.C. as a function of DAA concentration in solution.
(After Iwasaki and De Bruyn, Ref. 100, p.306)

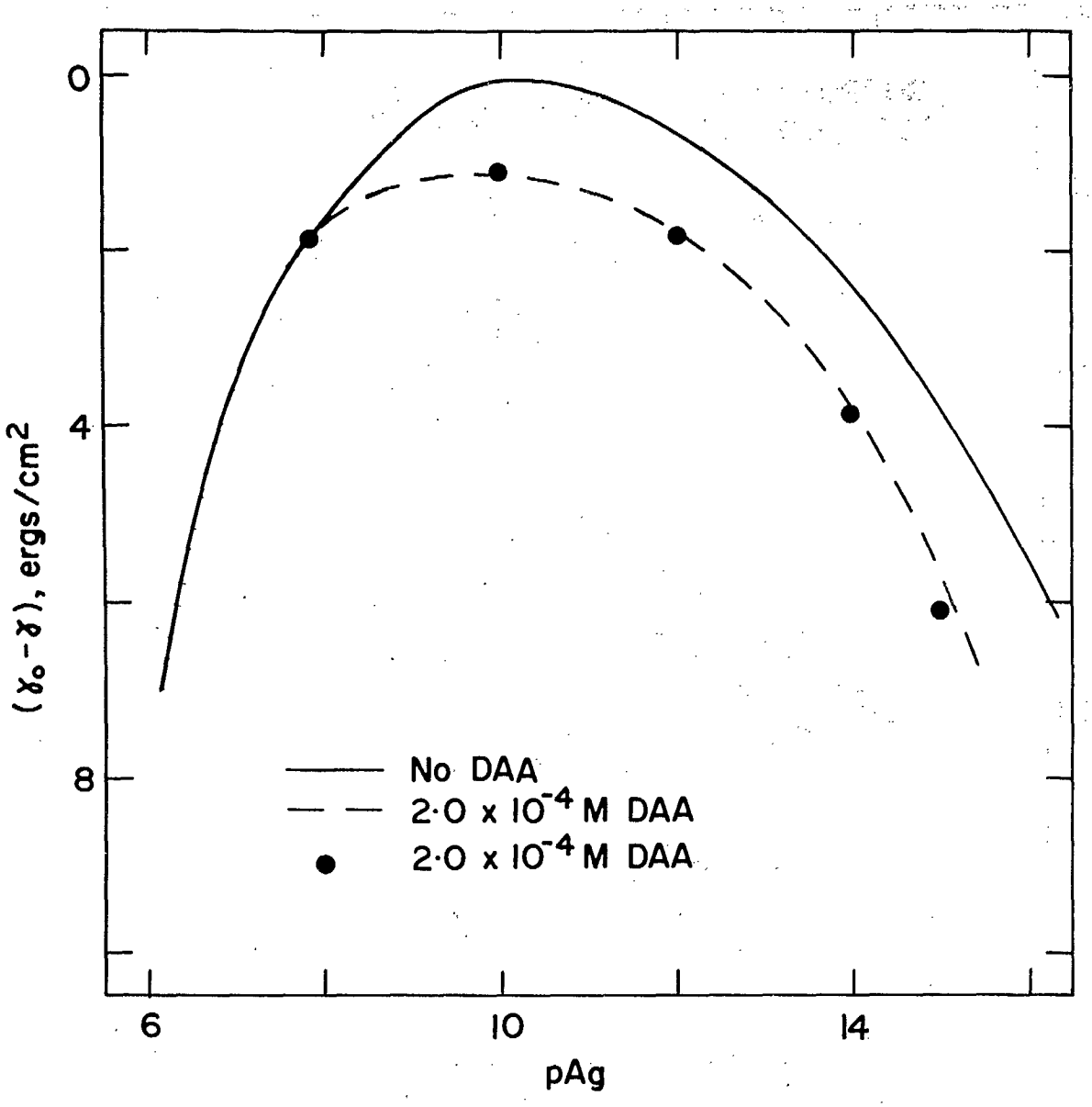

Figure 10. Lowering of interfacial tension at Ag_2S-solution interface as a function of pAg in presence and absence of DAA. Supporting electrolyte, 0·01M sodium acetate. The dotted curve and filled circles represent calculated values (cf. Eq.29). (After Iwasaki and De Bruyn, Ref. 100, p.309)

The Oxide-Solution Interface

The double layer at the oxide-solution interface has been investigated by studying the equilibrium distribution of the potential-determining ions (H^+ and OH^-) in the presence of an indifferent electrolyte. Several oxides -- α-Fe_2O_3 (22, 24, 102) in precipitate form and as specular hematite (105, 107), SiO_2 (quartz) (23), ZrO_2 (23, 105), ThO_2 (23), TiO_2 (rutile) (106), Al_2O_3 (25), and others (101, 108) -- have been investigated by several workers from different points of view. In most of the earlier work, the oxides, in a finely divided state, were allowed to equilibrate with solutions for several hours. Under these conditions, the z.p.c. of oxides was found (22, 25, 105, 106) to occur at the same pH as the isoelectric point (i.e.p.) of the solutions, i.e. where the activities of the dissolved, positive and negative metal complexes (from oxides) are equal. Parks and De Bruyn (22) have also demonstrated that a qualitative similarity exists between the charge density curves and the differential capacity curves of oxides, with those of AgI and Ag_2S. Later work (23, 24), using absolute values of surface areas, has shown that the experimental values of charge densities and differential capacities of the double layer, obtained under slow conditions of equilibrium (22, 24, 105, 106), show wide discrepancies with theory by several orders of magnitude. The primary equilibrium between the oxide surfaces and H^+ and OH^- has been shown to be attained rapidly (23), which was also pointed out by Verwey (27) as early as 1941. In recent work (23), using coarse, crystalline oxides of low, known surface areas,

the charge densities and differential capacities of the double layer, obtained under fast equilibrium conditions (2-6 minutes), were shown to agree quantitatively with the theoretically expected values. The slow changes in pH_s of the oxide-solution systems, that could last for days and weeks, have been attributed (23, 24) to several possible effects other than the primary surface effects. It was also suggested (23), from an analysis of the differential capacity curves, that O^{2-} ions play a special role at the interface which may lead to specific adsorption of cations at high, negative-surface-charge densities.

PART B. PRESENT STUDIES

VII. THE SCOPE OF THE PRESENT WORK ON THE OXIDE-SOLUTION INTERFACE

The present studies of the double layer on specular hematite, magnetite, cassiterite, rutile, alumina, zirconia and thoria, in different electrolyte solutions, is an extension of previous work on quartz, zirconia and thoria (23). The measurements are made on coarse, crystalline samples of the oxides. It is assumed that the primary interfacial equilibrium between the surface and H^+, OH^- and the electrolyte ions (NO_3^-, Cl^-, K^+, etc.) is attained rapidly (2 to 6 minutes). The work is based on the following considerations. There are about 1×10^{-9} moles of monovalent charge available per square centimetre of any ionic solid surface. For a total surface area of about 2000 cm^2/10 ml solution, as used in this work, there are about 2×10^{-6} moles of univalent surface charge available per 10 ml of solution. If the amount of the material in solution is kept below 10^{-6} moles/litre (i.e., 10^{-8} moles/10 ml), the secondary effects arising from the solubility of the material will be less than 1% of the total pH_s effects observed from the primary surface phenomenon that occurs in the first few minutes. The experimental conditions and the nature of material (coarse and crystalline) were chosen in this work so that the above conditions were satisfied. The validity of the above assumptions can be checked by

comparing the experimental values of the charge densities and the differential capacities of the double layer with the theoretical values, and for this purpose, materials of known surface areas have been used. In order to keep the solubility effects sufficiently low in the present work, fresh samples of oxides and solutions were used for each measurement and, also, corrections were made for the effects of solubility and slime formation. By comparing the experimental results obtained on the double-layer characteristics with theory, inferences can also be drawn as to the nature of ion-surface interactions. Such information will be useful in understanding several fundamental problems concerning mineral flotation, agglomeration, and similar industrial processes. This work is also expected to throw some light on the mechanism of the oxide electrodes. The oxide electrodes (30, 34, 35) have been known for a long time as 'electrodes of the second kind'(30). They are reversible to H^+ and obey the Nernst equation with respect to a_{H^+} within a limited range of pH, depending on the nature of the anions present in solution.

By comparing the behaviour of different oxides, it is also proposed to formulate theories of the general phenomena that occur at the oxide-solution interface.

VIII. EXPERIMENTAL

Materials

Naturally occurring samples of specular hematite and magnetite were supplied respectively by the Quebec Cartier Mining Co. and the Geological Survey of Canada. These samples were crushed and screened. A middle fraction of hematite was collected on a high-intensity Jones wet magnetic separator, rejecting the highly magnetic and non-magnetic portions. In a similar magnetic separation, the most magnetic portion was collected for magnetite. The material in the -150+200-mesh size (~0.1 mm) was selected for further work.

Concentrates of naturally occurring cassiterite were supplied by the Consolidated Mining and Smelting Co. of Trail, British Columbia. Naturally occurring rutile (Mexican origin) was obtained from the Ward's Natural Science Est., New York (U.S.A.). Rutile in the -100+ 200 mesh size was passed through a Jones wet magnetic separator and the non-magnetic material was collected for further work. Some quartz that was present in the rutile was removed by a heavy liquid separation, using tetrabromoethane. The final samples of rutile and cassiterite were leached with warm ethyl alcohol and subsequently washed with distilled water to remove the alcohol.

Samples of α-Al_2O_3 (produced by calcination of $Al_2O_3.3H_2O$) were supplied by the Aluminum Company of Canada. The material, in -100+ 150

mesh size, consisted of agglomerates of microcrystalline particles. Some work was also carried out on ZrO_2 and ThO_2. Details of these oxide samples have been given earlier (23). The oxides were finally leached with hot 10% HNO_3, to dissolve any soluble material from the surface and also to liberate the slimes that usually adhere to the material. The resultant material was washed free of excess acid, and deslimed. For desliming, the material was packed in a long glass tube with a fritted glass bottom and elutriated with a rising current of water. Then it was stored in degassed conductivity water which was replaced frequently. From spectrographic analysis, hematite, magnetite and rutile were found to be at least 99% pure, and cassiterite and alumina were 99.7% pure. The major impurity was SiO_2, the interference of which, on the basis of the previous work (23), is assumed to be negligible. The trace impurities were oxides of Mg, Cu, Al, Ca, etc. Many of the soluble impurities may, however, have been leached out of the surface in the acid treatment. On microscopic examination, all oxides except Al_2O_3 (microcrystalline) were found to be coarse and crystalline. Specular hematite possessed several smooth lustrous planes which, when uncontaminated, showed some degree of native hydrophobicity around the neutral pH_s, as tested by a flotation method.

Hematite and α-Al_2O_3 have similar crystal structures (109) which can be looked upon either as rhombohedral or hexagonal in nature. In α-Al_2O_3 (109, p. 96), each Al is surrounded by six oxygen atoms arranged octahedrally. Specular hematite was weakly magnetic, the co-ordination number of Fe^{3+} being also 6. Magnetite ($Fe^{2+}Fe_2^{3+}O_4$), which belongs to

the spinel group of oxides (109, p. 102), is hexoctahedral where Fe^{2+} and Fe^{3+} are in 4 and 6 co-ordination respectively; it is highly magnetic and a semiconductor.

Both rutile (TiO_2) and cassiterite (SnO_2) (109, p. 107) have a similar tetragonal crystal structure (109, p. 107). Each metal atom is surrounded by six oxygen atoms in an octahedron, where each oxygen atom, in turn, is surrounded by three metal atoms at the corners of an almost equilateral triangle.

Method

The oxide samples were given a blank stirring treatment in water under the same conditions as used in the experiment. The resultant samples were then used for surface area determinations, so that any increase in surface area due to stirring is also taken into account.

(a) Surface Area Measurements

The specific surface areas were determined by the krypton gas adsorption method, using the B.E.T. equation,

$$\frac{P}{v(P_o-P)} = \frac{1}{V_m C} + \frac{C-1}{V_m C}\ \frac{P}{P_o}\ , \qquad \text{(Eq. 33)}$$

where v is the volume (in cc S.T.P./g material) of the gas adsorbed at the equilibrium pressure P, V_m is the volume (cc S.T.P./g material) of the gas required to cover the entire surface with a monolayer of adsorbed gas (at liquid nitrogen temp., -195.8°C), P_o is the saturation vapour-pressure of liquid krypton, and C is a constant related to the net heat of adsorption.

Most of the gas-solid systems give an S-shaped isotherm on plotting P against V. For such systems, according to the B.E.T. equation, a plot of $\frac{P}{v(P_o-P)}$ against P/P_o is linear within certain ranges of the relative pressure, P/P_o, of 0.05-0.35 for nitrogen and 0.07-0.20 for krypton as adsorbates. Monolayer adsorption usually occurs in this relative pressure range. From the slope ($= \frac{C-1}{V_m C}$) and the intercept ($= \frac{1}{V_m C}$) of the linear portion of the B.E.T. plot, it can be shown that

$$V_m = \frac{1}{\text{Slope} + \text{Intercept}} \quad .$$

and, hence, the specific surface area, S, is given by

$$S = \frac{V_m \times N \times 10^{-16} \times \sigma_{Kr}}{22400} \quad , \qquad \text{(Eq. 34)}$$

where N is Avogadro's number and σ_{Kr} is the cross-sectional area of a krypton molecule in the condensed phase (19.5 Å^2 used). Theoretical details of the method may be found elsewhere (110-114). The apparatus used is as shown in Figure 11. A thermistor gauge (Figure 12) was used to measure the gas pressures. The thermistor gauge itself was calibrated, using a low-sensitivity McLeod gauge. Helium was used for such calibration purposes and also for dead-space determination. The experimental details and apparatus have been described in detail (115). Some of the B.E.T. plots obtained experimentally are shown in Figure 13. The specific surface areas were: 800 cm^2/g for magnetite, 451 and 308 cm^2/g for two samples of specular hematite, 420 cm^2/g for SnO_2, 2300 cm^2/g for TiO_2, and 4414 cm^2/g for Al_2O_3.

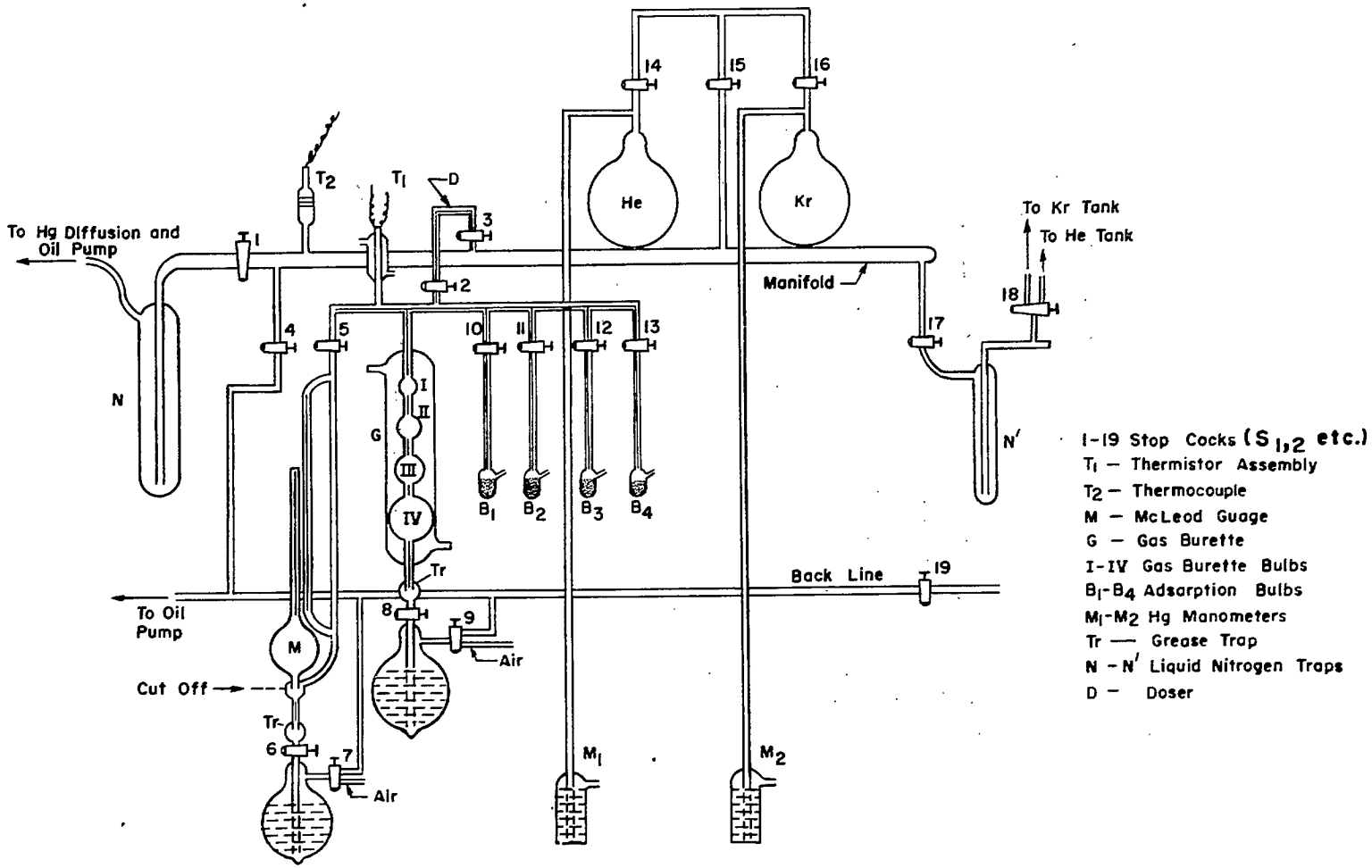

Figure 11. Apparatus for the determination of surface areas of powders by Kr gas adsorption.

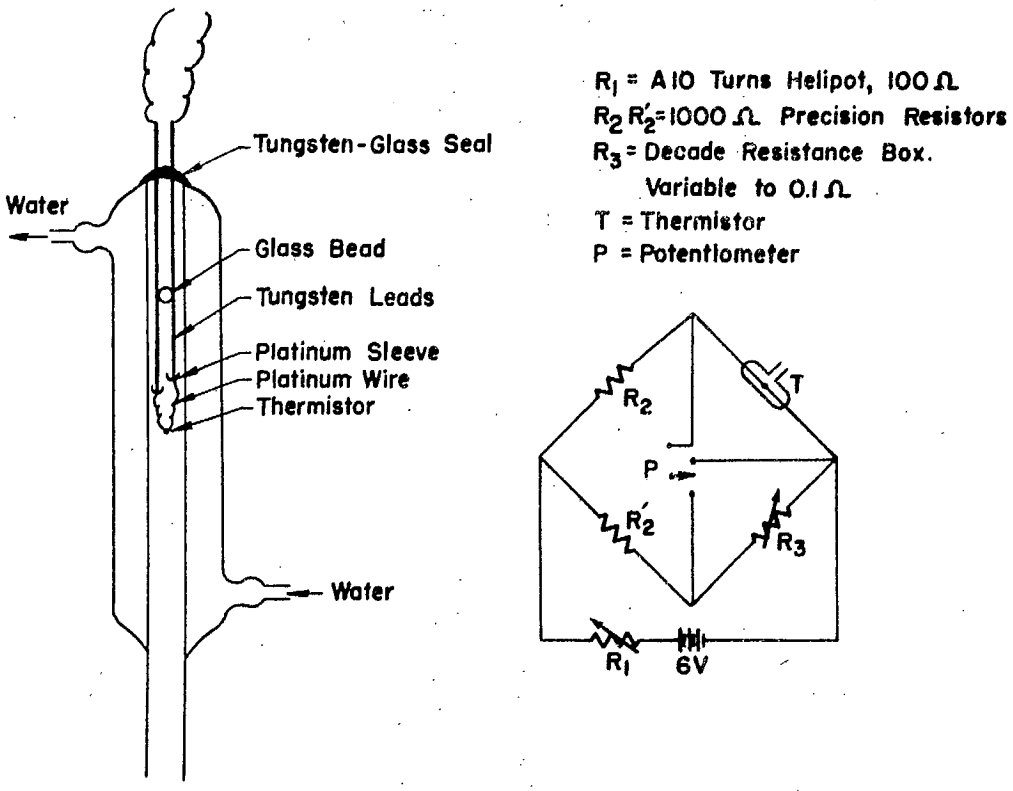

Figure 12. Thermistor gauge and electrical circuit used in measuring gas pressure.

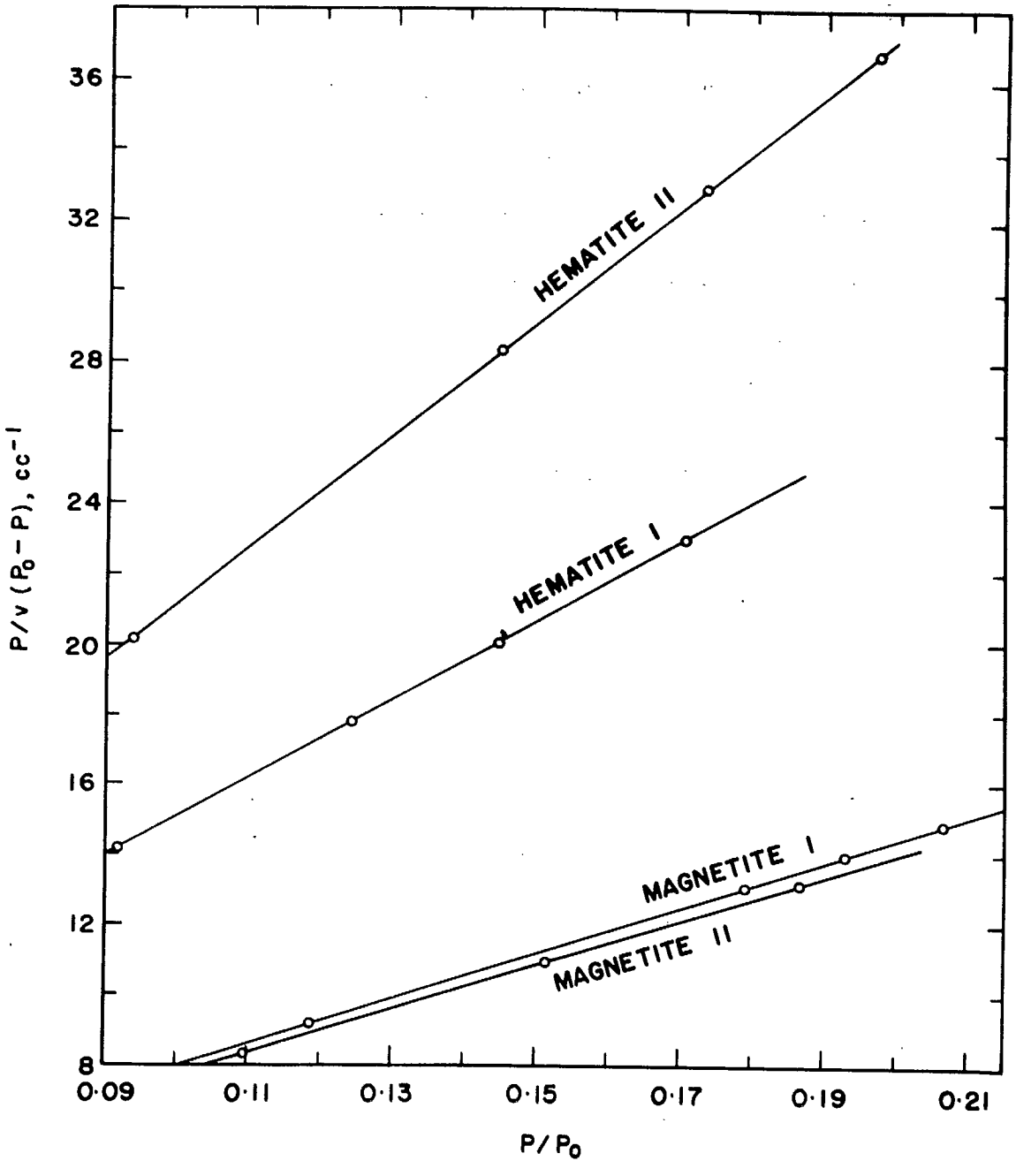

Figure 13. The B.E.T. plots for Kr gas adsorption on some mineral powders. (After Ahmed, Ref. 115, p. 15)

(b) Adsorption Studies

A Beckman Research pH Meter that could be read with a relative accuracy of 0.002 pH unit was enclosed in a constant-humidity (~50%) box, leaving the electrodes outside. The adsorption studies were carried out in a Pyrex glass tube (2-1/8 in. x 1-1/8 in.) provided with an outer jacket for the circulation of water at 25 $\pm$ 0.05°C. An inert atmosphere was maintained above the solutions by passing argon through two side vents fitted to the main chamber, which was also closed to the air by a flexible covering. Argon was purified to remove traces of CO_2 and other acidic impurities. A Beckman micro glass electrode and a KCl-saturated calomel electrode were used, the latter being separated from the experimental solution by a saturated KNO_3 solution bridge through a fibre junction. The glass electrode was calibrated against Beckman buffers in the pH_s (116) range 3.0 to 11.0. For the $NaClO_4$ solutions, a solution of KNO_3 and $NaNO_3$ in the molar ratio of 1:7 was used in the bridge, after the work of Mackor (19, p. 773). The liquid-junction potentials in both cases are small. As the calibration curves of pH_s against H^+ /OH^- concentration were obtained for each ionic strength separately under constant conditions of electrode combinations, small shifts may arise in the potential scale on increasing the ionic strength, but the calculations of charge densities should remain unaffected. The total shifts in the half-cell potential, as measured by the glass electrode, on increasing the ionic strength from 0.001 M to 0.1 M and to 1 M, were also determined and taken into account where necessary.

The oxide samples were taken directly out of water and rewashed, and the excess water was filtered out under suction in an atmosphere of argon. The resultant moist material (water, $\approx 2.5\%$ by weight of oxide) was used for the adsorption studies. Recrystallized reagent-grade KNO_3, KCl or $NaClO_4$ were used, as required, for adjusting the ionic strength of the solution. A 10-ml aliquot of the electrolyte solution was placed in the reaction vessel, and the dissolved CO_2 was then expelled by rapid stirring under a stream of argon. The pH_s was adjusted, as required, by means of HNO_3, HCl, $HClO_4$, or KOH, and the variation in pH_s on stirring the blank solution was followed at time intervals of two minutes. When the solution attained a steady reading of pH_s, a sample of the prepared oxide was added, and the variation in pH_s with time was again followed at intervals of two minutes. Fresh samples of the oxide and the solution were used for each run. Smaller quantities ($\sim$1.5 g) of oxide were used near the z.p.c. than at other values of pH_s ($\sim$2.5 to 3 g). It was found that almost all the change in pH_s occurred within 2 to 6 minutes of the addition of the oxide. This was followed by a much slower variation ($<5\%$ of the initial change) in the pH_s, which was attributed to secondary effects such as slime formation and solubility of the material. Corrections for these effects and for the blank were made. Verwey (27) has also reported that equilibrium is attained almost immediately in such oxide systems. The solubility* of the oxides

*Similar studies of the solubility of specular hematite near the z.p.c. indicate that, in a period of 1 hour, about 10^{-5} moles of Fe/litre goes into solution, whereas in the first few minutes, during which almost all the change in pH_s occurs, the solubility of iron is below detection limits (1 μ mole/litre).

under similar experimental conditions was also studied as a function of pH_s and of time, using standard colorimetric methods. No dissolved material could be detected (sensitivity, 1 μ mole/litre) at any pH_s under the present experimental conditions, whereas stirring for prolonged periods (~½ hour or more) produced dense colloidal solutions in some cases. Stirring was found to cause random variation in the liquid junction potentials and, hence, in the pH_s; stirring was therefore interrupted at the time of reading the meter at high sensitivity. It was also noted that any stirring method which crushed the material and produced more slimes gave erratic results. In the present work, a tiny glass stirrer was used.

Calibration curves of pH_s against molar concentrations of HNO_3, HCl and $HClO_4$ in solutions of KNO_3, KCl and $NaClO_4$ respectively, of 0.001 M, 0.1 M and 1 M concentrations, were obtained by potentiometric titrations. Similar calibration curves were obtained for KOH in KNO_3 solutions. These curves were used in calculating the charge densities, $q^{\pm}$, from the measured values of $\Delta a_{H^+/OH^-}$. Further experimental details may be found elsewhere (23).

IX. RESULTS

The Zero Points of Charge and the Charge Densities

Addition of the oxides to solutions of pH_s >their respective z.p.c. resulted in a decrease in pH_s, whereas below their respective z.p.c. the pH_s increased. The surfaces therefore have a negative charge in the former region of pH_s and a positive charge in the latter, according to the mechanism discussed earlier (23). This behaviour is similar to that of ZrO_2 and ThO_2 (23). In Table 1 are typical examples of the changes in pH_s that occur on adding magnetite samples to KNO_3 solutions, the pH_s being read at two-minute intervals. Although the absolute values of pH_s may not be significant to the accuracy shown in this table, the relative values are. It is also seen in Table 1 that almost all the changes in pH_s occurred within about 6 minutes of the addition of oxides to the solution. The later changes in pH_s are so slow that the initial equilibrium between the surface and the potential determining ions may be taken as practically complete. The slow changes in pH_s were attributed to secondary effects such as slime formation and solubility of the material, for which suitable corrections were made.

TABLE 1

Change in pH_s on Adding Hematite to 1 M KNO_3 Sol'n

pH_s, q^+ range, 0.001 M KNO_3		pH_s, q^- range, 1 M KNO_3
4.360		8.940
4.356	← Blank →	8.934
4.356		8.934
	← Oxide added →	
4.712		8.246
4.810		8.138
4.881		8.074
4.890		8.066

From the initial and final values of pH_s (if <7) or pOH_s (if >7), the respective values of a_{H^+} or a_{OH^-} were calculated. If necessary, corrections for blank, solubility and slime formation were made. The activities were converted into concentration terms C_{H^+} or C_{OH^-}, by multiplying by the respective activity coefficient factors*, which in turn were obtained from the calibration curves of pH_s against the molar concentration of acid or base. From the resulting data one can calculate (ΔC_{H^+} or ΔC_{OH^-})/10 ml/cm^2 oxide, and hence the charge densities $q^{\pm}$ (using Equation 4).

* $\frac{1}{f_{H^+}}$ (for pH_s<7) and $\frac{1}{f_{OH^-}}$ (for pH_s>7).

The $q^{\pm}$ values for hematite, magnetite, cassiterite, rutile and alumina are shown in Figures 14 to 19 as a function of final pH_s and potential relative to the z.p.c. The values of q^+ on hematite in $NaClO_4$ and KCl solutions are also shown, plotted against the final pH_s, in Figures 15A and 15B respectively. The values of q^+ in KCl solutions for SnO_2 and TiO_2 and Al_2O_3 were also obtained. These q^+ values for TiO_2 and Al_2O_3 in KCl solutions (not shown in Figures 18 and 19) were almost the same as their q^+ values in NO_3^- solutions (Figures 18 and 19). However, much higher values of q^+ were obtained for SnO_2 in 1 M KCl solutions, as shown in Figure 17. In order to investigate the general behaviour of oxides in the anodic region in different electrolyte solutions, q^+ values were also obtained for ZrO_2 and ThO_2 in $NaClO_4$ and KCl solutions. The results are shown in Figures 20 and 21. These should be compared with the previous values of q^+ obtained for ZrO_2 and ThO_2 in NO_3^- solutions (23).

In general, the $q^{\pm}$ values of all the oxides examined increase in magnitude with increasing half-cell potential ($\pm$) of the oxide electrode, relative to the z.p.c. In the cathodic region, the q^- values of all oxides increase not only with increasing pH_s (or negative potential) but also with increasing KNO_3 concentration or ionic strength of the solution. In the anodic region, however, the q^+ values depend on the nature of the oxide as well as of the anions present in solution. Thus, in KNO_3 and $NaClO_4$ solutions, the q^+ values of hematite (Figures 14 and 15A), rutile (Figure 18), cassiterite (Figure 17) and Al_2O_3 (Figure 19) are practically independent of KNO_3 and $NaClO_4$ concentration, and almost entirely depend on a_{H^+}. Similarly, the

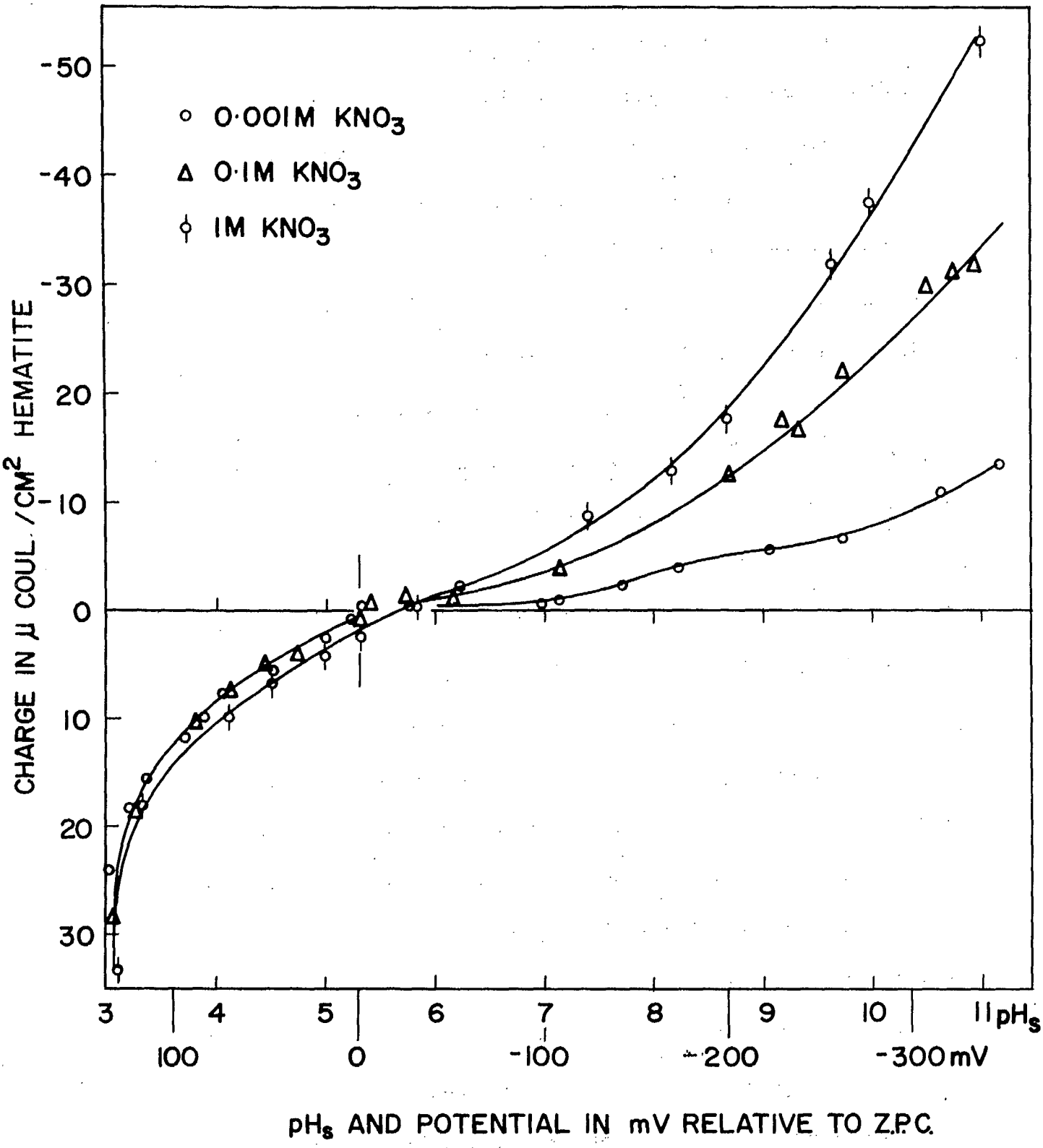

Figure 14. Variation in charge density ($q^{\pm}$) on hematite with final pH_s and potential difference relative to the Z.P.C. Indifferent electrolyte is KNO_3.

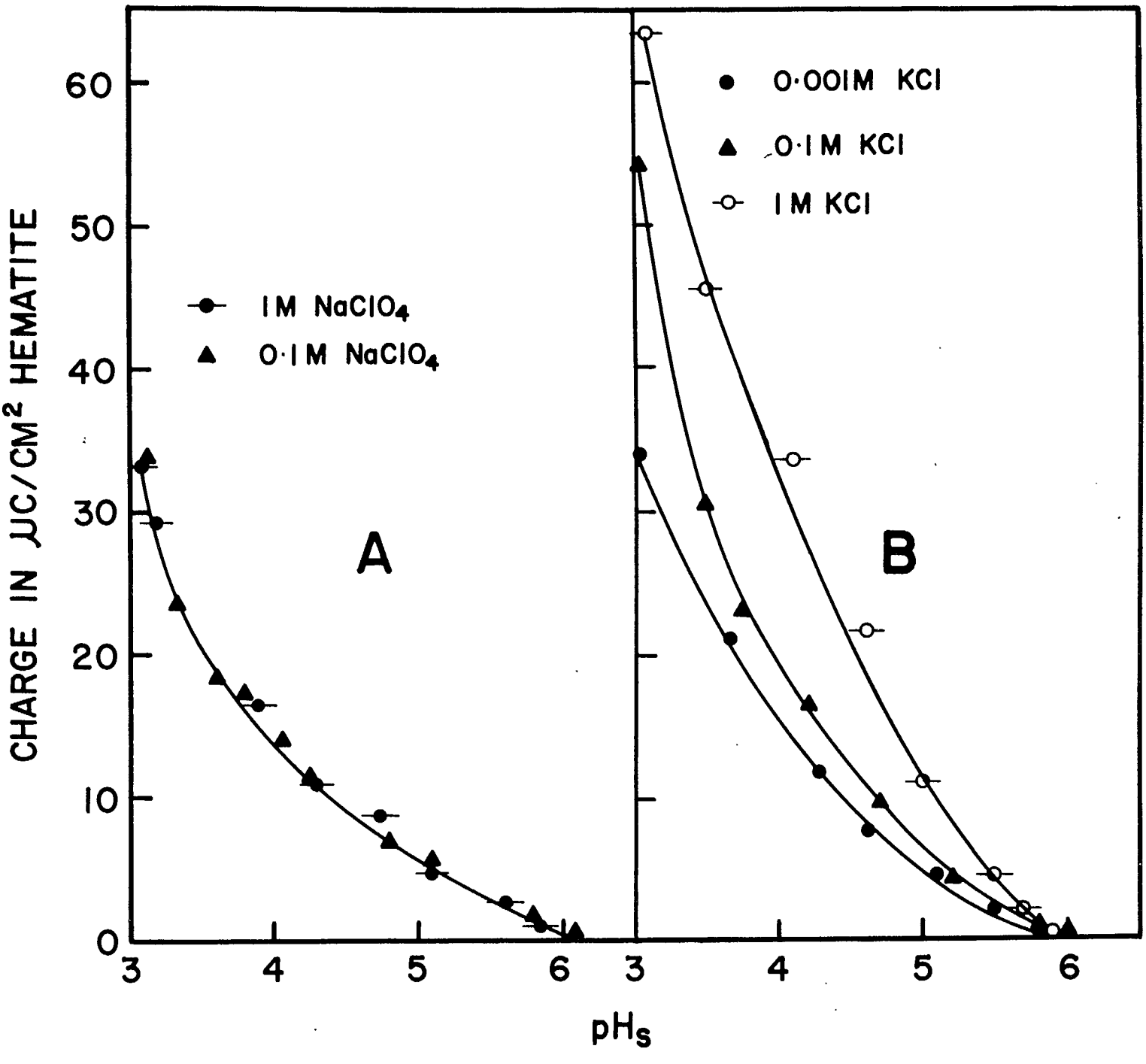

Figure 15. Variation in charge density (q^+) on hematite with final pH_s in: A - $NaClO_4$ solutions, B - KCl solutions.

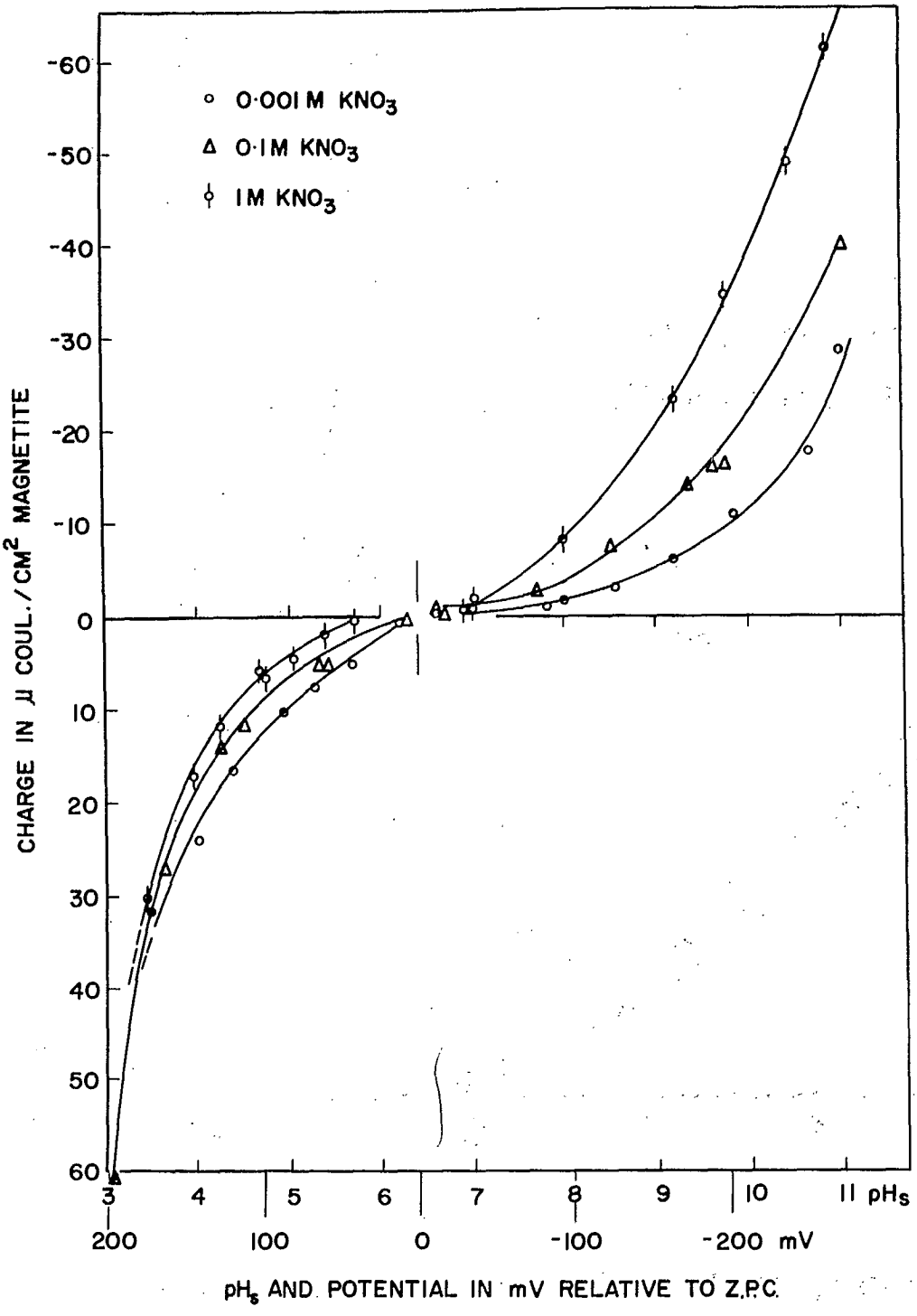

Figure 16. Variation in charge density ($q\pm$) on magnetite with final pH_s and potential relative to the Z.P.C. Indifferent electrolyte is KNO_3.

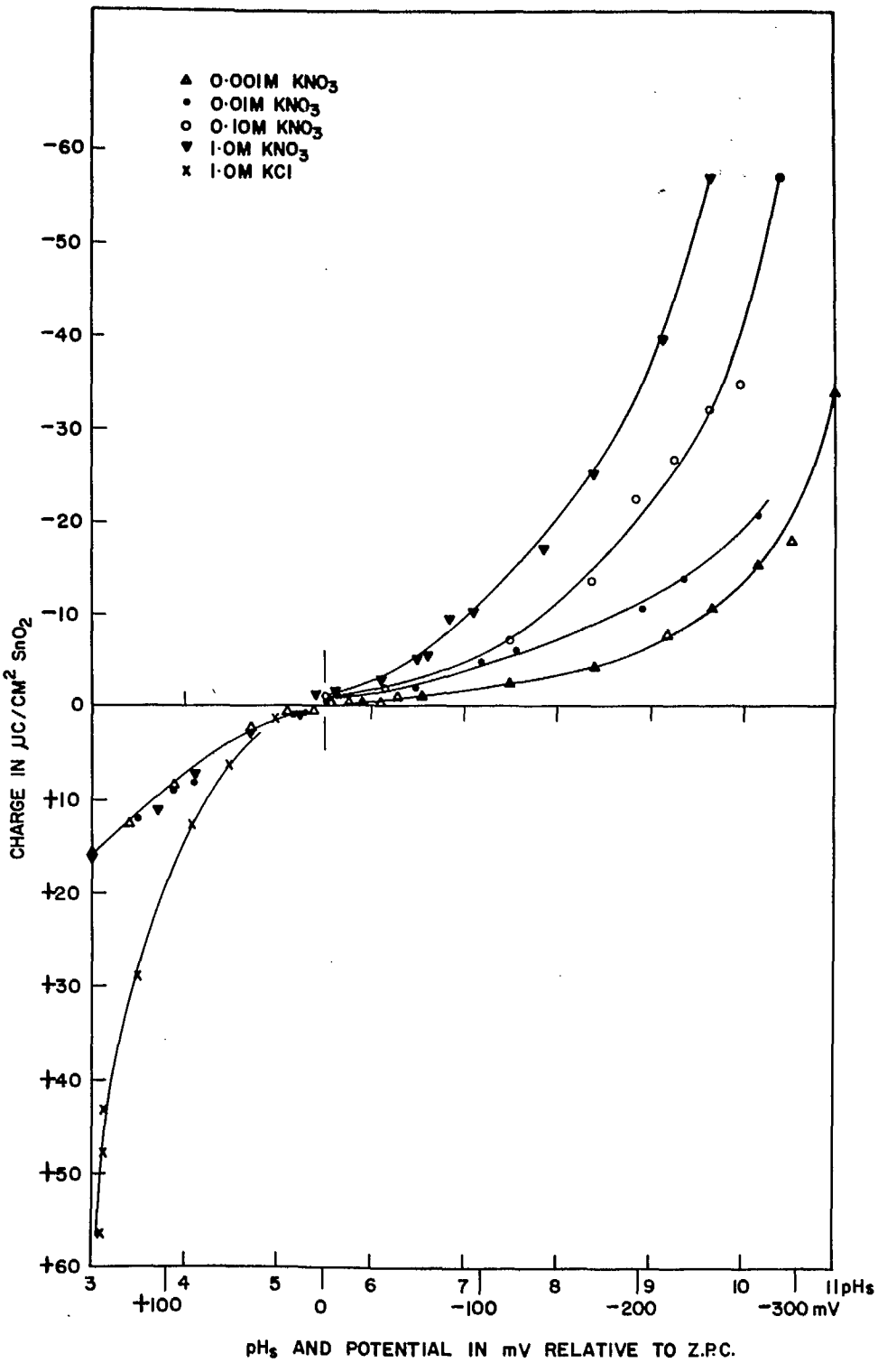

Figure 17. Variation in charge density ($q^{\pm}$) on SnO_2 with final pH_s and potential difference relative to the z.p.c., in KNO_3 solutions. The q^+ values of SnO_2 in 1 M KCl solution are also shown.

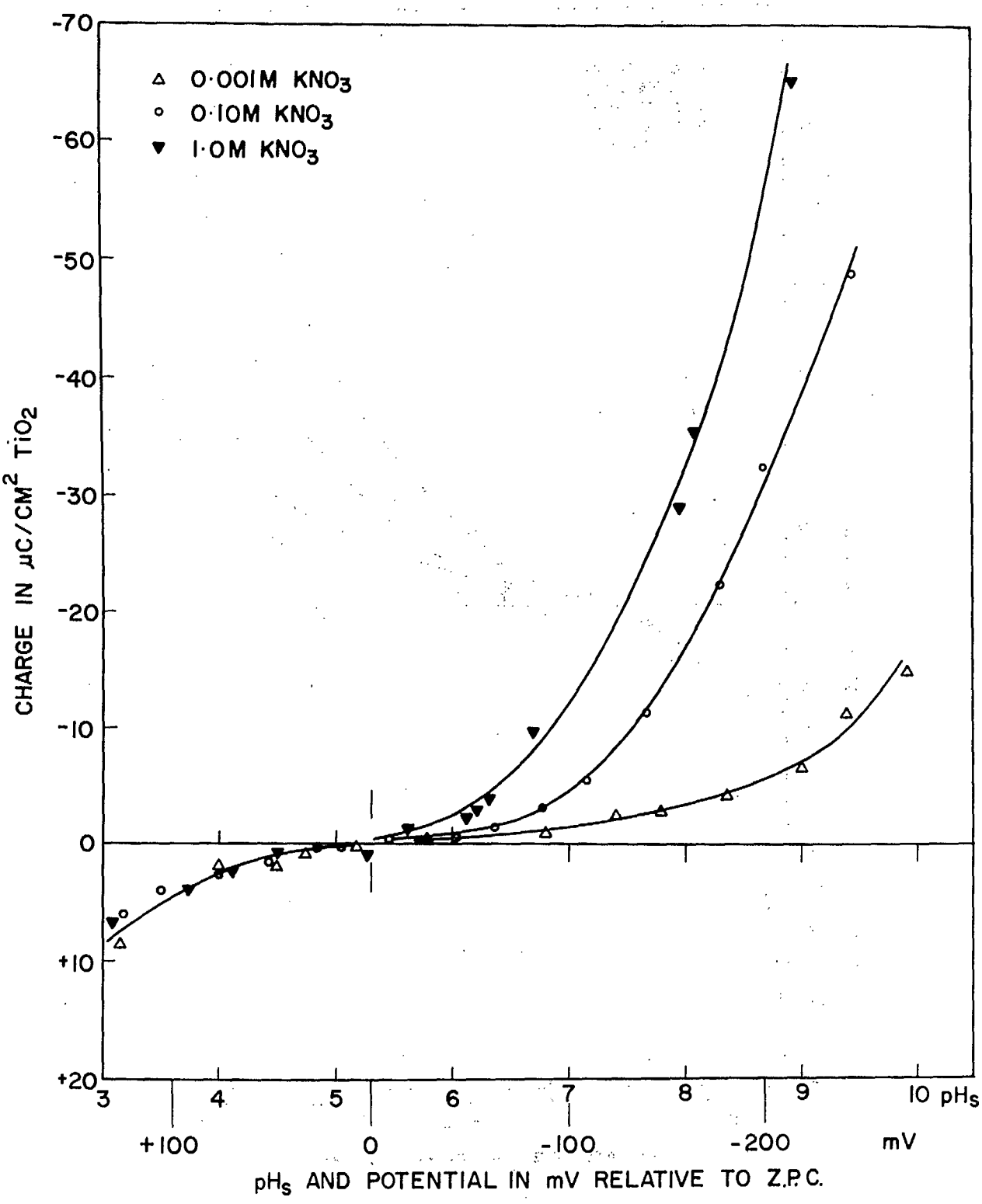

Figure 18. Variation in charge density ($q^{\pm}$) on TiO_2 with final pH_s and potential difference relative to the z.p.c., in KNO_3 solutions.

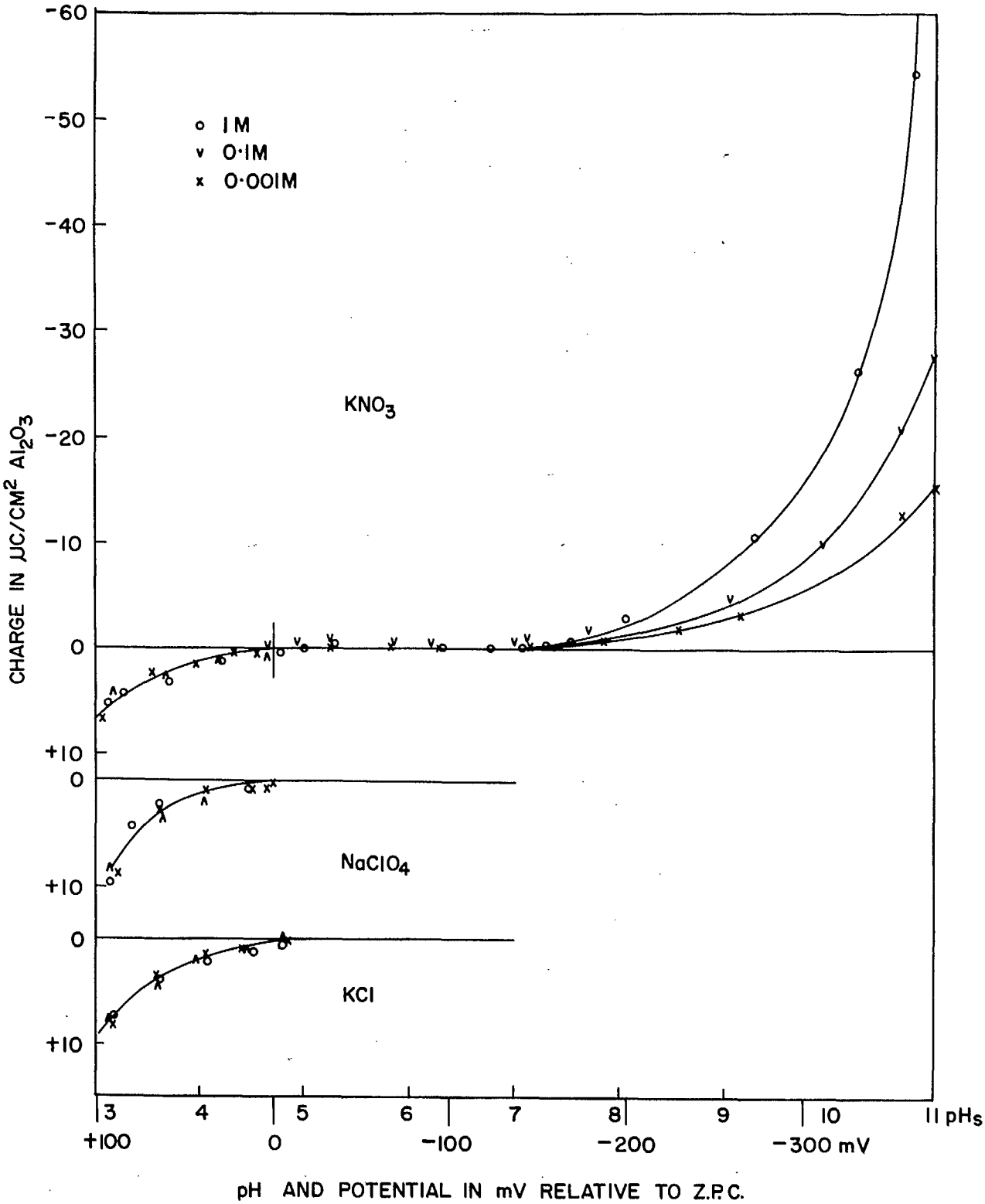

Figure 19. Variation in charge density (q^{+}_{-}) on Al_2O_3 with final pH_s and potential difference relative to z. p. c., in KNO_3, KCl and $NaClO_4$ solutions.

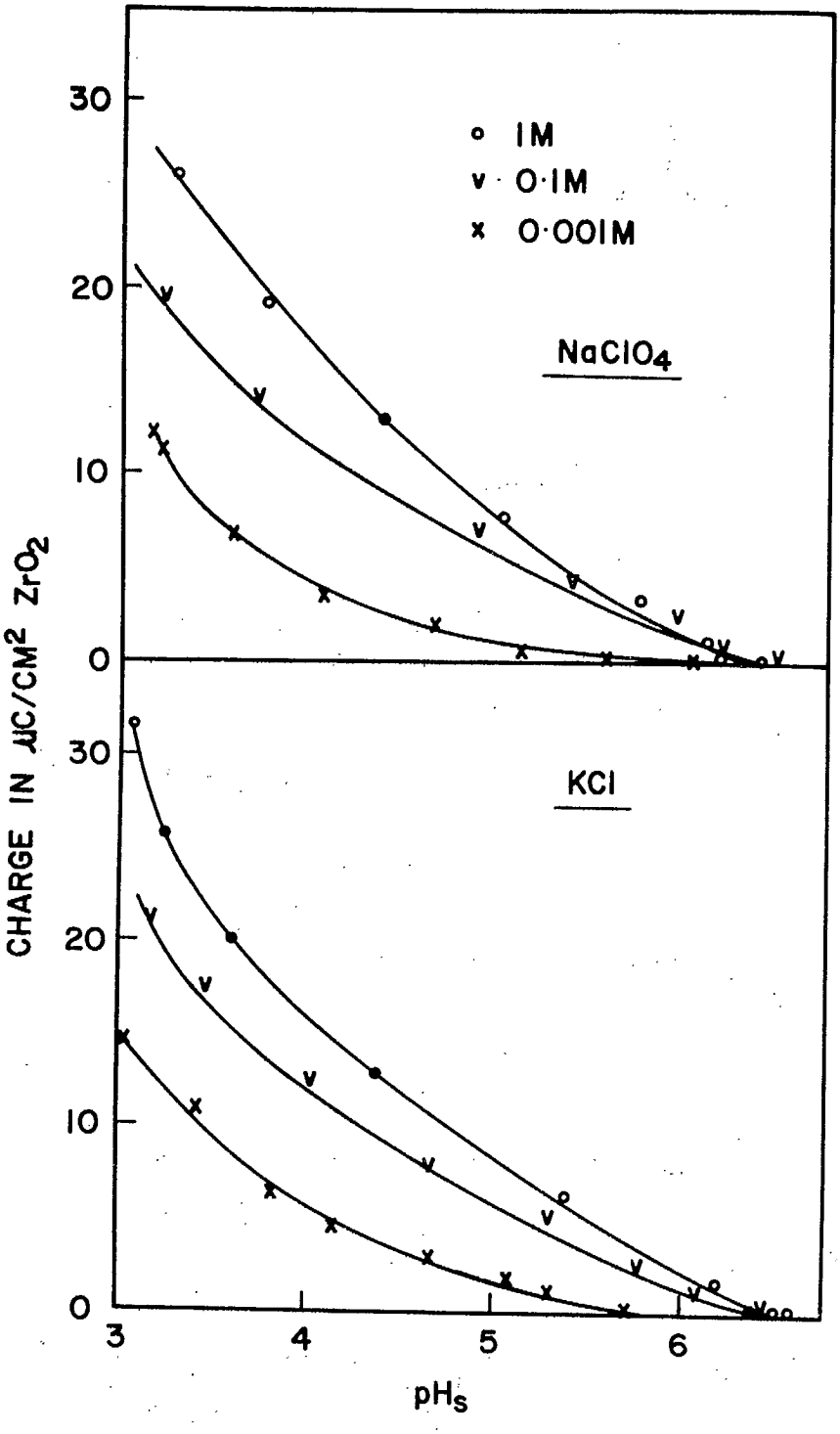

Figure 20. Variation in charge density (q^+) on ZrO_2 with final pH_s in $NaClO_4$ and KCl solns.

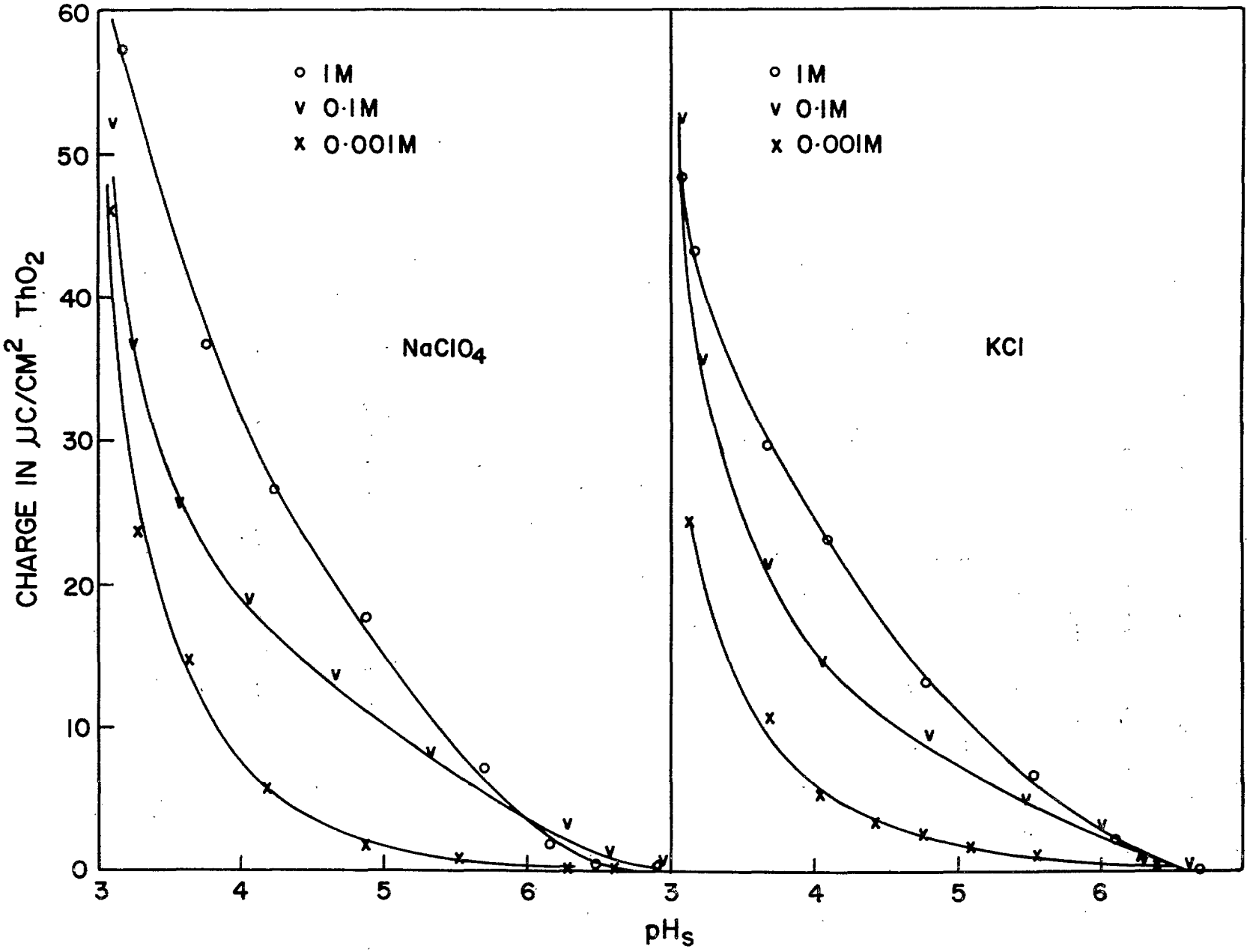

Figure 21. Variation in charge density (q^+) on ThO_2 with final pH_s in $NaClO_4$ and KCl solutions.

q^+ values of rutile and alumina in KCl solutions were also found to be independent of KCl concentration and depend mainly on a_{H^+}. However, the q^+ values of hematite and cassiterite in KCl solutions (Figures 15B and 17), and of zirconia (Figure 20) and thoria (Figure 21) in $NaClO_4$ as well as in KCl (and in KNO_3 (23)) solutions, increase with the increasing anion concentration in solution at any given pH_s. These variations of q^+ with the electrolyte concentrations should be adequately explained in any theories concerning the oxide-solution equilibria. The behaviour of magnetite in the q^+ region was somewhat ambiguous. As seen in Figure 16, comparatively high values of q^+ were obtained in 0.001 M KNO_3 solution and, also, the q^+ values slightly decreased in magnitude with increasing concentration of KNO_3 in solution. This behaviour of magnetite was quite reproducible. The magnetite samples under investigation were found to be strongly magnetic and n-type semiconductors. Similar work on magnetite samples of different origin gave very low values of q^+. The behaviour of magnetite, therefore, is inconsistent with the general behaviour of the other oxides investigated and shall be discussed further in the next section.

Experiments were also carried out with several oxides under somewhat different conditions. A series of oxide samples (1.5 g to 3 g each) were rewashed and dried at room temperature in a vacuum desiccator that was subsequently opened in an argon atmosphere. (Published data (117, 118) indicated that the chemisorbed water is retained on the surfaces of quartz through the formation of hydroxyl bonds, and other oxides were assumed to behave similarly.) The oxide samples, thus prepared, were used for

further work. The same results of $q^{\pm}$ were obtained with the samples dried in this manner as were obtained in the present work with slightly wet samples of oxides. The z.p.c. was found to lie at a slightly lower pH, however, when dry samples of oxides were used.

The Differential Capacity and the γ-γ_o Curves

The differential capacity C ($\mu F/cm^2$) of the whole double layer (C(+) in the anodic region and (C-) in the cathodic region) on different oxides was obtained by the graphical differentiation of the smoothed charge-density curves (Equation 5) of different oxides. The results are shown in Figures 22 to 24, for different oxides.

The changes in the interfacial energy (γ-γ_o), in ergs/cm^2, have been obtained for different oxides, by the graphical integration (cf. Equations 7 and 29) of the charge density plots of Figures 14 and 16 to 19. The results are plotted for each oxide in Figures 25 to 29.

X. DISCUSSION

The Zero Points of Charge

The pH_s at which the z.p.c. of different oxides occurred in KNO_3 solutions of different concentrations are summarized in Table 2. It should be emphasized here that these values of pH_s for the z.p.c. of oxides are for the initial primary equilibria (2-6 minutes) between the oxides and the potential-determining ions (H^+ and OH^-) in electrolyte solutions that are

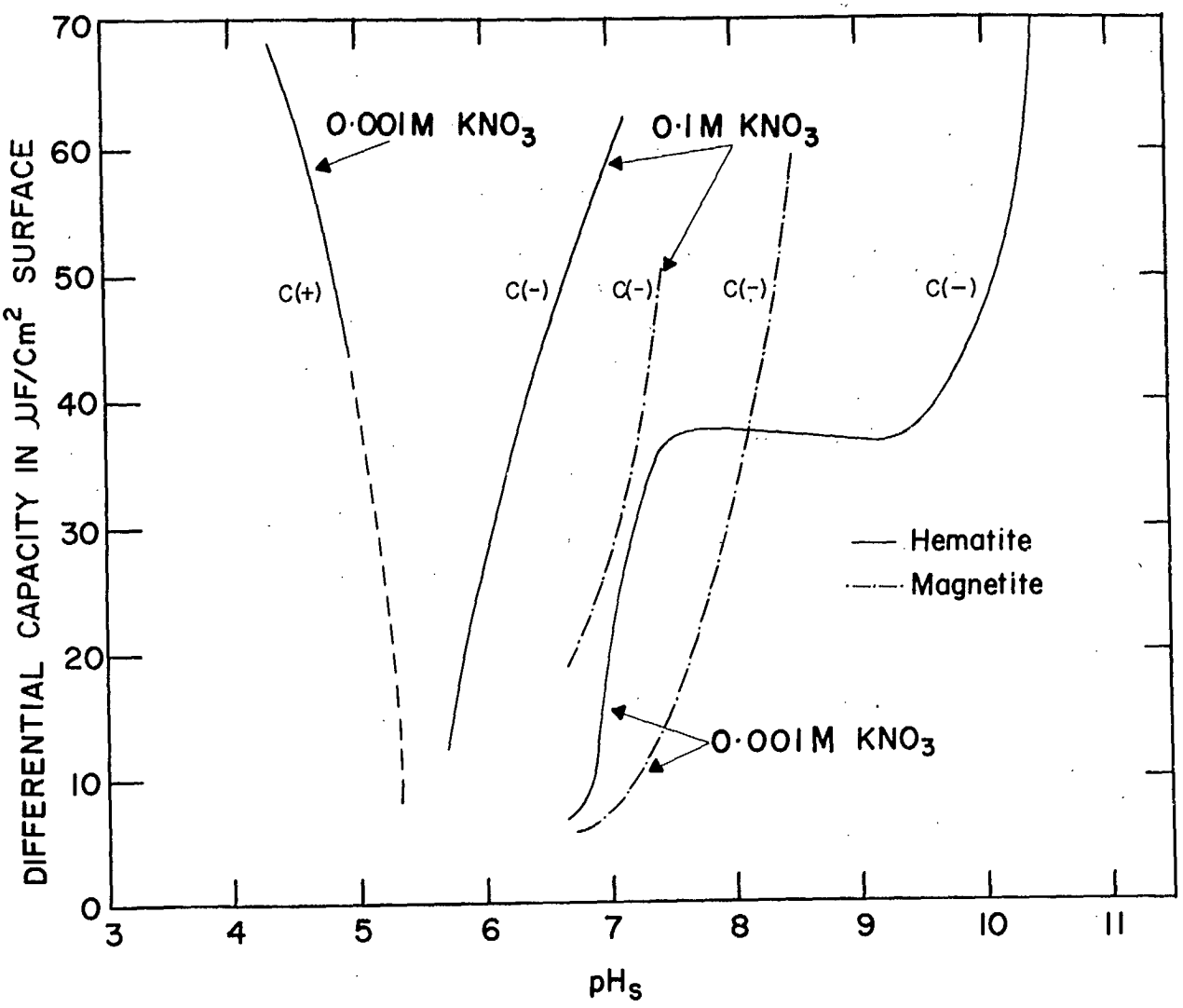

Figure 22. Variation in the differential capacity of the double layer on hematite and magnetite (C(-) only) with pH_s. Indifferent electrolyte is KNO_3.

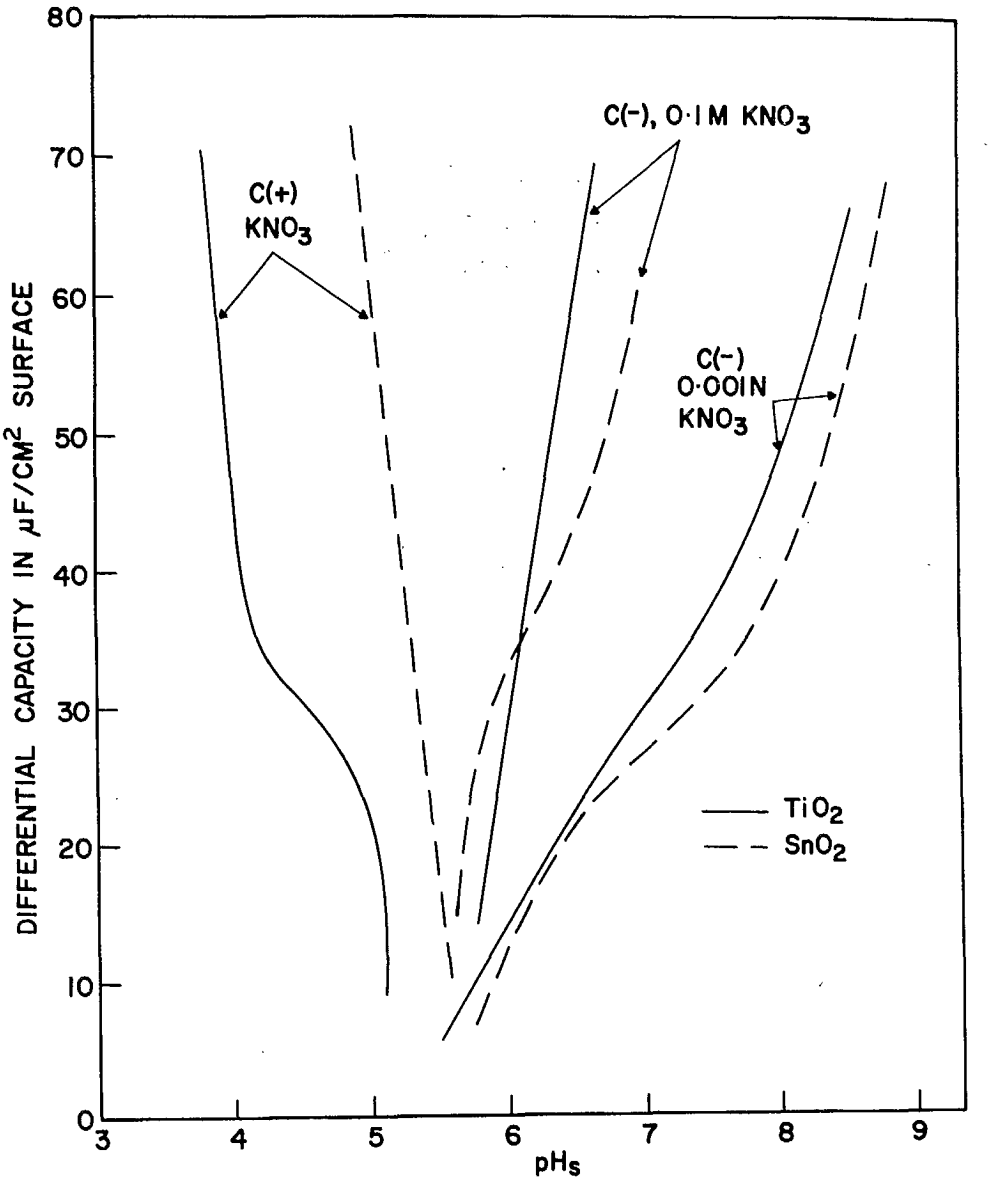

Figure 23. Variation in the differential capacity of the double layer on cassiterite and rutile in KNO_3 solutions, with pH_s.

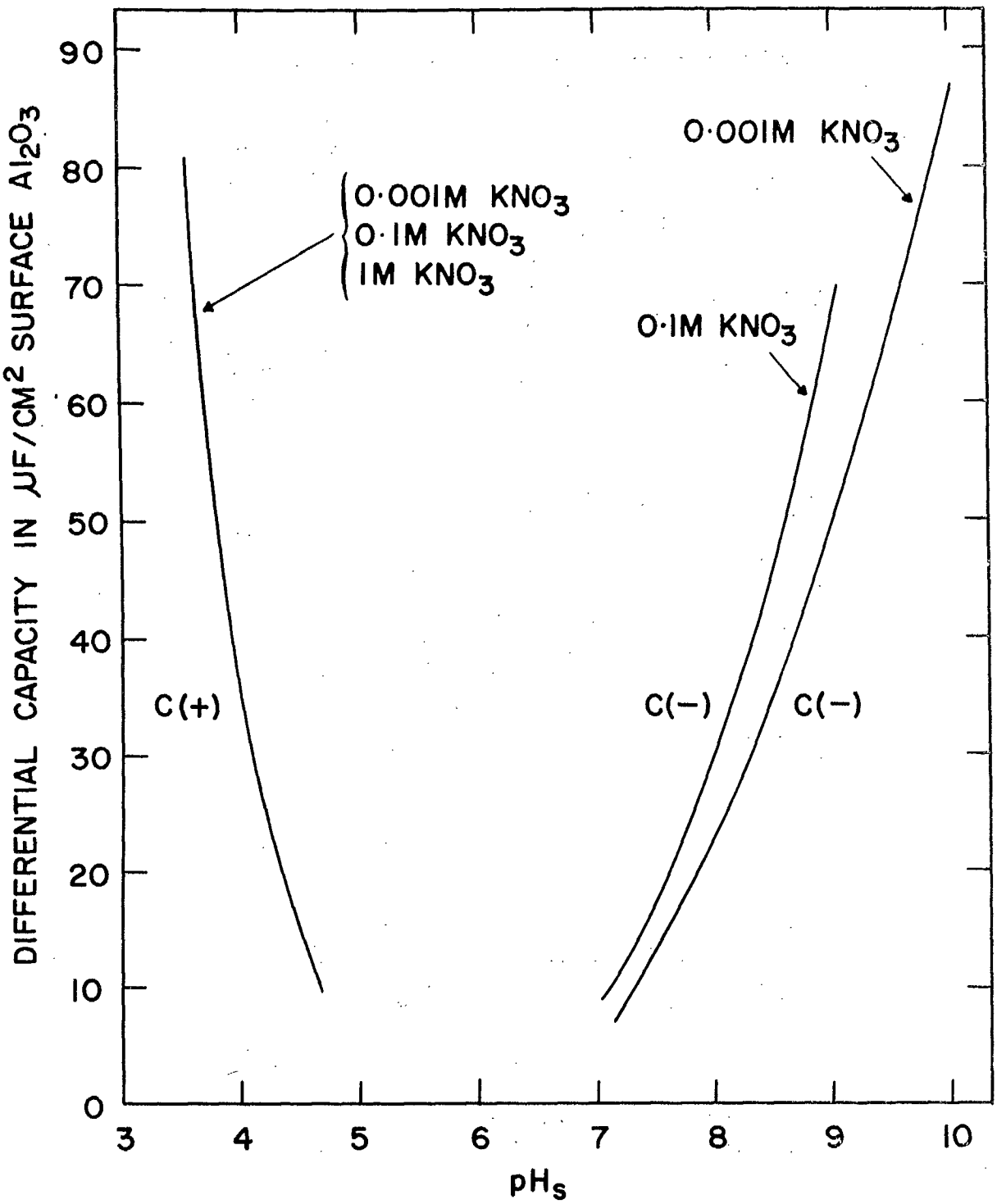

Figure 24. Variation in the differential capacity of the double layer on Al_2O_3 in KNO_3 solutions, with pH_s.

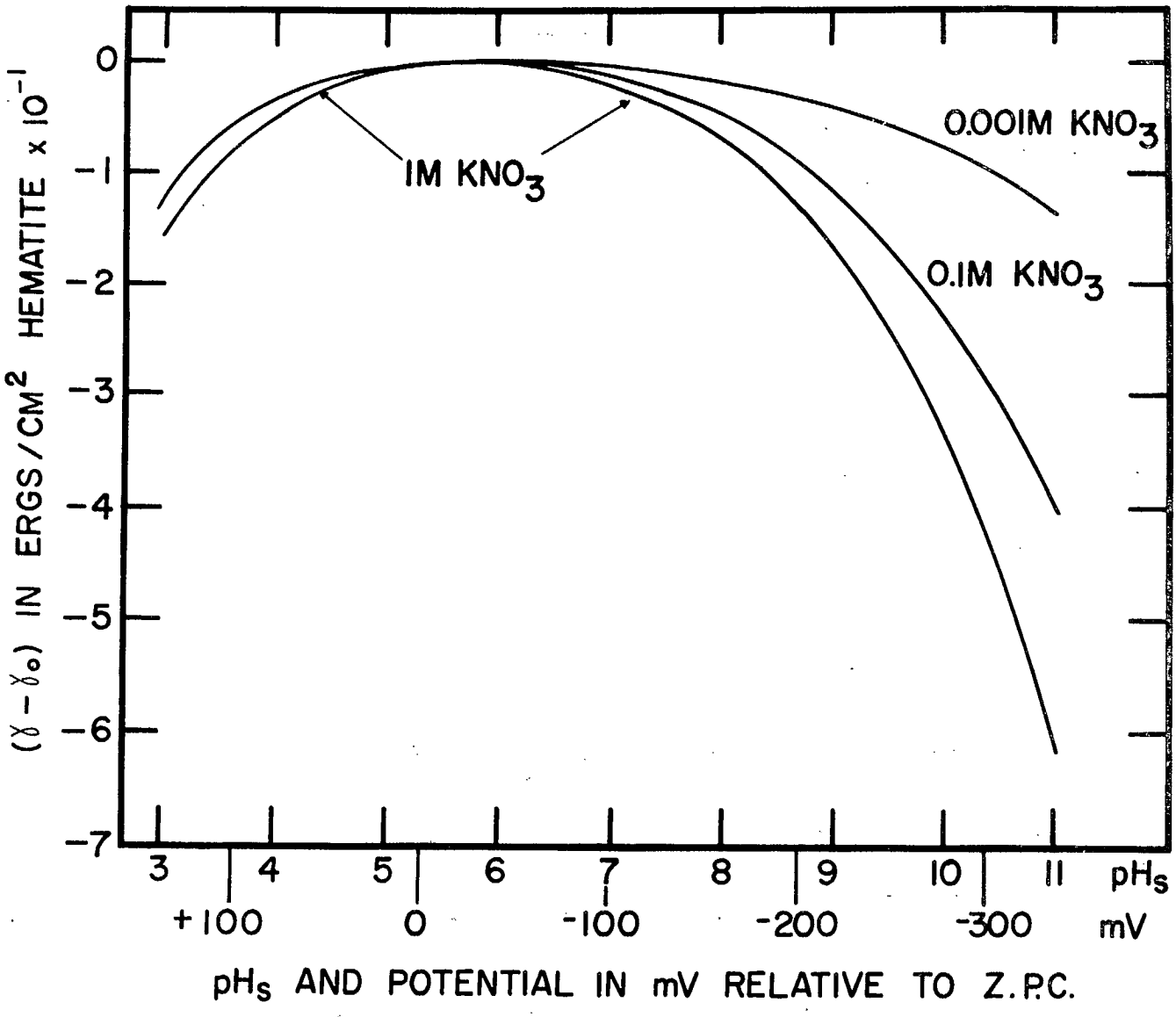

Figure 25. Changes in the interfacial tension at the hematite-solution interface with pH_s and potential difference relative to the z.p.c. Indifferent electrolyte is KNO_3.

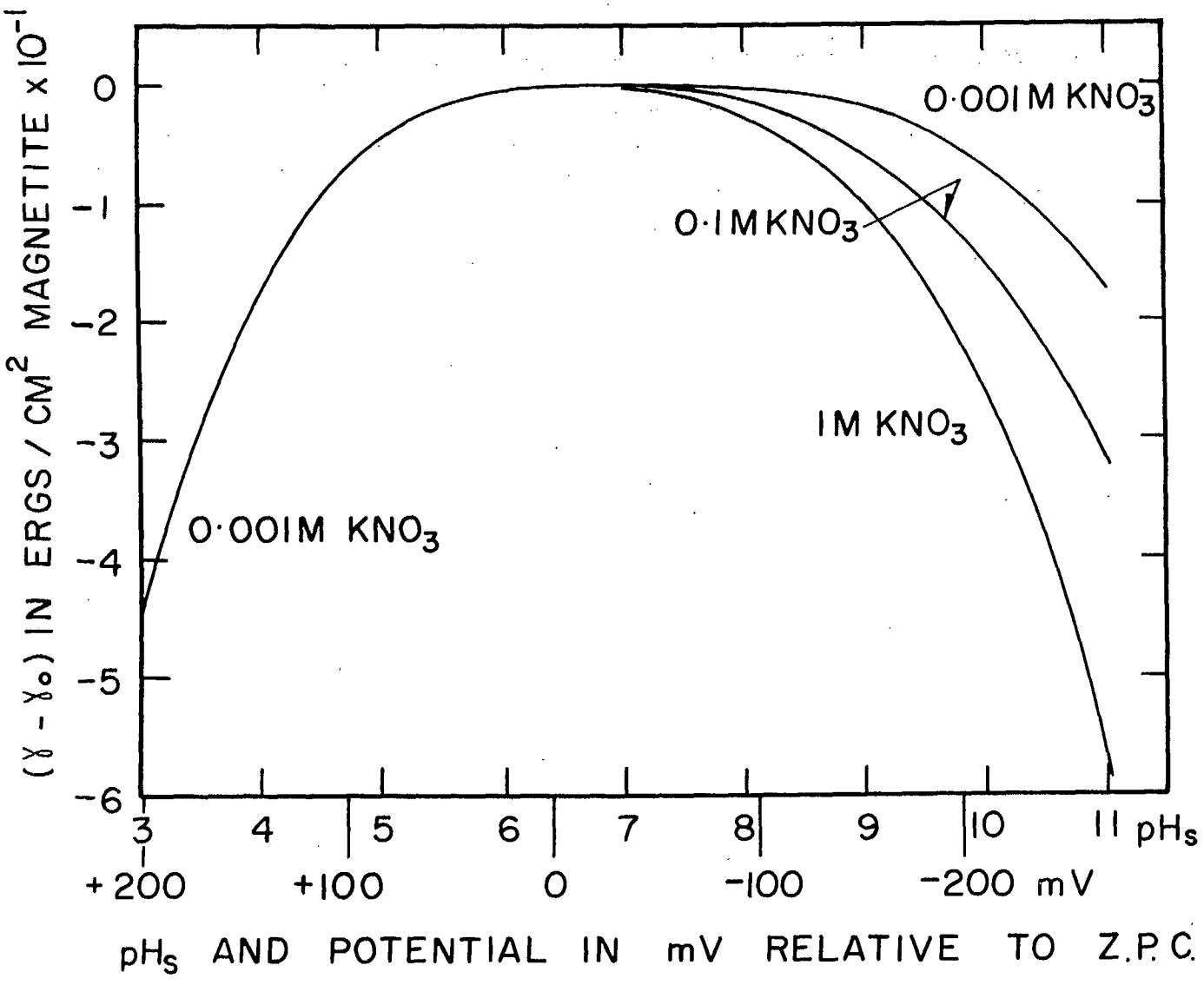

Figure 26. Changes in the interfacial tension at the magnetite-solution interface with pH_s and potential relative to the z.p.c. Indifferent electrolyte is KNO_3.

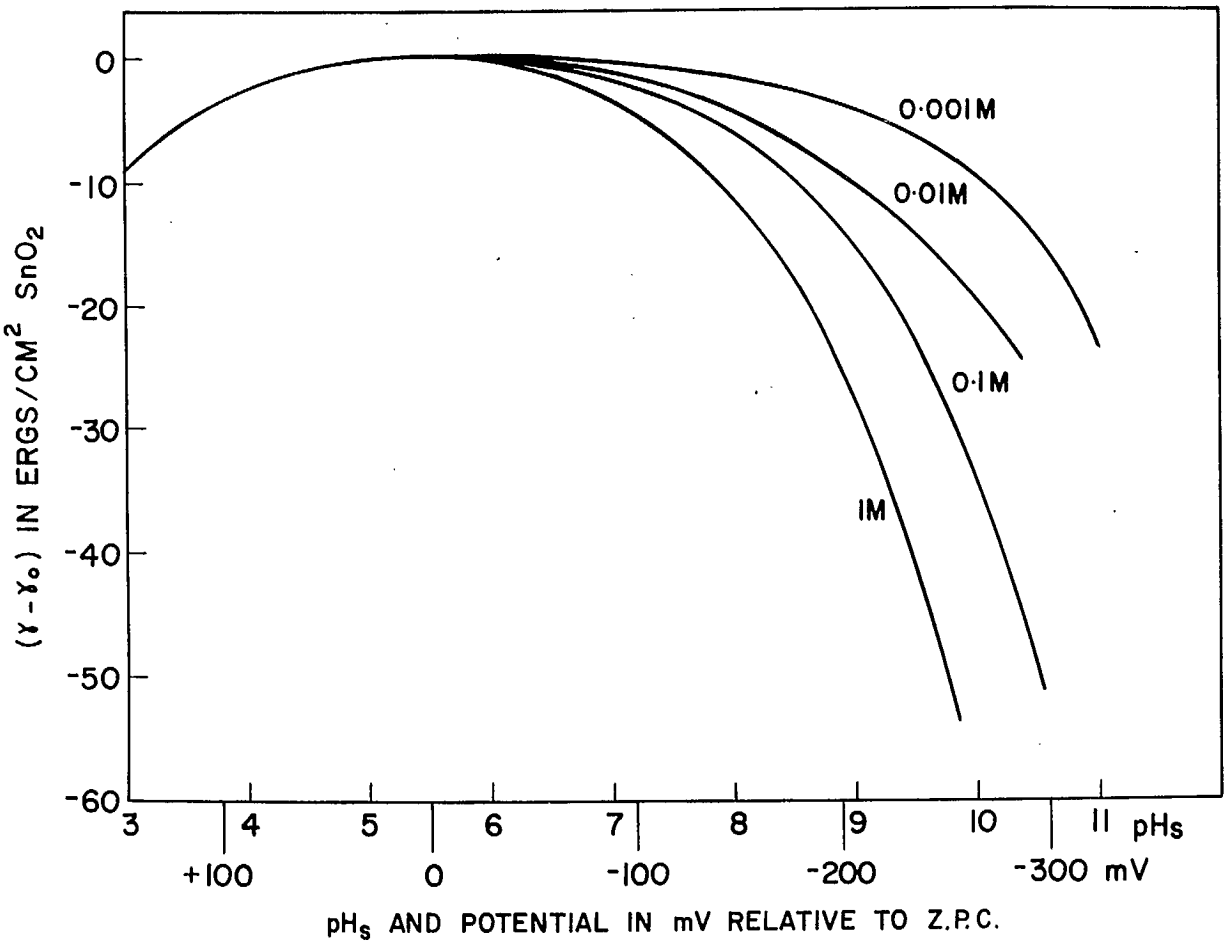

Figure 27. Changes in the interfacial tension at the cassiterite-solution (KNO_3) interface with pH_s and potential relative to the z.p.c.

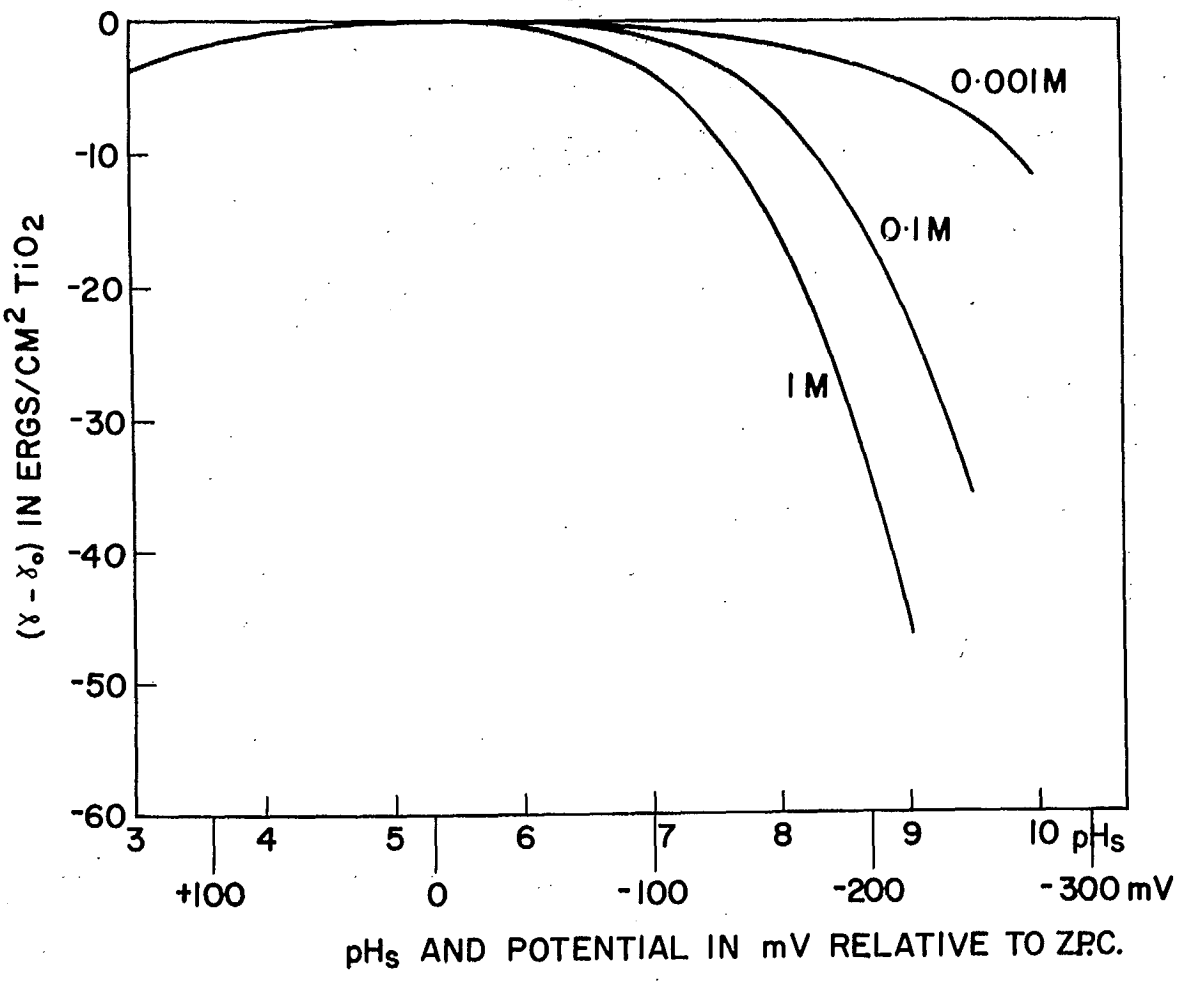

Figure 28. Changes in the interfacial tension at the rutile-solution (KNO_3) interface with pH_s and potential relative to the z.p.c.

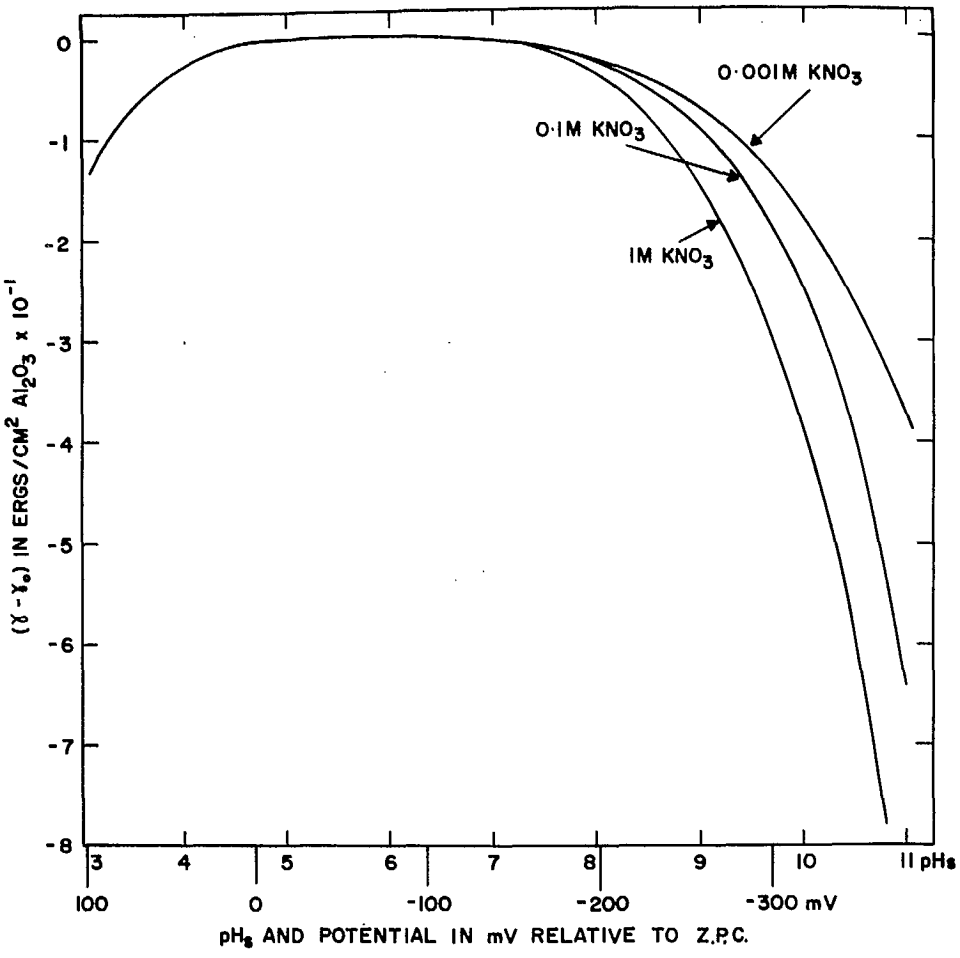

Figure 29. Changes in the interfacial tension at the Al_2O_3-solution (KCl or KNO_3) interface with pH_s and potential relative to the z.p.c.

practically free of the dissolved complexes of the metals that constitute the oxides. The significance of the above statement will be elaborated later. For comparison, the z.p.c. of quartz, zirconia and thoria (23) are also included.

TABLE 2

Z.P.C. of Oxides in KNO_3 Solutions

Oxide	Electrolyte Concentration	pH_s of Z.P.C.
Quartz (dry samples)	1 M KNO_3	3.6 ± 0.05
ZrO_2 (" ")	0.001 M KNO_3	5.5 ± 0.05
ZrO_2 (" ")	1 M KNO_3	6.2 ± 0.05
ThO_2 (" ")	0.001 M KNO_3	5.9 ± 0.05
ThO_2 (" ")	1 M KNO_3	6.8 ± 0.1
Fe_2O_3 (specular hematite, moist)	0.001 M KNO_3	5.3 ± 0.05
Fe_2O_3 " " "	0.1 M KNO_3	5.4 ± 0.05
Fe_2O_3 " " "	1 M KNO_3	5.7 ± 0.1
Fe_3O_4 (magnetite, moist)	0.001 M KNO_3	6.4 ± 0.1
SnO_2 (cassiterite, moist)	0.001 M KNO_3	5.5 ± 0.1
SnO_2 " "	0.1 and 1 M KNO_3	5.4 ± 0.1
TiO_2 (rutile, moist)	0.001 M KNO_3	5.3 ± 0.05
TiO_2 " "	0.1 M KNO_3	5.0 ± 0.05
TiO_2 " "	1 M KNO_3	4.8 ± 0.1
α-Al_2O_3 (moist)	0.001 M KNO_3	4.7 ± 0.1
α-Al_2O_3 "	0.1 M KNO_3	4.8 ± 0.1
α-Al_2O_3 "	1 M KNO_3	5.0 ± 0.1

When the concentration of KNO_3 in a blank solution was increased from 0.001 M to 1 M, the glass electrode measured a decrease in pH_s of 0.3 ± 0.05 unit in the vicinity of the z.p.c. Hence, in order to compensate for the above shift in the half-cell potential, a corresponding shift in the z.p.c. of the oxides towards a higher pH_s, by about 0.3 pH_s unit, is expected from theory. Such a shift in the z.p.c. of hematite, zirconia and thoria, towards a higher pH_s, was found to occur with increasing concentration of KNO_3 in solution, as seen from Table 2. But, in the case of rutile and cassiterite, the z.p.c. shifted towards a lower pH_s (or a more positive potential). It is also known, from theories of the electrical double-layer, that if cations are specifically adsorbed (in the inner Helmholtz layer) on the surface at the z.p.c., the z.p.c. itself would shift towards a more positive potential. Similarly, if anions are specifically adsorbed on the surface at the z.p.c., the z.p.c. would shift towards a more negative potential. Thus, according to the Esin and Markov effect (8, p. 650), in the presence of specific adsorption the z.p.c. is known to vary with the electrolyte concentration at a rate $>RT/nF$. Hence, the observed shift in the z.p.c. of cassiterite and rutile towards a more positive potential, on increasing the KNO_3 concentration, indicates some specific adsorption of K^+ on the oxide surfaces at the z.p.c. Although the pH_s measurements near the z.p.c. were not very precise, the trend, however, could be definitely established. Further evidence of the specific adsorption of K^+ on the oxide surfaces can be obtained from the differential capacity : pH_s curves (Figures 22-24).

The z.p.c. of the different forms of iron oxides, as reviewed by Parks (119), are widely different, depending on oxide composition, crystalline form, size, and the method of surface preparation. The basic reason for such variations in the z.p.c., sometimes of the same material (23, 105), is not obvious. A direct relationship has been established between the z.p.c. of the oxides on the pH scale, their electrostatic field strength and their heats of immersion (103, 104). It is also known that the specific heats of immersion and the surface energies of oxides (118) are greater when the oxides are coarse and crystalline than when they are in a finely divided condition. Hence, the z.p.c. of oxides may also vary with the particle size. However, the major cause for the differences in the reported values of the z.p.c. lies in the kinetic stage of the oxide-solution equilibria. The present values for the z.p.c. of iron oxides are for the primary equilibrium (first few minutes) that occurs between the oxide surfaces and the potential-determining ions (H^+ and OH^-) in the presence of K^+, NO_3^-, etc., in solutions that are practically free of dissolved iron complexes. However, if the oxides are allowed to equilibrate with solutions for a long time ($\sim$15 hours) (22, 24 25, 105, 106), the solutions become saturated with the dissolved complexes that may also be adsorbed on the surfaces, or be precipitated. The hydrolysis of iron salts, for example, is also known to be a very slow process (120). Under such conditions, the experimental z.p.c. of oxides should occur at the same pH_s as the isoelectric point (i.e.p.) of the soluble complexes. Thus, Parks and De Bruyn (22) found that the z.p.c. of precipitated iron oxide, under slow conditions of equilibria, occurs at the same

pH_s (≈ 8.5) as the i.e.p. of the soluble complexes of iron. A similar agreement between the z.p.c. of titania surfaces with the i.e.p. (~pH 7) (106) of titanium complexes and the z.p.c. of alumina with the i.e.p. of aluminum complexes (pH 9.1) has been reported (25). Further, the adsorption on oxide surfaces of the dissolved complex ions in solution would itself shift the z.p.c. considerably. Thus, the important conclusion is drawn here that the z.p.c. of oxides will depend on the kinetic stages of the equilibria that one is working with and also on the experimental conditions. Thus, for example, the z.p.c. of rutile could vary from an initial pH_s value of 5.3 to a final pH_s value of 7 (which is the i.e.p. of Ti^{4+} complexes), depending on the experimental conditions and the solution composition. Similarly, the z.p.c. of hematite would vary from an initial pH_s value of 5.3 to a final pH_s value of 8.5 (which is the i.e.p. of Fe^{3+} complexes), depending on the experimental conditions and the solution composition. Since precipitated or finely divided material, having a large surface area, can dissolve in solution more easily, the resultant z.p.c. of fine precipitates will be closer to the i.e.p. of the dissolved complexes than to the initial z.p.c. of oxides. On the same basis, the z.p.c. of colloidal or finely divided particles, determined by electrophoretic methods in a closed system, will be closer to or identical with the i.e.p. (or z.p.c. final) of the soluble complexes of metals that constitute the oxide. The pH_s of the zero zeta potential obtained by streaming potential methods, using fresh electrolyte solutions, will be closer to the initial z.p.c. of the oxides as obtained in the present work under fast conditions of oxide-solution equilibria. Thus,

the present pH_s values of 5.5, 5.3 and 3.6 for the z.p.c. of cassiterite, specular hematite and quartz in 0.001 M KNO_3 solutions, respectively, are in close agreement with the pH_s of the zero zeta potential obtained by streaming potential methods (107, 121, 122).

The Oxide-Solution Equilibria

When a sparingly soluble oxide is added to an electrolyte solution, the following reactions will occur: (a) hydrolysis and complex formation of the surface atoms, and dissociation of the surface groups, as a primary step; accompanied by (b) dissolution of the oxide leading to secondary reactions, such as hydrolysis, complex formation and dissociation of the dissolved complexes, adsorption of the dissolved complexes on the surface, and precipitation in colloidal form. Whereas the primary equilibrium of the surface (type a) with the potential-determining ions (H^+ and OH^-) is known to be complete (23, 24, 27) within minutes after the addition of the oxides to the solution, the secondary reactions (type b) arising from the solubility of the material are known to be very slow (120) and may last for days or weeks. The surface structure, the equilibrium constants, and the zero point of charge of the oxide surfaces that are in primary equilibrium with H^+ and OH^- (type a), will be much different from the respective properties when the same surface is under slow equilibrium (several hours) with the dissolved complexes. What is studied, therefore, under such slow equilibrium conditions, is the over-all result of all the reactions listed above under "a" and "b". It is, therefore, not unexpected that Onoda and De Bruyn (24)

found that the apparent values of the charge densities and differential capacities of the double layer on iron oxide, under conditions of slow equilibrium, disagreed with the theoretical values by several orders of magnitude. Similarly, the charge densities and differential capacities of the double layer on titania, reported by Smith and Salman (106), are too high to be attributed to the surface phenomenon alone. Similar discrepancies may also be found in work with other oxides (102, 105) under slow conditions of equilibrium. A considerable amount of work has been carried out (22, 24, 102, 105, 106, 108, 123, 124) on the slow equilibrium that occurs between metal oxides and solutions saturated with their metal complexes. In aqueous suspensions of metal oxides, such as M_2O_3 (e.g., Fe_2O_3) and $M'O_2$ (e.g., SnO_2, TiO_2, ZrO_2 and ThO_2), several dissolved aquo-complexes in six co-ordination, such as $\left[M(H_2O)_3(OH)_3\right]$, $\left[M(H_2O)_{3+n}(OH)_{3-n}\right]^{n+}$, $\left[M(OH)_4 \cdot nH_2O\right]^-$ and similar compounds of M'^{4+}, are known to exist in equilibrium with the oxide surfaces at different values of pH_s. Under such equilibria, the electrode potentials of metals and metal oxides at any given pH_s will depend on the activities and the equilibrium constants of such complexes. Pourbaix (123) and Delahay et al. (124) have carried out detailed thermodynamic analyses of such systems and the data have been presented as pH-potential diagrams.

The present work and the following thermodynamic analysis of the double layer on oxides are, however, concerned with the primary equilibrium (fast, 2-6 minutes) that occurs between the oxide surfaces and the potential-determining ions (H^+ and OH^-) in solutions (of KNO_3, KCl or $NaClO_4$) that

are practically free of the dissolved metal (from oxides) complexes.

The Primary Oxide-Solution Equilibria and the Surface Charge

(a) The Positive Surface Charge

The thermodynamics of the double layer at reversible interfaces, including the oxide-solution interface, has already been considered in relation to the theory of electrocapillarity. The surface of reference relative to which the surface excess, Γ, is considered needs some clarification in the present system. Grahame (7, p. 454) and Mackor (19, p. 666) have discussed the above subject elsewhere, for the Hg-solution interface and the AgI-solution interface respectively. For the sake of discussion, assume $\left[\rightarrow M(H_2O)(OH)_2\right]$ to be the structure of the neutral aquo-complex on oxide surfaces at the z.p.c. (M = Ti^{4+}, Sn^{4+} or Fe^{3+} in six co-ordination), such that three of the co-ordination sites, including two valence states of M, are exposed to the solution. This structure at the z.p.c. may be taken as the reference plane for the thermodynamic treatment and an interfacial energy, γ_o, assigned to it. Although the charge densities would depend on the location of the reference plane, the interfacial energy is independent of it. At equilibrium, the chemical potentials -- and, hence, the activities of the potential-determining ions on the two sides of the reference plane -- are equal. The surface charge, $q^{\pm}$, then originates from the surface excess (Γ) of H^+ or OH^- on the solid side of the reference plane, and is compensated in the double layer by the excess charge, of opposite sign,

composed of the counter ions such as NO_3^- and K^+. It should be noted that, at the z.p.c., Γ_{H^+} and $\Gamma_{OH^-} \neq 0$ but that, with respect to the dehydrated surface, $\left(\Gamma'_{H^+} - \Gamma'_{OH^-}\right)_{z.p.c.} = 0$. Because the surface charge originates through a chemical reaction at the interface, it is necessary to understand the relevant mechanism in order to account for the origin and the variation of q^+ with pH_s (potential) and with the ionic strength of the solution. The increase in pH of the solution on adding the oxide may be ascribed to the chemisorption of H^+ on the neutral surface with the replacement of the surface hydroxyl groups by anions such as Cl^- (mechanism A), or without the replacement of such surface-OH groups by anions (mechanism B). The two mechanisms are shown, schematically, below:

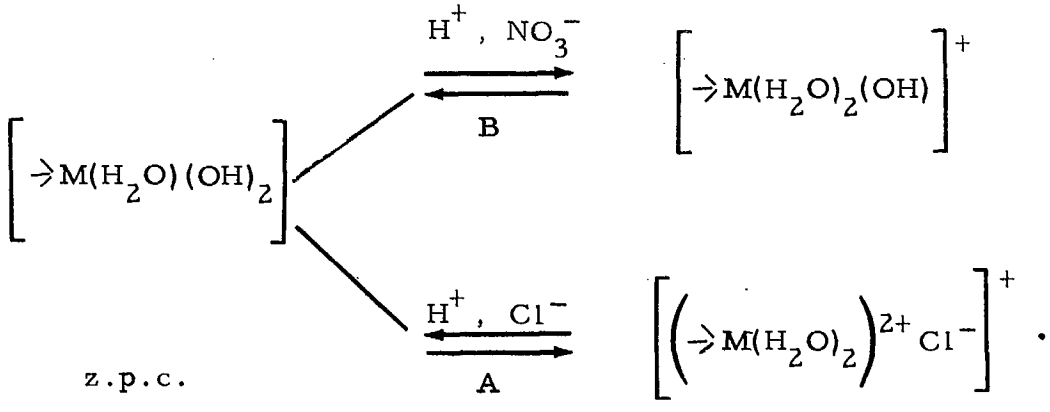

If the anions present in solution (e.g. NO_3^-, ClO_4^-) are such that their interaction with the metal atom M (e.g. Fe, Sn, Ti, Al) is very weak in comparison with that of the OH-ligands in the aquo complex, q^+ as shown in mechanism B will be entirely due to H^+ adsorption. The positive charge densities, q^+, therefore, will depend mainly on a_{H^+} and not on the anionic concentration. Some increase in the q^+ values of oxides is, however,

expected on increasing the ionic strength of the solution as a result of compressing the diffuse double layer.

The charge densities of the diffuse double layer, (η^d), as a function of electrolyte concentration and double-layer potential (outer Helmholtz layer), are given by Equation 16. Using a similar equation, Russell (67) has tabulated values of q^d for different values of electrolyte concentrations and electrode potentials for the case z = 1. It may be seen from his data that for a potential of about 100 mV relative to the z.p.c. (the rational potential, ψ^r, (7, p. 452)), an increase in η^d (and hence in q) of only about 2 μ coul./cm^2 is expected on increasing KNO_3 concentration from 0.001 M to 1 M. This small increase in the q^+ values of oxides on increasing the ionic strength of the solution from 0.001 M to 1 M for a uni-univalent salt, is within the experimental error of the present work. Thus, the effect of ionic strength on the diffuse double layer is small in comparison with the effect on the q^+ values due to chemisorption of H^+ on the oxide surfaces under investigation. Because of the exceptionally high ionic mobility of H^+ in aqueous solutions, the effect of ionic strength on a_{H^+} is also small for common electrolytes. Hence, within the above limitations, the q^+ values of oxides obeying mechanism B should depend almost entirely on a_{H^+}. This explains the results of q^+ for:

(1) Fe_2O_3 (specular hematite) in NO_3^- and ClO_4^- solutions (Figures 14 and 15A);

(2) SnO_2 in NO_3^- solutions (Figure 17);

(3) TiO_2 in NO_3^-, ClO_4^- and Cl^- solutions (Figure 18);
(4) Al_2O_3 in NO_3^-, ClO_4^- and Cl^- solutions (Figure 19).

From the above argument, it follows that the particular anions listed above are not specifically adsorbed on the corresponding oxide surfaces, but these anions stay as counter ions in the outer Helmholtz layer. The positive surface charge on oxides is obtained by the chemisorption of H^+ ions, and the oxide is then reversible to H^+ only.

If the anions present in solution are more electronegative than NO_3^- (e.g. Cl^-), they can replace the hydroxyl ligands of the surface aquo-complex through a covalent interaction with the metal M (e.g. Fe, Sn) in addition to H^+ adsorption on the surface, according to mechanism A. This will result in higher experimental values of q^+ which increase, not only with increasing a_{H^+}, but also with increasing anion concentration. These oxides, therefore, will be reversible to H^+ as well as to the anion. This explains the results of q^+ for:

(1) Fe_2O_3 (hematite) in Cl^- (Figure 15B);
(2) SnO_2 in Cl^- (Figure 17);
(3) ZrO_2 in NO_3^- (23), ClO_4^-, and Cl^- (Figure 20);
(4) ThO_2 in NO_3^- (23), ClO_4^- and Cl^- (Figure 21).

These particular anions, therefore, are specifically adsorbed on the oxide surfaces listed above, in their q^+ region.

Magnetite, however, shows unusual behaviour in that q^+ decreases in value on increasing the KNO_3 concentration from 0.001 M to 0.1 M and 1 M (Figure 16). This behaviour, which was found to be reproducible, is probably due to a different kind of adsorption of H^+, presumably in the space-

charge layer of magnetite. Then the decrease in q^+ with increasing KNO_3 concentration could be attributed to the predominant effect of the increase in ionic strength retarding the chemisorption of H^+ on magnetite. Some other samples of magnetite, however, gave very low values of q^+. The behaviour of magnetite is by no means clear, and requires more detailed study.

If Γ'_{H^+} and Γ'_{OH^-} are the surface excess of H^+ and OH^- adsorbed on the dehydrated oxide surfaces to form the aquo-complex at the z.p.c., then $\left(\Gamma'_{H^+} - \Gamma'_{OH^-}\right)_{z.p.c.} = 0$. There is additional adsorption of H^+ (mechanism B) or removal of OH^- (by Cl^- for example, mechanism A) from the neutral surface on decreasing the pH_s below the z.p.c., so that the Gibbs' adsorption equation, for the general case, may be written at constant temperature and pressure as:

$$d\gamma = -\left[\left(\Gamma'_{H^+} - \Gamma'_{OH^-}\right)_{z.p.c.} + \left(\Gamma_{H^+} - \Gamma_{OH^-}\right)\right] d\bar{\mu}_{HX} - \left(\Gamma_{X^-}\, d\bar{\mu}_{KX}\right) - \left(\Gamma_{K^+}\, d\bar{\mu}_{KX}\right), \qquad \text{(Eq. 35)}$$

where γ is the interfacial energy (in ergs/cm^2), $\bar{\mu}$ is the electrochemical potential, X^- is the anion, and Γ is the surface excess. In the above equation, $\left(\Gamma'_{H^+} - \Gamma'_{OH^-}\right)_{z.p.c.} = 0$. In the q^+ region, adsorption of K^+ is almost zero, and, applying the above equation for mechanism B, $d\bar{\mu}_{KX}$ at constant ionic strength may be taken as almost zero. This is because the anions X^- (e.g., NO_3^- or ClO_4^-) remain as counter ions only in the diffuse double layer and their adsorption is negligibly small on oxide surfaces, and also because, as discussed previously, no surface hydroxyl groups are replaced by anions. Hence, for the q^+ region of oxides, according to

mechanism B, where the anions are not specifically adsorbed on the surface, the above equation simplifies to:

$$d\gamma = \left[-\Gamma_{H^+}\right]_{\mu_{KX}} d\bar{\pi}_{HX}. \qquad \text{(Eq. 36)}$$

Thus, in the interfacial reactions following mechanism B, the decrease in interfacial energy is mainly due to H^+ adsorption on the surface. This conclusion is in agreement with the results of q^+ for:

(1) Fe_2O_3 in NO_3^- and ClO_4^- solutions (Figures 14 and 15A);
(2) SnO_2 in NO_3^- solutions (Figure 17);
(3) TiO_2 in NO_3^-, ClO_4^- and Cl^- solutions (Figure 18);
(4) Al_2O_3 in NO_3^-, ClO_4^- and Cl^- solutions (Figure 19).

The above conclusion is also in agreement with the known properties of these metal oxides which can behave as electrodes of the second kind (30, 35), reversible to H^+, depending on the nature of the ions present in solution. The half-cell potential (E) of the oxide electrodes, under the above set of conditions, has been given by the Nernst equation:

$$E = E_o + \frac{2.303RT}{F} \log a_{H^+}. \qquad \text{(Eq. 37)}$$

Kortüm and Bockris (30, p. 296) have also indicated that proton adsorption may be the primary mechanism for ideal behaviour of an oxide-electrode.

When the interfacial reactions occur according to mechanism A (e.g., Fe_2O_3 and SnO_2 in Cl^- solutions), in addition to H^+ adsorption on the surface, the surface hydroxyl groups are also replaced by Cl^-. As the specific adsorption of anions (X^-) on oxides is appreciable, the product $\Gamma_X - d\bar{\pi}_{KX}$ can no longer be taken as zero (cf. mechanism B). Hence, the general Gibbs'

adsorption equation, at constant temperature and pressure for mechanism A, is simplified to:

$$d\gamma = -\left[\Gamma_{H^+} - \Gamma_{OH^-}\right] d\bar{\mu}_{HX} - \Gamma_{X^-} d\bar{\mu}_{KX}. \qquad \text{(Eq. 38)}$$

At constant pH_s, the decrease in the interfacial energy is due to Cl^- adsorption, so that

$$d\gamma = -\left[\Gamma_{Cl^-}\right]_{pH_s} d\bar{\mu}_{KX}. \qquad \text{(Eq. 39)}$$

Thus, the oxides' surfaces, reacting with electrolyte solutions according to mechanism A, are reversible to H^+ as well as to X^-. This conclusion is in agreement with the results of q^+ for:

(1) Fe_2O_3 (hematite) and SnO_2 in Cl^- solutions (Figures 15B and 17);
(2) ZrO_2 in NO_3^- (23), ClO_4^- and Cl^- (Figure 20) solutions;
(3) ThO_2 in NO_3^- (23), ClO_4^- and Cl^- (Figure 21) solutions.

(b) The Negative Surface Charge

The negative surface charge on oxide surfaces originates in solutions of $pH_s >$ the pH_s of the z.p.c., from acidic dissociation of the surface hydroxyl groups, and this leads, subsequently, to the adsorption of K^+ on the surface. As is seen in Figure 14 and Figures 16 to 19, the q^- values of all oxides increase with increasing values of pH_s as well as with increasing K^+ concentration. This behaviour is similar to that of quartz, zirconia and thoria that were studied earlier (23). The general Gibbs' adsorption equation (Equation 35), in the q^- region, may be written as:

$$d\gamma = -\left[\Gamma_{H^+} - \Gamma_{OH^-}\right] d\bar{\mu}_{KOH} - \Gamma_{K^+}\, d\bar{\mu}_{KX}, \qquad \text{(Eq. 40)}$$

where the adsorption of anions (X^-) is assumed to be negligibly small. At constant pH_s, the decrease in interfacial energy is due to adsorption of K^+, so that:

$$d\gamma = -\left[\Gamma_{K^+}\right]_{pH_s} d\bar{\mu}_{KX}. \qquad \text{(Eq. 41)}$$

The oxide electrodes are reversible to OH^- in the q^- region, and, hence, indirectly to H^+. The half-cell electrode potential of oxides, in the q^- region, has been given (30) as:

$$E = E_o + \frac{RT}{nF} \ln \frac{Ks}{Kw} + \frac{RT}{F} \ln a_{H^+}, \quad \text{or}$$

$$E = E_o' + \frac{2.303RT}{F} \log a_{H^+}, \qquad \text{(Eq. 42)}$$

where Ks is the constant for the acidic dissociation of the surface-hydroxyl groups, and Kw is the ionic product of water. The oxide electrode can obey the Nernst equation with respect to a_{H^+} at low K^+ concentration, and up to a pH_s where the specific adsorption of K^+ is negligible. The nature of adsorption of K^+ on the negatively charged surfaces of oxides will be discussed in conjunction with the differential capacity of the double layer.

The Differential Capacity of the Double Layer and the Interfacial Energy

The thermodynamic and experimental methods of obtaining the differential capacity, $C(\pm)$, and the decrease in the interfacial energy $(\gamma-\gamma_o)$ of the double layer on oxides, have already been discussed. In 0.001 M and 0.1 M solutions of 1-1 valent salts, differential capacities of 6

and 14 $\mu F/cm^2$ are expected (7; 8, p. 642; 9) at the zero point of charge in the absence of any specific adsorption. As seen in Figures 22 to 24, the minimum values of C, as obtained from the graphical differentiation of the q-E plots, are in fair agreement with the theory. At higher $\pm$ potentials relative to the z.p.c., a constant base capacity (8, p. 642) of 17 $\mu F/cm^2$ (due to the layer of water molecules on the surface), in the absence of specific adsorption, is expected from theory. Any increase in the double-layer capacity over 17 $\mu F/cm^2$ is attributed to the adsorption of either cations or anions in the inner Helmholtz layer of the interface through the displacement of the water molecules on the surface (specific adsorption). Thus the steep rise in the C(+) values of the double layer on Fe_2O_3, Fe_3O_4, SnO_2 and TiO_2 in KNO_3 solutions, as seen in Figures 22 to 24, may be attributed to the chemisorption of H^+ on the surface, as was also discussed in the previous section. In the presence of Cl^-, however, C(+) is expected to vary with Cl^- adsorption as well, and comparatively high values of C(+) will be obtained. In general, many anions that are less hydrated and more polarizable than cations -- for example, Cl^-, Br^- and I^- -- show a greater tendency for specific adsorption on solid surfaces. Thus, for the same surface potential, both the surface charge and the differential capacity will be higher on the positive side than on the negative side.

The C(-) curve of hematite, in Figure 22, shows a plateau between pH_s 7.5-9.5 (C(-) $\approx$ 30-40 $\mu F/cm^2$), followed by a steep rise in C(-). The steep rise in C(-) at $pH_s > 9.5$ is similar to that obtained for quartz and zirconia (23) in the q^- region, and is most probably due to the specific

adsorption of cations to the metal atoms of the surface through chemisorbed $O^{=}$, as discussed earlier (23). These plateaus probably correspond to the characteristic "hump" in the C curves of the polarized Hg surface, except that in this work the hump has been smoothed in the graphical differentiation of the q^{-} curves. The hump, as discussed in part A, has been attributed to two opposing effects, the specific adsorption of ions and dielectric saturation. If the specific adsorption of ions is intense, e.g. I^{-} on Hg, the hump is found to be masked. In the case of magnetite, titania, cassiterite, etc. (Figures 22-24), the intense specific adsorption of ions appears to have masked the effects which give rise to such humps.

The curves of $(\gamma-\gamma_o)$ against pH_s (or potential) for different oxides, as shown in Figures 25 to 29, represent the decrease in the interfacial energy relative to that (γ_o) of the same surface at the z.p.c. The decrease in the interfacial energy occurs as ions are adsorbed on the surface, and the greater the adsorption the larger is the decrease in the interfacial energy. As seen in Figures 25 to 29, the interfacial energy is a maximum at the zero point of charge as predicted from theory (Equation 2). The coincidence of the $(\gamma-\gamma_o) : pH_s$ curves (Figures 25, 27-29) at the left-hand side of the z.p.c. indicates that the interface has a structure or composition which is practically unaffected by the salt concentration, as discussed in a previous section. This behaviour is comparable to that of the cathodic surfaces of Hg or AgI (99), where the cations stay in the outer Helmholtz plane.

Applications of Double-Layer Studies in Some Industrial Processes

The information obtained on the double-layer characteristics such as the z.p.c., charge densities ($\pm$), differential capacities, the interfacial tension, etc., could prove of considerable use in solving many industrial problems in such areas as mineral flotation, agglomeration, adhesion, surface spreading, corrosion, etc. In the foregoing discussion, for example, several inferences were drawn as to (a) the nature ($\pm$) and magnitude of the surface charge, and the space charge on the solution side of the double layer; (b) the chemical structure of the surface; (c) the nature of ion-surface interactions and the type of adsorption (specific or non-specific) of cations and anions on the surface; and (d) the shift in the zero point of charge. The nature ($\pm$) and the amount of the activators, collectors and depressants that are used in mineral flotation should depend on the nature ($\pm$) and magnitude of the surface charge. In a mixture of minerals whose z.p.c. are sufficiently separated, the surface of one mineral will be positively charged and that of the other negatively charged, in the range between their respective z.p.c. In such cases, selective or collective flotation may be achieved by selecting activators and depressants of appropriate charge. In selecting these flotation reagents, it is also important to know the chemical composition of the surface, and whether the counter ions are specifically adsorbed (through covalent interaction) on the surface or if they stay in the diffuse double-layer. Solid surfaces, in general, possess water of hydration which makes them hydrophilic. If ions such as Cl^- (but not

NO_3^- or ClO_4^-) are present in solution, they can displace the water molecules of the surface (e.g., of hematite and cassiterite, but not of rutile) when specifically adsorbed, and the surface would subsequently behave as a chloride surface. Polyvalent anions, if specifically adsorbed, can serve as anionic activators or depressants in flotation. The differential capacity curves can provide information on the specific adsorption of ions on the surface. Thus, by an analysis of the C(-) curves of quartz, zirconia and thoria in the q^- region (23), and similarly for the other oxides in the present investigations, it was shown in what pH range and electrolyte concentrations the specific adsorption of anions or cations becomes considerable. This subject has also been considered in some detail in a previous publication (23).

It was also pointed out, earlier in this paper, that the z.p.c. would strongly depend on the kinetics of the solid-solution equilibria and on the extent of dissolution of the solid, in addition to the nature and concentration of other electrolytes present in solution. The z.p.c. shifts towards a higher or a lower pH_s when cations or anions are specifically adsorbed on the surface in the vicinity of the z.p.c. Neutral organic molecules, such as alcohols, having a smaller surface tension (and dielectric constant) than water, tend to accumulate at the interface and this also shifts the z.p.c. It was also pointed out earlier that polyvalent complex ions in solution, arising from the solubility of the solid, may have a different or an opposite charge from that of the surface and hence can be re-adsorbed on the surface. This would not only shift the z.p.c. but would also result in what may be called

"self-activation" of the surface. Hence, the z.p.c. at the initial stage of equilibrium (a few minutes) could be much different from the z.p.c. of the same material when allowed to equilibrate in solutions for longer times. This could probably explain why the rate of flotation often falls off rapidly after a few minutes of initial reaction.

ACKNOWLEDGEMENTS

The authors are grateful to Dr. J. D. Keys (Head, Mineral Physics Section, Mineral Sciences Division, Mines Branch 1964-1967) for his continued encouragement during the course of this work and to Professor B. E. Conway, University of Ottawa, for offering critical suggestions. Thanks are also due to Dr. H. P. Dibbs, Head, Surface Science Group, of the Mines Branch's Mineral Sciences Division, and to P. E. Shannon, the Mines Branch editor, for suggestions and substantial assistance in the preparation of this report. The authors would like to thank the Consolidated Mining and Smelting Co. of Canada and the Quebec Cartier Mining Company for providing, respectively, samples of cassiterite and specular hematite for this work.

One of us (D.M.) is particularly grateful to the Mines Branch, Department of Energy, Mines and Resources, Ottawa, for providing the research facilities.

REFERENCES

1. Gaudin, A.M., "Flotation", 2nd ed. (McGraw-Hill, New York, 1958).

2. Sutherland, K.L. and Wark, I.W., "Principles of Flotation", published by the Australian Inst. of Mining and Metallurgy, Melbourne, in 1955.

3. De Bruyn, P.L. and Agar, G.E., in "Froth Flotation", 50th Anniversary Volume, published by the AIME, New York, in 1962.

4. Proceedings of Symposium on Recent Developments in Mineral Dressing, London, September 1952 (published by the Institution of Mining and Metallurgy, London, 1953).

5. Klassen, V.I. and Mokrousov, V.A., "An Introduction to the Theory of Flotation" (Butterworths, London, 1963). This is a translation from the Russian, made by J. Leja and G.W. Poling.

6. Adams, N.K., "The Physics and Chemistry of Surfaces", 3rd ed. (Oxford University Press, London, 1941).

7. Grahame, D.C., Chem. Rev., 41, 441 (1947).

8. Devanathan, M.A.V. and Tilak, B.V.K., Chem. Rev., 65, 635 (1965).

9. Delahay, P., "Advances in Electrochemistry and Electrochemical Engineering", Vol. I (Interscience, New York, 1961).

10. Bockris, J. O'M., Müller, K., Wroblowa, H. and Kovac, Z., J. Electroanal. Chem., 10, 416 (1965).

11. Levine, S. and Matijevic, E., J. Colloid and Interface Sci., 23, 188 (1967).

12. Proceedings of Symposium on the Chemistry and Physics of Interfaces, Washington, D.C., June 1964, sponsored and published by the American Chemical Society, 1964.

13. Adamson, A.W., "The Physical Chemistry of Surfaces" (Interscience, New York, 1960).

14. Walters, G.K., J. Phys. Chem. Solids, 14, 43 (1960).

15. Kokes, R.J., J. Phys. Chem. Solids, 14, 51 (1960).

16. Eischens, R.P., J. Phys. Chem. Solids, 14, 56 (1960).

17. Zettlemoyer, A.C., Chem. Rev., 59, 937 (1959).

18. Mohilner, D., J. Phys. Chem., 66, 724 (1962).

19. Mackor, E.L., Rec. Trav. Chim., 70, 663, 747, 763 (1951).

20. Overbeek, J. Th. G., "Semi-Centennial Symposium on Electrochemical Constants", Circular No. 524, p. 213, U.S. Bureau of Standards, Washington, D.C. (1953).

21. Bijsterbosch, B.H. and Lyklema, J., J. Colloid Sci., 20, 665 (1965).

22. Parks, G.A. and De Bruyn, P.L., J. Phys. Chem., 66, 967 (1962).

23. Ahmed, S.M., Can. J. Chem., 44, 1663, 2769 (1966).

24. Onoda, G.Y. Jr. and De Bruyn, P.L., Surface Sci., 4, 48 (1966).

25. Yopps, J.A. and Fuerstenau, D.W., J. Colloid Sci., 19, 61 (1964).

26. Li, H.C. and De Bruyn, P.L., Surface Sci., 5, 203 (1966).

27. Verwey, E.J.W., Rec. Trav. Chim., 60, 625 (1941).

28. Freyberger, W.L. and De Bruyn, P.L., J. Phys. Chem., 61, 586 (1957).

29. Iwasaki, I. and De Bruyn, P.L., J. Phys. Chem., 62, 594 (1958).

30. Kortüm, G. and Bockris, J. O'M., "Textbook of Electrochemistry", (Elsevier Pub. Co., New York, 1951), p. 293.

31. Janz, G.J. and Taniguchi, H., Chem. Rev., 53, 397 (1953).

32. Goates, J.R., Cole, A.G., Gray, E.L. and Faux, N.D., J. Am. Chem. Soc., 73, 707 (1951).

33. Golding, R.M., J. Chem. Soc., 1838 (1959).

34. Ives, D.J.G. and Janz, G.J., "Reference Electrodes, Theory and Practice" (Academic Press, New York, 1961), p. 322.

35. Stock, J.T., Purdy, W.C. and Garcia, L.M., Chem. Rev., 58, 611 (1958).

36. Verwey, E.J.W. and Overbeek, J. Th. G., "Theory of the Stability of Lyophobic Colloids" (Elsevier, New York, 1948).

37. Conway, B.E., "Theory and Principles of Electrode Processes" (Ronald Press Co., New York, 1965).

38. Parsons, R., "Modern Aspects of Electrochemistry", Vol. I, J.O'M. Bockris, ed. (Academic Press Inc., New York, 1954), p. 103.

39. Frumkin, A.N. and Damaskin, B.B., "Modern Aspects of Electrochemistry", Vol. 3, J.O'M. Bockris and B.E. Conway, eds. (Butterworths, London, 1964), p. 149.

40. Leja, J., Proceedings of Second International Congress on Surface Activity, London, 3, 273 (1957).

41. Grahame, D.C., Proceedings of International Committee of Electrochemical Thermodynamics, III Meeting, Berne (1951), p. 330.

42. Conway, B.E. and Gordon, L.G.M., J. Electroanal. Chem., 15, 7 (1967).

43. Riney, J.S., Schmid, G.M. and Hackerman, N., Rev. Sci. Instr., 32, 588 (1961).

44. Grahame, D.C. and Whitney, R.B., J. Am. Chem. Soc., 64, 1548 (1942).

45. Ramaley, L. and Enke, C.G., J. Electrochem. Soc., 112, 943 (1965).

46. Butler, J.N., J. Phys. Chem., 70, 2312 (1966).

47. Rouse, T.O. and Weininger, J.L., J. Electrochem. Soc., 113, 184 (1966).

48. Delahay, P., "New Instrumental Methods in Electrochemistry" (Interscience, New York, 1954).

49. Grahame, D.C., J. Chem. Phys., 21, 1054 (1953).

50. Grahame, D.C. and Soderberg, B.A., J. Chem. Phys., 22, 449 (1954).

51. Grahame, D.C., Poth, M.A. and Cummings, J.I., J. Am. Chem. Soc., 74, 4422 (1952).

52. Grahame, D.C., J. Electrochem. Soc., 98, 343 (1951).

53. Frumkin, A., "Proceedings of Symposium on Electrode Processes", Philadelphia (Wiley, New York, 1959), p. 2.

54. Delahay, P. and Susbielles, G.G., J. Phys. Chem., 70, 647 (1966).

55. Conway, B.E., Bockris, J.O'M. and Amar, I.A., Trans. Faraday Soc., 47, 756 (1951).

56. Grahame, D.C., J. Chem. Phys., 18, 903 (1950).

57. Macdonald, J.R. and Barlow, C.A. Jr., J. Chem. Phys., 36, 3062 (1962).

58. Watts-Tobin, R.J., Phil. Mag., 6, 133 (1961).

59. Bockris, J.O'M., Devanathan, M.A.V. and Müller, K., Proc. Roy. Soc. (Lon.), Series A, 274, 55 (1963).

60. Delahay, P., J. Electrochem. Soc., 113, 967 (1966).

61. Levine, S., Mingins, J. and Bell, G.M., J. Electroanal. Chem., 13, 280 (1967).

62. Grahame, D.C., Z.Electrochem., 62, 264 (1958).

63. Macdonald, J.R. and Barlow, C.A. Jr., J. Electrochem. Soc., 113, 978 (1966).

64. Levine, S., Bell, G.M. and Calvert, D., Can. J. Chem., 40, 518 (1962).

65. Grahame, D.C., J. Am. Chem. Soc., 80, 4201 (1958).

66. Grahame, D.C. and Parsons, R., J. Am. Chem. Soc., 83, 1291 (1961).

67. Russell, C.D., J. Electroanal. Chem., 6, 486 (1963).

68. Dutkiewiez, E. and Parsons, R., J. Electroanal, Chem., 11, 100 (1966).

69. Parsons, R., Trans. Faraday Soc., 51, 1518 (1955).

70. Susbielles, G.G., Delahay, P. and Solon, E., J. Phys. Chem., 70, 2601 (1966).

71. Devanathan, M.A.V. and Tilak, B.V.K., Indian J. Chem., 3, 373 (1965).

72. Parsons, R., Trans. Faraday Soc., 55, 999 (1959).

73. Dutkiewiez, E., J. Electroanal. Chem., 15, 1 (1967).

74. Payne, R., J. Electrochem. Soc., 113, 999 (1966).

75. Wroblowa, H., Kovac, Z. and Bockris, J.O'M., Trans. Faraday Soc., 61, 1523 (1965).

76. Grahame, D.C., J. Am. Chem. Soc., 76, 4819 (1954).

77. Grahame, D.C., J. Am. Chem. Soc., 79, 2093 (1957).

78. Mott, N.F. and Watts-Tobin, R.J., Electrochim. Acta, 4, 79 (1961).

79. Staicopolus, D.N., J. Electrochem. Soc., 108, 900 (1961).

80. Sparnaay, M.J., Surface Sci., 1, 213 (1964).

81. Hampson, N.A., Larkin, D. and Morley, J.R., J. Electrochem. Soc., 114, 817 (1967).

82. Hampson, N.A. and Larkin, D., J. Electrochem. Soc., 114, 933 (1967).

83. Popat, P.V. and Hackerman, N., J. Phys. Chem., 62, 1198 (1958).

84. Brodd, R.J. and Hackerman, N., J. Electrochem. Soc., 104, 704 (1957).

85. McMullen, J.J. and Hackerman, N., J. Electrochem. Soc., 106, 341 (1959).

86. Green, M., "Modern Aspects of Electrochemistry", No. 2, J.O'M. Bockris, ed. (Butterworths, London, 1959), Chapter 5.

87. Garrett, C.B.G. and Brattain, W.H., Phys. Rev., 99, 376 (1955).

88. Many, A., J. Phys. Chem. Solids, 8, 87 (1959).

89. Proceedings of Symposium on the Surface Chemistry of Metals and Semiconductors, H.C. Gatos, ed. (Wiley, New York, 1960).

90. Proceedings of the Conference on the Physics of Semiconductor Surfaces, Philadelphia, June 1956, R. H. Kingston, ed. (University of Pennsylvania Press, Philadelphia, 1957).

91. "Progress in Semiconductors", Vol. 5, A. F. Gibson, ed. (Wiley, New York, 1960).

92. Many, A., Goldstein, Y. and Grover, N.B., "Semiconductor Surfaces" (Wiley, New York, 1965).

93. "The Electrochemistry of Semiconductors", P.J. Holmes, ed. (Academic Press, New York, 1962).

94. Frankl, D.R., "Electrical Properties of Semiconductor Surfaces" (Pergamon Press, New York, 1967).

95. Dewald, J.F., J. Phys. Chem. Solids, 14, 155 (1960).

96. Honig, J.M., J. Chem. Edn., 43, 76 (1966).

97. Mular, A.L., Trans. AIME, 232, 204 (1965).

98. Sparnaay, M.J., Proceedings of Third International Congress on Surface Activity, Cologne, 2, 232 (1960).

99. Lyklema, J. and Overbeek, J. Th. G., J. Colloid Sci., 16, 595 (1961).

100. Iwasaki, I. and De Bruyn, P.L., Surface Sci., 3, 299 (1965).

101. Herczynska, E., J. Inorg. Nucl. Chem., 26, 2127 (1964).

102. Atkinson, R.J., Posner, A.M. and Quirk, J.P., J. Phys. Chem., 71, 550 (1967).

103. Healy, T.W. and Fuerstenau, D.W., J. Colloid Sci., 20, 376 (1965).

104. Healy, T.W., Herring, A.P. and Fuerstenau, D.W., J. Colloid and Interface Sci., 21, 435 (1966).

105. Smith, G.W. and Salman, T., Can. Met. Quart., 5, 93 (1966).

106. Smith, G.W. and Salman, T., Can. Met. Quart., 6, 167 (1967).

107. Joy, A.S., Watson, D. and Cropton, R.W.G., Trans. AIME, 229, 5 (1964).

108. Healy, W.T. and Jellett, V.R., J. Colloid and Interface Sci., 24, 41 (1967).

109. Bragg, L. and Claringbull, G.F., "The Crystalline State", Vol. 4 (Bell and Sons, Ltd., London, 1965).

110. Brunauer, J., Emmet, P.H. and Teller, E., J. Am. Chem. Soc., 60, 309 (1938).

111. Emmet, P.H., "Catalysis", Vol. 1 (Reinhold, New York, 1954), pp. 31-74.

112. Brunauer, S., Vol. 33, Advances in Chemistry Series (Amer. Chem. Soc., 1961), p. 5.

113. Beebe, R.A., Beckwith, J.B. and Honig, J.M., J. Am. Chem. Soc., 67, 1554 (1945).

114. Rosenberg, A.J., J. Am. Chem. Soc., 78, 2929 (1956).

115. Ahmed, S.M., Mines Branch, Technical Bulletin TB 84, Dept. of Energy, Mines and Resources, Ottawa (1966).

116. Bates, R.G., J. Res. Nat. Bur. Std., A, 66, 179 (1962).

117. Egorov, M.M. and Kiselev, V.F., Zh. Fiz. Khim., 36, 318 (1962).

118. Wade, W.H., Cole, H.D., Meyer, D.E. and Hackerman, N., Advan. Chem. Ser., 33, 35 (1961).

119. Parks, G.A., Chem. Rev., 65, 177 (1965).

120. Biedermann, G. and Chow, J.T., Acta Chem. Scand., 20, 1376 (1966).

121. Buchanan, A.S. and O'Connor, D.J., Austral. J. Chem., 6, 278 (1953).

122. Gaudin, A.M. and Fuerstenau, D.W., Trans. AIME, 202, 66 (1955).

123. Pourbaix, M.J.N., "Thermodynamics of Dilute Aqueous Solutions" (English translation by J.N. Agar), Arnold, London (1949).

124. Delahay, P., Pourbaix, M. and Rysselberghe, P.V., J. Chem. Edn., 27, 683 (1950).

= = =

SMA:DM:(PES)vb